Energy Island Baltic Sea

Metocean Assessment

Part B: Data Analyses

Report
IO Number 4500092960

2024-02-22

Prepared for Energinet Eltransmission A/S

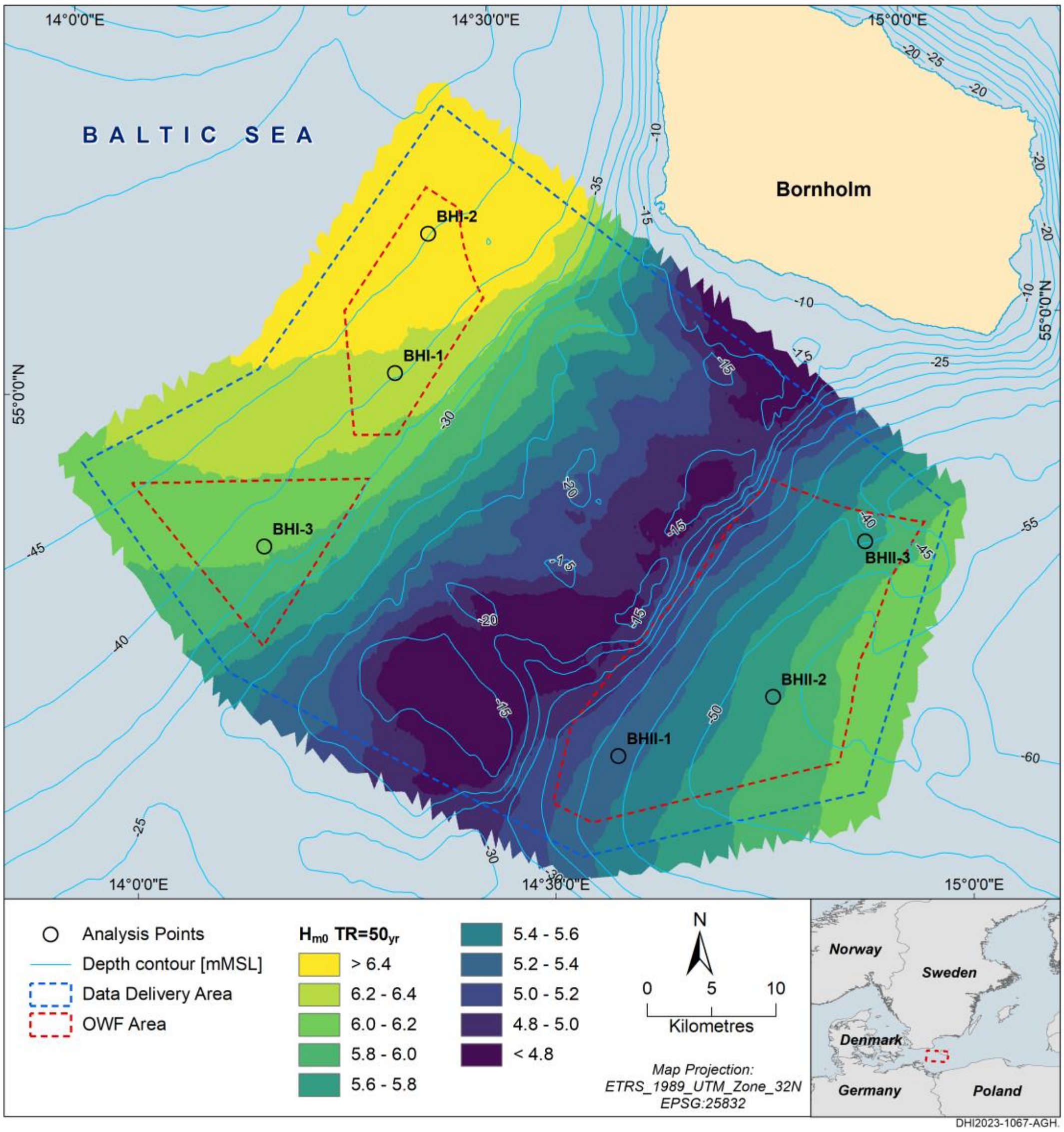

Energy Island Baltic Sea

Metocean Assessment
Part B: Data Analyses

Report
IO Number 4500092960

Prepared for: Energinet Eltransmission A/S
Represented by Mr Kim Parsberg Jakobsen

Front page: Spatial variation across EIBS OWFs area of H_{m0} for return period of 50 years.

Contact person:	Morten Rugbjerg, mnr@dhigroup.com, +45 45 16 94 18
Project Manager:	Morten Rugbjerg
Quality Supervisor:	Jacob Berg Jørgensen
Author:	Arief Rullyanto
Project No.:	11829021
Approved by:	Jacob Berg Jørgensen
Approval date:	2024-02-22
Revision:	Final 1.2
Classification:	**Confidential**
=	
File name:	11829021_DHI_EIBS_Metocean_PartB_Data_Analysis.docx

DHI A/S • Agern Allé 5 • DK-2970 Hørsholm • Denmark
Telephone: +45 4516 9200 • dhi@dhigroup.com • www.dhigroup.com • Company Reg. No.: DK36466871

Contents

Figures

Tables

Appendices

Nomenclature

Variable	Abbreviation	Unit
Atmosphere		
Wind speed @ 10 m height	WS_{10}	m/s
Wind direction @ 10 m height	WD_{10}	°N (clockwise from)
Air pressure @ mean sea level	P_{MSL}	hPa
Air temperature @ 2 m height	$T_{air,2m}$	°C
Relative humidity @ 2 m height	RH_{2m}	-
Downward solar radiation flux	DSWR	W/m^2
Ocean		
Water level	WL	mMSL
Current speed	CS	m/s
Current direction	CD	°N (clockwise to)
Water temperature	T_{sea}	°C
Water Salinity	Salinity	PSU
Waves		
Significant wave height	H_{m0}	m
Peak wave period	T_p	s
Mean wave period	T_{01}	s
Zero-crossing wave period	T_{02}	s
Peak wave direction	PWD	°N (clockwise from)
Mean wave direction	MWD	°N (clockwise from)
Direction standard deviation	DSD	°

Definitions	
Coordinate System	WGS84 EPSG 4326 (unless specified differently)
Direction	Clockwise from North Wind: °N coming from Current: °N going to Waves: °N coming from
Time	Times are relative to UTC
Vertical Datum	MSL (unless specified differently)

Abbreviations	
2D	2-dimensional
3D	3-dimensional
ADCP	Acoustic Doppler Current Profiler
CEM	Coastal Engineering Manual, Meteorology and Wave Climate
CFSR	Climate Forecast System Reanalysis
DEA	Danish Energy Agency
DNV	Det Norske Veritas
DNVGL	Det Norske Veritas Germanischer Lloyd
ECMWF	European Centre for Medium-Range Weather Forecasts
EIBS	Energy Island Baltic Sea
EMODnet	The European Marine Observation and Data Network
ERA5	ECMWF Re-analysis v5
FEED	Front-End Engineering Design
HD	Hydrodynamic
IEC	International Electrotechnical Commission
ISO	International Organization for Standardization
mMSL	Metres above Mean Sea Level
MSL	Mean Sea Level
NORA3	3 km NOrwegian ReAnalysis atmospheric dataset
OWF	Offshore Wind Farm
PR	Peak Ratio
PSU	Practical Salinity Unit
SW	Spectral Wave
UTC	Coordinated Universal Time
WGS84	World Geodetic System 1984

Revision

Version	Date	Revision log
Draft 0.1	13 October 2023	Draft version for client review
Final 1.0	21 December 2023	Final version incorporating comment to draft report from client
Final 1.1	21 February 2024	Final version incorporating comment to final report from client
Final 1.2	22 February 2024	Minor changes to report structure (sections 5.3, 6.3 and 6.4)

Executive Summary

Energinet Eltransmission A/S (Energinet) commissioned DHI A/S (DHI) to carry out a metocean study that shall serve as a basis for Front-End Engineering and Design (FEED) of two offshore wind farms named Bornholm I and Bornholm II, being part of Energy Island Baltic Sea (EIBS). The offshore wind farms are to be located southwest of the island Bornholm in the Baltic Sea. This report presents the metocean study made by DHI.

The results of the metocean study consist of three reports: a metocean data basis report (Part A), a metocean data analysis report (Part B, this report), and a hindcast revalidation note. Additionally, a metocean hindcast database is provided.

The study provides detailed metocean conditions for EIBS offshore wind farm (OWF) and establishes a metocean database around the OWF area as shown in Figure 0.1.

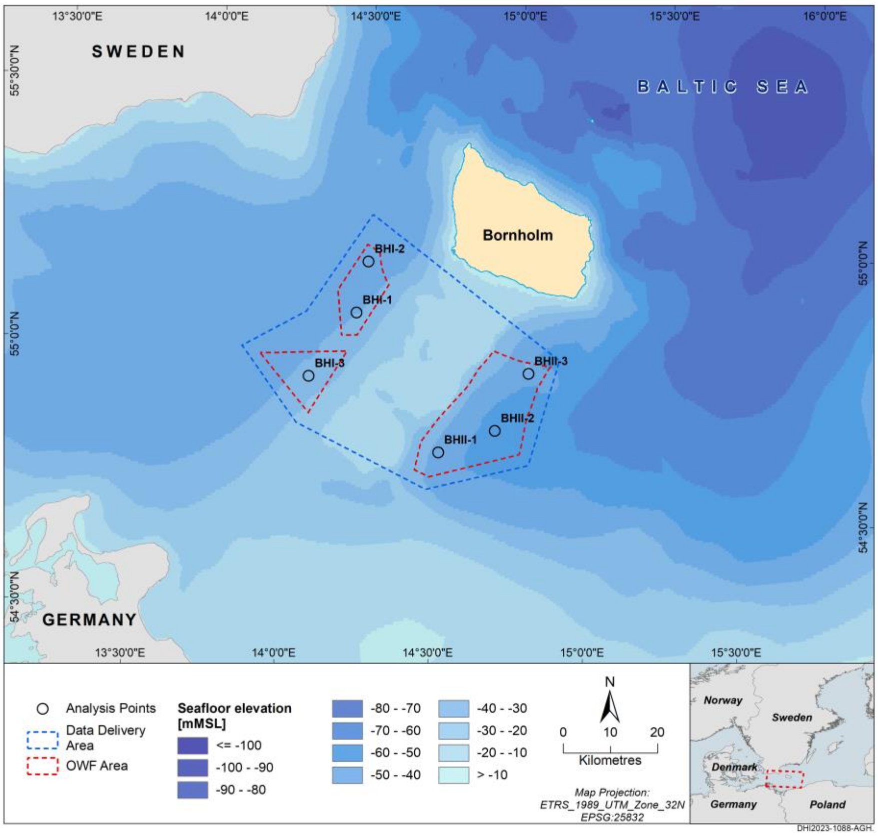

Figure 0.1 Location of the Energy Island Baltic Sea, the related offshore wind farm development area

In order to establish the metocean conditions, DHI performed high-resolution numerical modelling (wave and hydrodynamic) and state-of-the-art analyses of the model results (both normal and extreme conditions), which are presented in this report. Six points are selected for the analysis, denoted as BHI-1, BHI-2, BHI-3, BHII-1, BHII-2, and BHII-3. BHI-2 is selected as representative point in this report.

Normal conditions

Across the EIBS OWF areas, the mean wind speed is 7.6 m/s, and the mean significant wave height is 0.9 – 1.0 m with peak wave periods most frequently at 9 - 11 s. The wave conditions are predominantly from the west and southwest.

The tides are weak at BHI-2 with HAT = 0.06 mMSL and LAT = -0.08 mMSL, giving a tidal range of 0.14 m. The highest and lowest total water levels in the hindcast period (1979 - 2022) are +1.26 mMSL and -1.35 mMSL and occur during winter. The mean current speed of near-surface, mid-depth and near-seabed are 0.2, 0.09, and 0.06 m/s, respectively, dominated by residual (especially during extreme events).

Extreme conditions

Extreme metocean conditions were established using Traditional Extreme Value Analysis (T-EVA) following the methodology and settings derived and described in Appendix B Sensitivity of T-EVA to Distribution, Threshold, and Fitting.

The estimated extreme values within the EIBS OWF area are given for return periods of 1, 5, 10, and 50 years for waves (H_{m0}, H_{max}, and C_{max} including conditioned/joint variables), water level and currents at six (6) analysis points (see Figure 2.1). Table 0.1 presents a summary of the 50-year omni-extreme values at all analysis points.

The water depth at the analysis points varies within -37 to -54 mMSL. The 50-year significant wave height, $H_{m0,50yr}$, varies within 5.3 – 6.0 m at the analysis points. The maximum wave height, H_{max}, is a factor 1.9 - 2 times H_{m0}, depending on local water depth. The 50-year maximum wave crest height with respect to MSL (i.e., convoluted with the simultaneous water level), $C_{max,MSL}$, varies within 6.8 to 7.3 mMSL.

The 50-year total high and low water levels, HWL_{tot} and $LWL_{tot,}$ are within +1.3 mMSL and -1.3 mMSL, and the 50-year total near-surface current speed, $CS_{tot,50yr}$, varies within 0.85 – 1.28 m/s across the analysis points.

Table 0.1 **Summary of the 50-year omni-directional extreme values at all six analysis points**
Results at BHI-2 are presented in the main body of this report, while results at all six analysis points are given in the data reports attached to this report.

Variable		50-year omni-directional extreme values at analysis points					
Abbrev.	Unit	BHI-1	BHI-2	BHI-3	BHII-1	BHII-2	BHII-3
d	mMSL	-40.5	-45.2	-37.0	-43.0	-53.6	-42.2
HWL_{tot}	mMSL	1.3	1.3	1.3	1.2	1.2	1.2
LWL_{tot}	mMSL	-1.3	-1.3	1.4	1.2	1.2	1.1
$CS_{surf.,tot}$	m/s	1.28	1.09	1.35	0.85	0.89	1.00
$CS_{mid.,tot}$	m/s	0.63	0.57	0.7	0.56	0.43	0.47
$CS_{seabed,tot}$	m/s	0.28	0.35	0.27	0.32	0.26	0.27
H_{m0}	m	6.4	6.6	6.0	5.3	5.8	5.7
$T_p\|H_{m0}$ *	s	9.7	9.7	9.4	9.2	10.5	10.3
H_{max}	M	12.2	12.7	11.5	10.8	11.6	11.1
T_{Hmax}	s	8.7	8.7	8.4	8.3	9.4	9.3
$C_{max,MSL}$	mMSL	7.1	7.3	6.8	6.8	7.2	6.8

*: $T_p|H_{m0}$ is 0.5 quantile

1 Introduction

This study provides detailed metocean conditions to use in the Front-End Engineering and Design (FEED) of two offshore wind farms named Bornholm I and Bornholm II, being part of Energy Island Baltic Sea (EIBS). The offshore wind farms are to be located southwest of the island Bornholm in the Baltic Sea. The study consists of three reports: a metocean data basis (Part A) [1], a metocean data analysis (Part B) which is the present report, and a hindcast revalidation note [2]. Additionally, a metocean hindcast database is provided.

Energinet Eltransmission A/S (Energinet) was instructed by the Danish Energy Agency (DEA) to initiate site investigations, including a metocean assessment, for offshore wind farms in an area to the southwest of Bornholm in the Baltic Sea. Following this, Energinet commissioned DHI A/S (DHI) to provide a detailed metocean site condition assessment for use in FEED as described in "CONSULTANCY CONTRACT REGARDING SITE METOCEAN CONDITIONS ASSESSMENT FOR OFFSHORE WIND FARMS – BALTIC SEA" signed on 7 March 2023.

The study consists of several deliverables:

- Part A: Description and Verification of Data Basis (report) [1]
- Part B: Data Analyses and Results (this report)
- Long-term hindcast data (digital time series)
- Measurement data (digital time series)
- Hindcast revalidation note [2]

The study refers to the following common practices and guidelines:

- DNV-RP-C205 [3]
- IEC 61400-3-1 [4]

2 Analysis Points

This section presents the points within the EIBS OWF area selected for analysis of the metocean conditions as presented in this study.

Figure 2.1 shows a map of the six (6) analysis points and Table 2.1 presents the coordinates and water depths of the analysis points.

The analysis points were defined by Energinet considering the anticipated locations of the wind farms, and the spatial distribution of highest waves (see Section 6.2.4), strongest currents (see Section 5.2.2), and water depths (~35-55 mMSL).

Results at BHI-2, the deepest location in the offshore wind farm area north of Ronne Bank with the highest H_{max} (amongst the 6 points), are presented in the body of this report, while results at all six locations are given in the data reports attached to this report (listed in Appendix A: List of Data Reports).

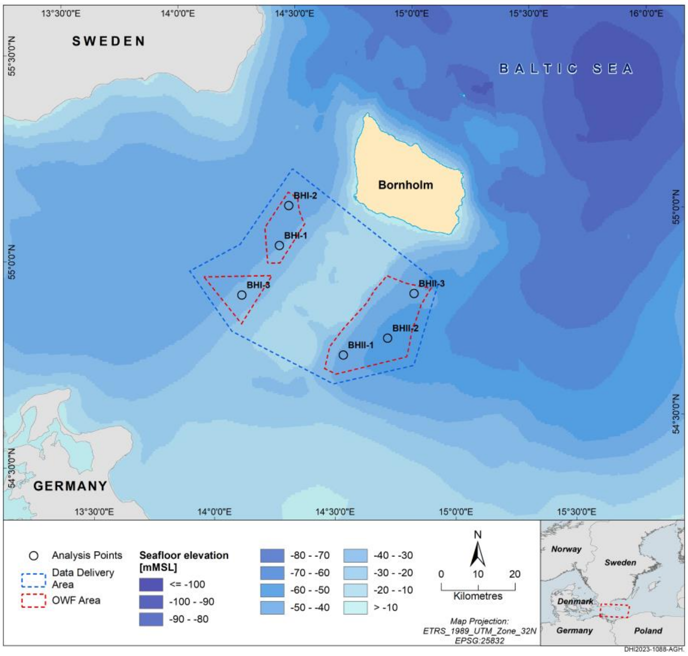

Figure 2.1 Map of the EIBS OWF areas and the selected analysis points

Table 2.1 Coordinates and water depth of the EIBS OWF area analysis points

#	Name	Longitude WGS84 [°E]	Latitude WGS84 [°N]	Depth, SW_{EIBS} [mMSL]
1	BHI-1	14.35560	54.99480	-40.4527
2	BHI-2	14.40847	55.08976	-45.1720
3	BHI-3	14.18206	54.88130	-37.0191
4	BHII-1	14.58820	54.71700	-43.0427
5	BHII-2	14.77962	54.74930	-53.6456
6	BHII-3	14.90577	54.85194	-42.2479

3 Wind Conditions

This section presents a summary of the modelled wind data, followed by a presentation of normal wind conditions.

Note that wind data is included only to assess the misalignment relative to waves. Other wind conditions are addressed in a separate study assessing the wind conditions within the EIBS areas.

The wind data was adopted from [1] and consisted of NORA3 [5] data during the period 1979 – 2022 (44 years). For convenience, we interpolated the NORA3 data from its native resolution (3km and 1 hour) to the mesh and output time step of the wave model of this study (~500 m and 1 hour). The wind dataset is denoted EIBS-AT-NORA3. Table 3.1 summarises the metadata of the EIBS-AT-NORA3 dataset.

Table 3.1 Metadata of the EIBS-AT-NORA3 atmospheric dataset
Time series data was provided to Energinet (.dfs0).

Name	Value
Dataset ID:	EIBS-AT-NORA3
Start Date [UTC]:	1979-01-15 00:00:00
End Date [UTC]:	2022-12-31 23:00:00
Time Step [s]:	3600s

The NORA3 wind is considered representative of a 1-hour averaging period at 10 m height [1]. Conversion for various averaging periods and heights can be found in Section 3.2 on [1].

The wind analyses cover the entire period and are presented in speed bins of 1.0 m/s and directional bins of 22.5° at 10 m height.

Table 3.2 presents the variables of the EIBS-AT-NORA3 dataset, including the bin sizes applied in the analyses of the normal conditions.

Table 3.2 Wind variables of the EIBS-AT-NORA3 dataset

Variable name	Abbrev.	Unit	Bin size
Wind speed at 10 m height (MSL)	WS_{10}	m/s	1.0
Wind direction at 10 m height (MSL)	WD_{10}	°N-from	22.5

3.1 Normal wind conditions

The normal wind conditions are presented at the six analysis points in terms of:

- Time series
- Wind roses

3.1.1 Timeseries

Figure 3.1 shows a time series of wind speed at BHI-2 during the 44-year hindcast period. The mean speed is 7.5 m/s, and the maximum speed is 32.9 m/s.

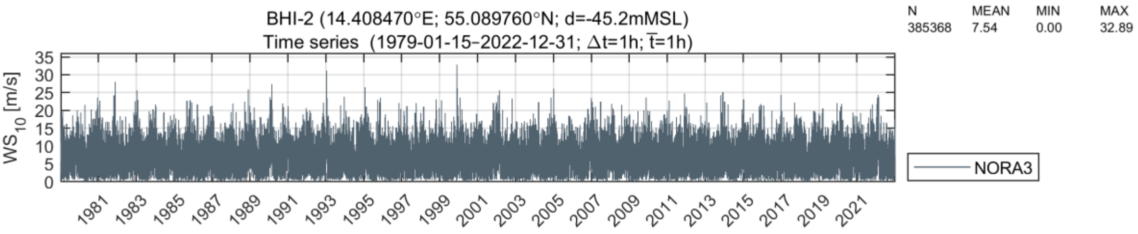

Figure 3.1 Time series of wind speed, WS_{10}, at BHI-2

3.1.2 Wind rose

Figure 3.2 shows a wind rose at BHI-2, showing the dominant wind coming from the west.

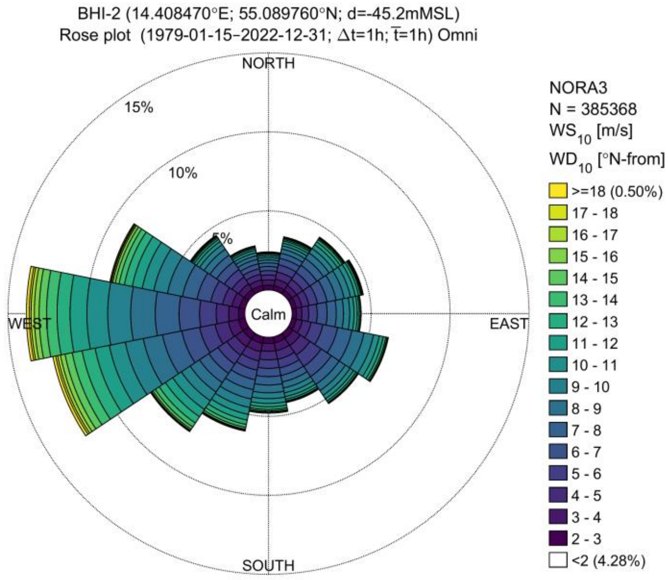

Figure 3.2 Wind rose of WS_{10} and WD_{10} at BHI-2

4 Water Levels

This section presents a summary of the water level data basis established in [1], followed by a presentation of normal and extreme water level conditions.

The water level data was adopted from the hydrodynamic model forced by ERA5, ($HD_{NE,ERA5}$) in [1]. The water level at EIBS consists of a tidal and a non-tidal (residual) component. The two components were separated by harmonic analysis (see Section 4.1.2). The water level dataset is denoted EIBS-HD2D-ERA5. Table 4.1 summarises the metadata of the EIBS-HD2D-ERA5 dataset.

Table 4.1 Metadata of the EIBS-2DHD-ERA5 water level dataset
Time series data is provided to Energinet (.dfs0).

Name	Value
Dataset ID:	EIBS-2DHD-ERA5
Start Date [UTC]:	1979-01-15 00:00:00
End Date [UTC]:	2022-12-31 23:00:00
Time Step [s]:	3600
Cell Size [m]:	~500 (OWF area)

The water level data is relative to mean sea level (MSL).

The water level analyses are presented in bins of 0.1 m. Table 4.2 presents the water level variables of the EIBS-HD-ERA5 dataset, including the bin sizes applied in figures and tables throughout this report.

Table 4.2 Water level variables of the EIBS-2DHD-ERA5 water level dataset

Variable name	Abbrev.	Unit	Bin size
Water Level – Total	WL_{total}	mMSL	0.1
Water Level – Tide	WL_{tide}	mMSL	0.1
Water Level – Residual	$WL_{residual}$	m	0.1

4.1 Normal water level conditions

The normal water level conditions are presented in terms of:

- Time series
- Tidal levels
- Histograms
- Monthly statistics

4.1.1 Timeseries

Figure 4.1 shows a time series of water level at BHI-2 during the 44-year period, for total, tidal, and residual components. The 'de-tiding' of water levels is explained in Section 4.1.2. The highest total and residual water levels are 1.26 mMSL and 1.21 m. The tidal levels are given in Section 4.1.2.

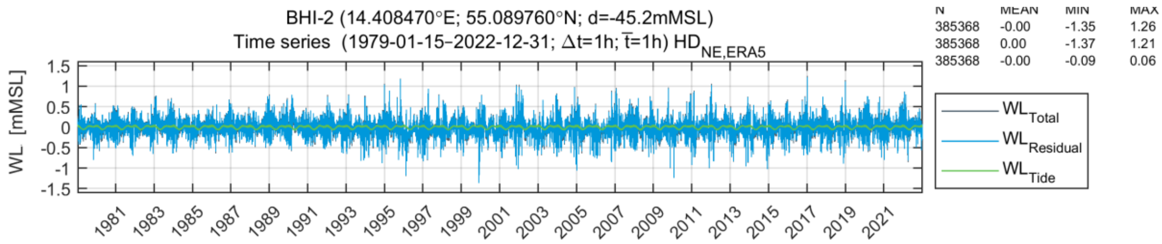

Figure 4.1 Time series of water level at BHI-2

4.1.2 Tidal levels

The tides are weak at EIBS, but to quantify this, astronomical water levels (tidal levels) are provided below. The levels were calculated using harmonic analysis to separate the tidal and non-tidal (residual) components of the total water level time series from the hydrodynamic model (after subtracting the mean of the data).

Figure 4.1 shows the time series of the total, astronomical tidal and residual water level at BHI-2, while Table 4.3 summarises the astronomical water levels. The HAT is +0.06 mMSL and LAT -0.08 mMSL, giving a total tidal range of 0.15 m.

The harmonic analysis was conducted using the U-tide toolbox, [6], which is based on the IOS tidal analysis method by the Institute of Oceanographic Sciences as described in [7], and integrates the approaches defined in [8] and [9]. The residual water level was derived by subtracting the predicted tidal level from the total water level. The astronomical water levels are defined as (https://ntslf.org/tgi/definitions):

- HAT: Maximum predicted tidal WL
- MHWS: Average of the two successive high waters reached during the 24 hours when the tidal range is at its greatest (spring tide)
- MHWN: Average of the two successive high waters reached during the 24 hours when the tidal range is at its lowest (neap tide)
- MLWN: Average of the two successive low waters reached during the24 hours when the tidal range is at its lowest (neap tide)
- MLWS: Average of the two successive low waters reached during the 24 hours when the tidal range is at its greatest (spring tide)
- LAT: Minimum predicted tidal WL

Table 4.3 Tidal levels at BHI-2

Tidal level	Abbreviation	Value	Unit
Highest astronomical tide	HAT	+0.06	mMSL
Mean high water springs	MHWS	+0.02	mMSL
Mean high water neaps	MHWN	+0.00	mMSL
Mean sea level	MSL (z0)	0.00	mMSL
Mean low water neaps	MLWN	-0.01	mMSL
Mean low water springs	MLWS	-0.02	mMSL
Lowest astronomical tide	LAT	-0.08	mMSL

4.1.3 Histogram

Figure 4.2 shows a histogram of total water level at BHI-2.

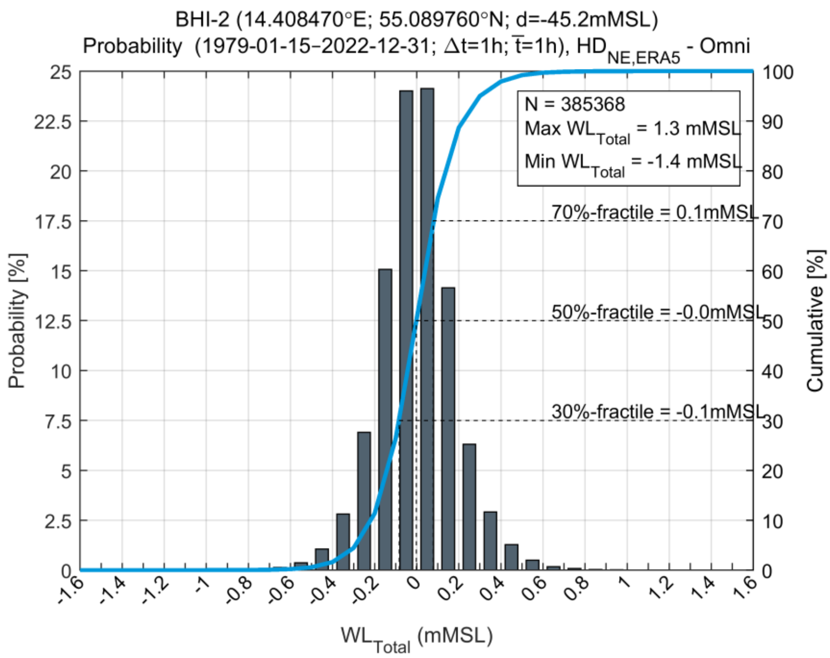

Figure 4.2 Histogram of total water level, WL_{Total}, at BHI-2

4.1.4 Monthly statistics

Figure 4.3 shows monthly statistics of total water level at BHI-2. Variation of the monthly mean water level is small, less than 0.1 m during the year. The highest (+1.3 mMSL) as well as the lowest (-1.4m MSL) water levels occur during winter.

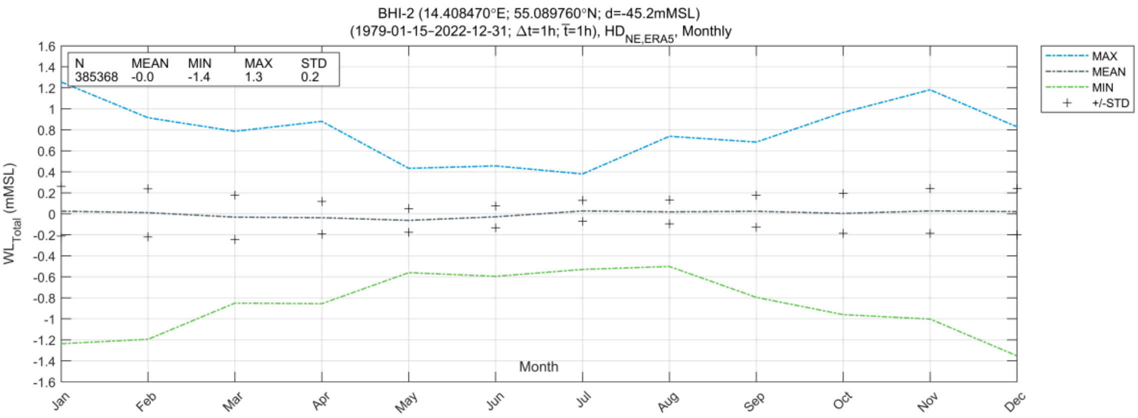

Figure 4.3 Monthly statistics of total water level, WL_{Total}, at BHI-2

4.2 Extreme water level conditions

Extreme water level conditions were established using Traditional Extreme Value Analysis (T-EVA) following the methodology and settings derived and described in Appendix B Sensitivity of T-EVA to Distribution, Threshold, and Fitting.

For high water level, the 2-p Weibull distribution was fitted by the least square method to 176 high peak events separated by at least 36 hours (annual average of 4 events).

For low water level, the 2-p Weibull distribution was fitted by the least square method to 176 high peak events separated by at least 36 hours (annual average of 4 events)

4.2.1 Extreme high-water levels

Table 4.4 and Figure 4.4 present the extreme total high-water level at BHI-2. The fitted distribution aligns very well to the hindcast data points, also at the tail, and all events are within the confidence levels, which gives confidence in the derived values. The 50-year total high-water level is 1.3 ± 0.2 mMSL (the 2.5- and 97.5%-tile confidence levels).

Table 4.4 Extreme total high-water level, $WL_{Total,high}$, at BHI-2

$WL_{Total,high}$ [mMSL]	Return period, T_R [years]			
	1	5	10	50
2.5%-tile	0.7	0.9	1.0	1.1
Central estimate	0.7	1.0	1.0	1.3
97.5%-tile	0.8	1.0	1.1	1.4

As mentioned in [1], the sea level rise in Northern Europe will amount to between 0.0m (5 percentile) and 0.5m (95 percentile) with a median of 0.25m in year 2055, which is assumed to be the end of the lifetime for the EIBS OWFs.

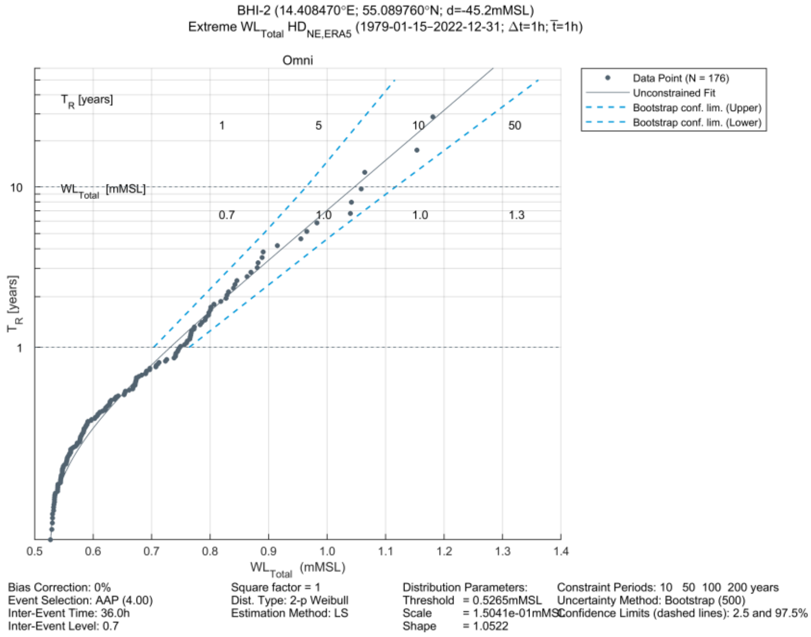

Figure 4.4 Extreme total high-water level, $WL_{Total,high}$, at BHI-2

Table 4.5 Extreme residual high-water level, $WL_{Residual,high}$, at BHI-2

$WL_{Residual,high}$ [mMSL]	Return period, T_R [years]			
	1	5	10	50
2.5%-tile	0.7	0.9	0.9	1.1
Central estimate	0.7	0.9	1.0	1.2
97.5%-tile	0.7	1.0	1.1	1.3

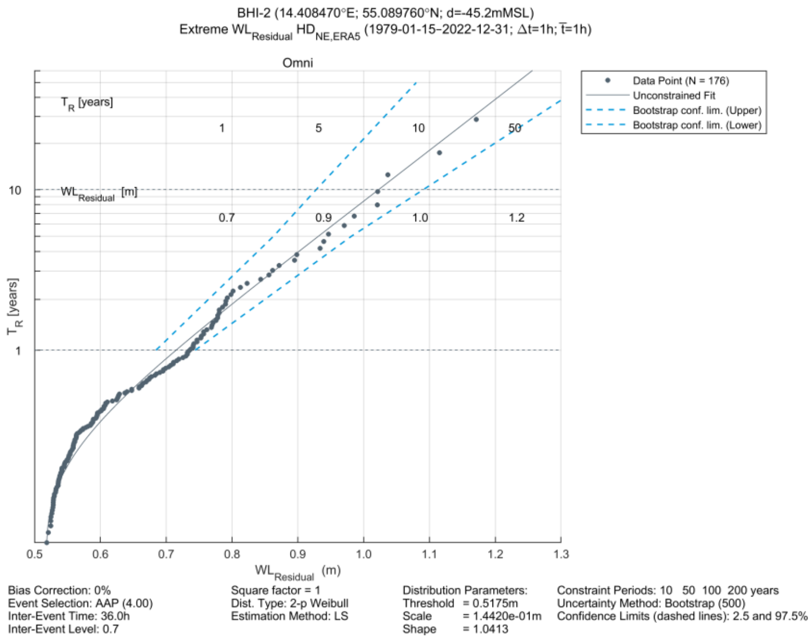

Figure 4.5 **Extreme total residual water level, $WL_{Residual,high}$, at BHI-2**

4.2.2 Extreme low water levels

Table 4.6 and Figure 4.6 present the extreme total low water level at BHI-2. The fitted distribution aligns well to the hindcast data points and within the confidence levels. The 50-year total low water level is -1.3 ± 0.2 mMSL (the 2.5- and 97.5%-tile confidence levels).

Table 4.6 **Extreme total low water level, $WL_{Total,low}$, at BHI-2**

$WL_{Total,low}$ [mMSL]	Return period, T_R [years]			
	1	5	10	50
2.5%-tile	-0.7	-0.9	-1.0	-1.1
Central estimate	-0.7	-1.0	-1.1	-1.3
97.5%-tile	-0.8	-1.0	-1.2	-1.4

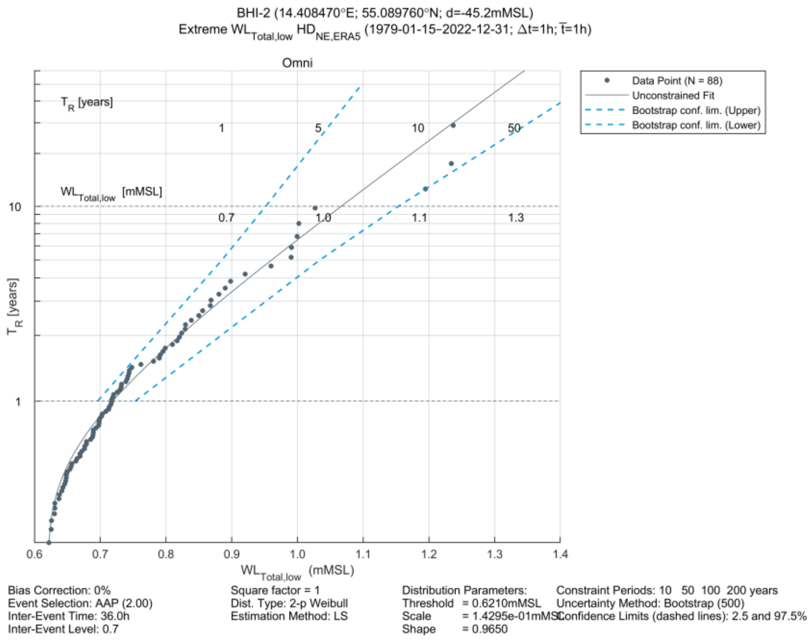

Figure 4.6 Extreme total low water level, $WL_{Total,low}$, at BHI-2

Table 4.7 Extreme total residual low water level, $WL_{Residual,low}$, at BHI-2

$WL_{Residual,low}$ [mMSL]	Return period, T_R [years]			
	1	5	10	50
2.5%-tile	-0.7	-0.9	-1.0	-1.1
Central estimate	-0.7	-1.0	-1.1	-1.3
97.5%-tile	-0.8	-1.0	-1.2	-1.5

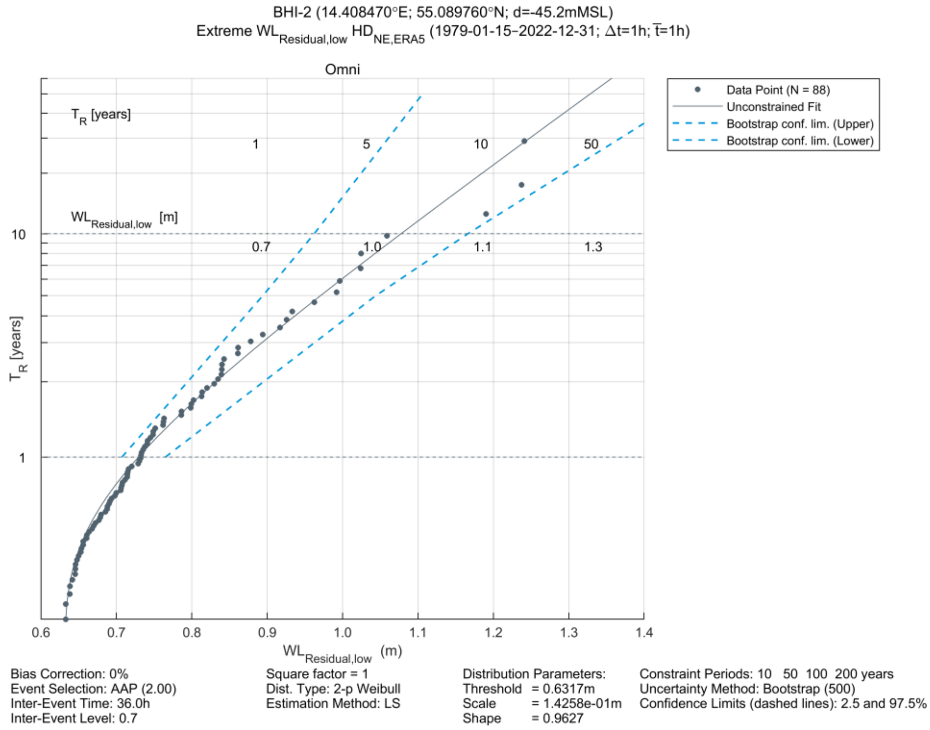

Figure 4.7 Extreme total residual low water level, $WL_{Residual,low}$, at BHI-2

5 Current Conditions

This section presents a summary of the current data basis established in [1], followed by a presentation of normal and extreme current conditions at the selected six analysis points of EIBS.

The generated current data set, denoted EIBS-3DHD contains current speed and direction, temperature, and salinity for all layers in the model. Table 5.1 summarises the metadata for the EIBS-3DHD dataset. Note that current presented here are not scaled but represent the modelled values.

Table 5.1 Metadata of the EIBS-3DHD current dataset
Time series data is provided to Energinet (.dfs0).

Name	Value
Dataset ID:	EIBS-3DHD
Start Date [UTC]:	1998-01-01 00:00:00
End Date [UTC]:	2022-12-31 23:00:00
Time Step [s]:	3600
Cell Size [m]:	~600-1000 (OWF area)

The current analyses are presented in speed bins of 0.05 m/s and directional bins of 22.5°. Table 5.2 presents the variables of the EIBS-3DHD dataset, including the bin sizes applied in figures and tables throughout this report.

Table 5.2 Current variables of the EIBS-3DHD dataset
U-velocity, V-velocity, current speed, and current direction were provided for all layers used in the model (20 σ-layers to -20 m, 2m z-levels below) in .dfsu format. The analyses were performed for the current speed and current direction.

Variable name	Abbrev.	Unit
U-velocity (all layers)	U	m/s
V-velocity (all layers)	V	m/s
Current speed (all layers)	CS	m/s
Current direction (all layers)	CD	°N-to

The current analyses cover the data period 1998-01-01 – 2022-12-31 (25 years).

The main body of this report presents results at BHI-2, while results at all six analysis points are given in the data reports (listed in Table A.1) which are attached to this report. The data reports contain all (scatter) tables and figures presented below.

5.1 Normal current conditions

The normal current conditions are presented in terms of:

- Normal current profiles
- Time series
- Current roses
- Histograms
- Monthly statistics
- Directional statistics
- Maps of mean current speed

5.1.1 Time series

Figure 5.1 shows a time series of current speed at BHI-2 during the 25 years hindcast period, for total, tidal, and residual at three level (near-surface, mid-depth, and near-seabed). The ‘de-tiding’ of current speed follows the method given in Section 4.1.2 for water level. The highest total and residual current speeds are approximately 1.11 m/s, indicating a small tidal current magnitude (maximum of 6 cm/s)

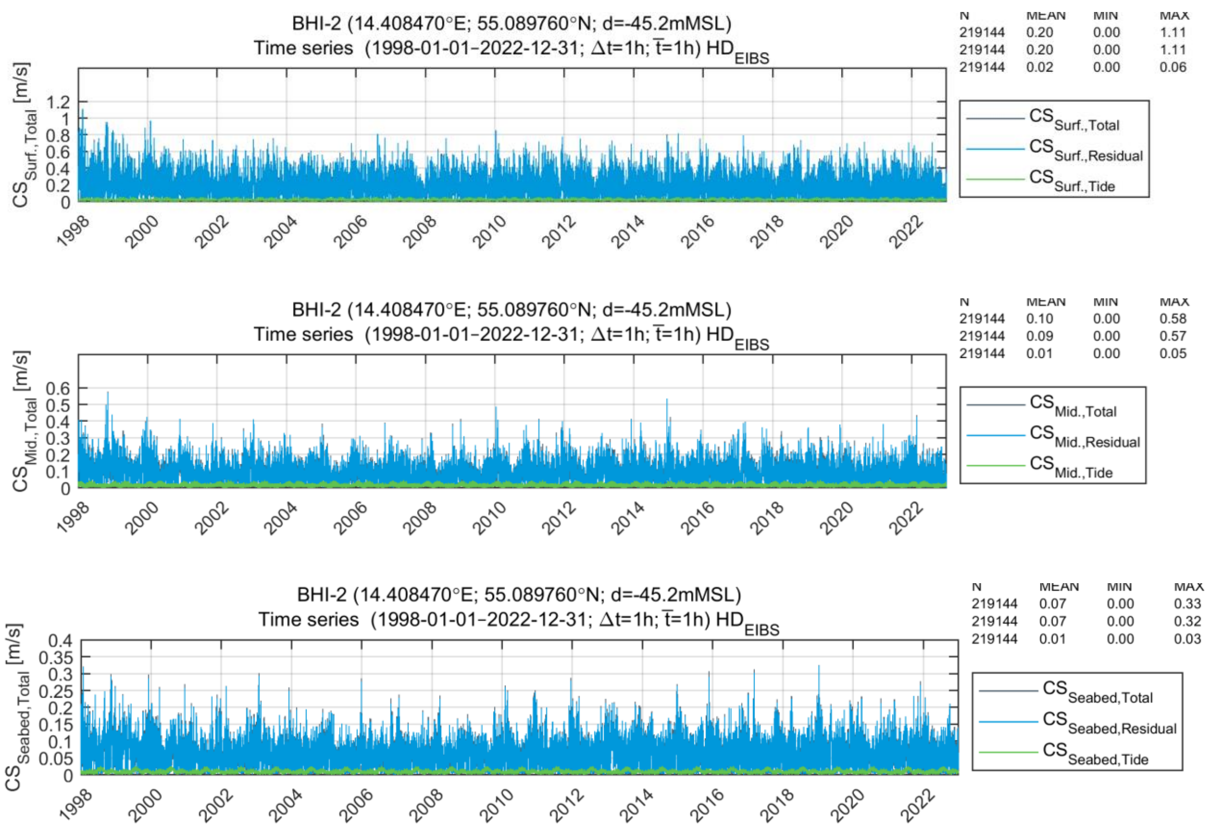

Figure 5.1 Time series of near-surface, mid-depth, and near-seabed current speeds at BHI-2

5.1.2 Current roses

Figure 5.2 to Figure 5.10 show roses of current speed at near-surface, mid-depth, and near-seabed at BHI-2. The near-surface current shows currents predominantly towards east-northeast. At near-seabed, the currents predominantly more towards north-northeast. Figure 5.11 to Figure 5.19 show the scatter plots of current speed against current direction.

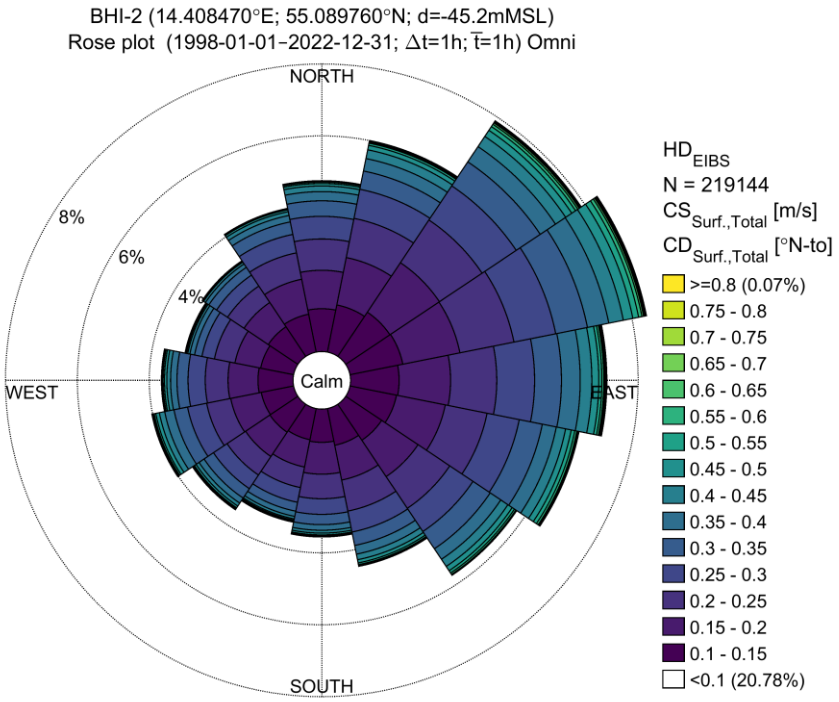

Figure 5.2 Near-surface total current rose at BHI-2

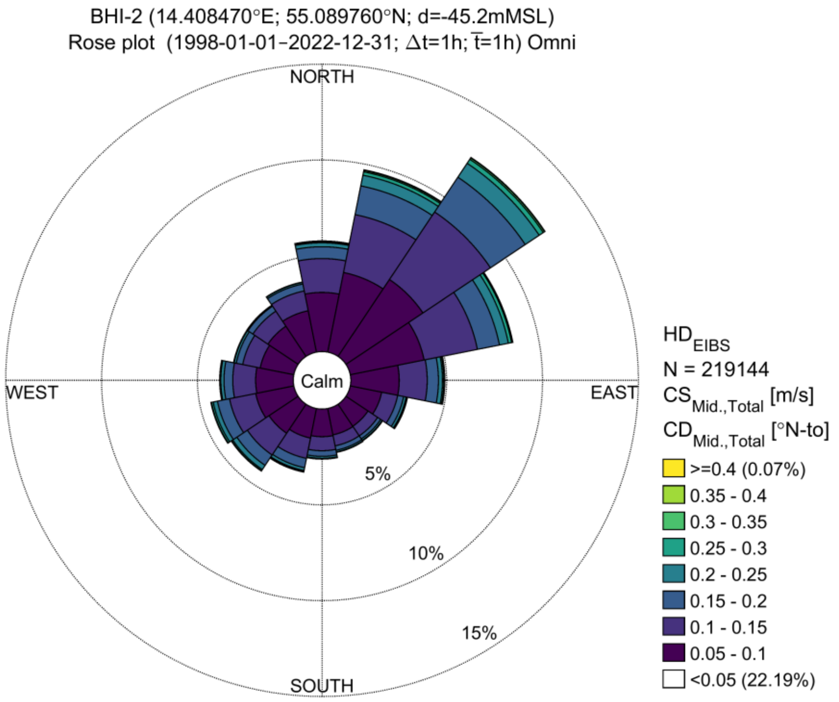

Figure 5.3 Mid-depth total current rose at BHI-2

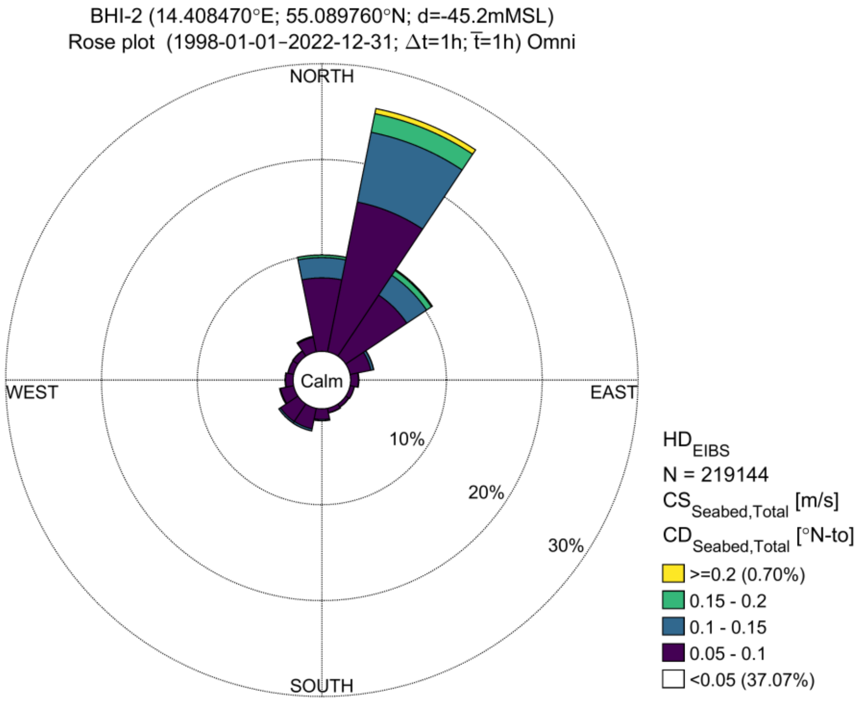

Figure 5.4 Near-seabed total current rose at BHI-2

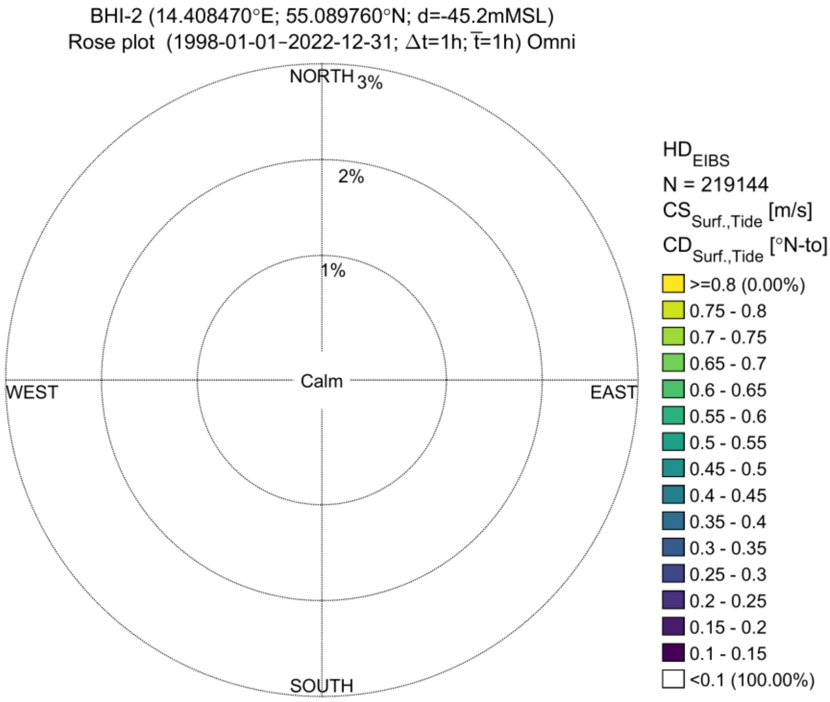

Figure 5.5 Near-surface tidal current rose at BHI-2

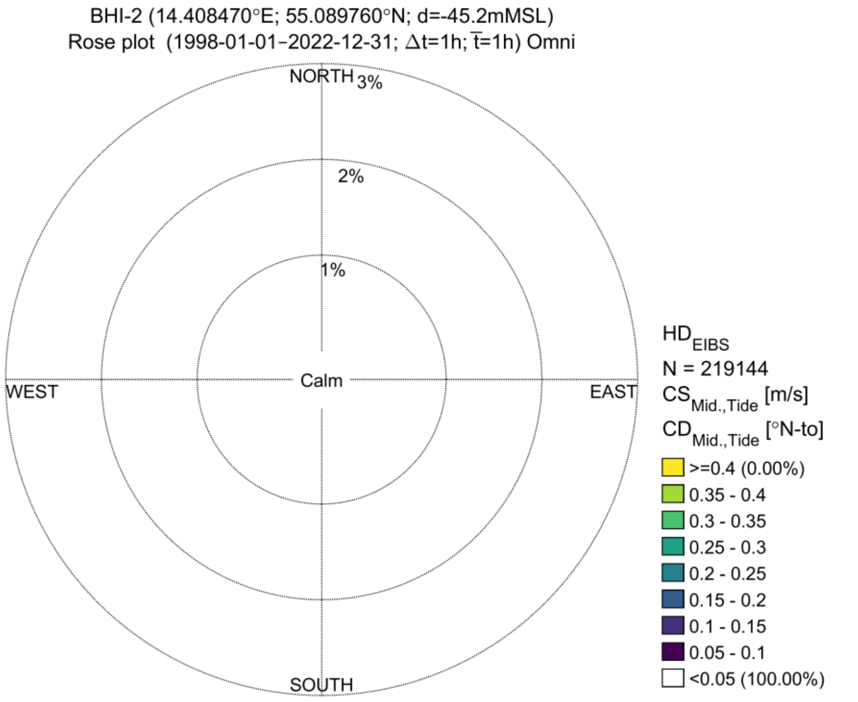

Figure 5.6 Mid-depth tidal current rose at BHI-2

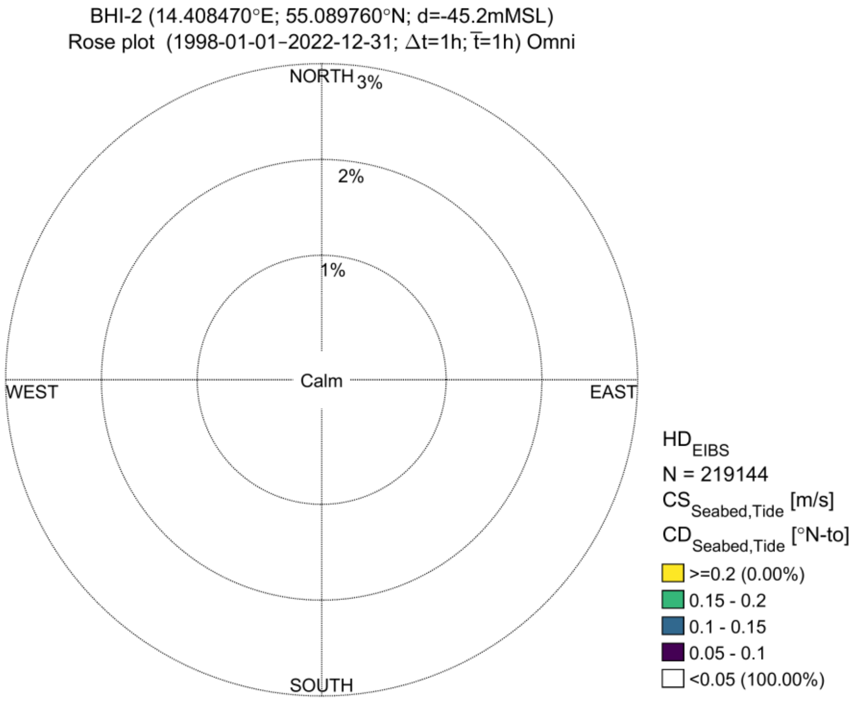

Figure 5.7 Near-seabed tidal current rose at BHI-2

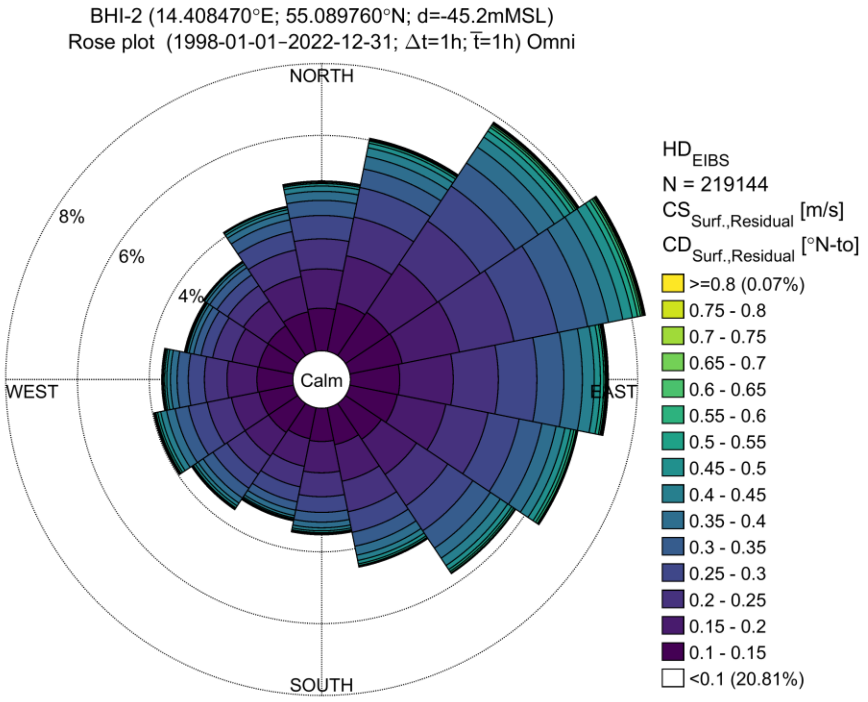

Figure 5.8 Near-surface residual current rose at BHI-2

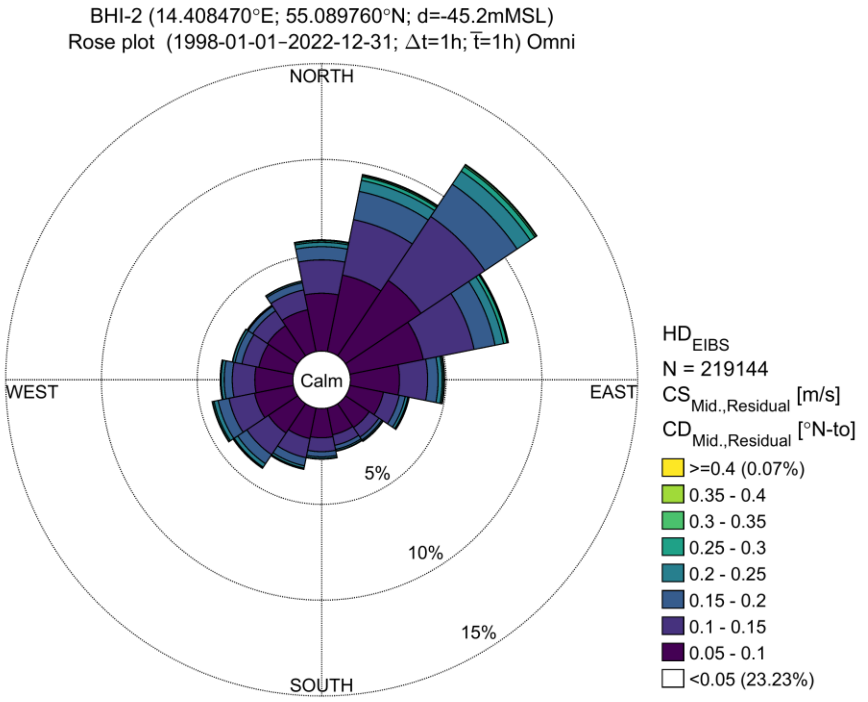

Figure 5.9 Mid-depth residual current rose at BHI-2

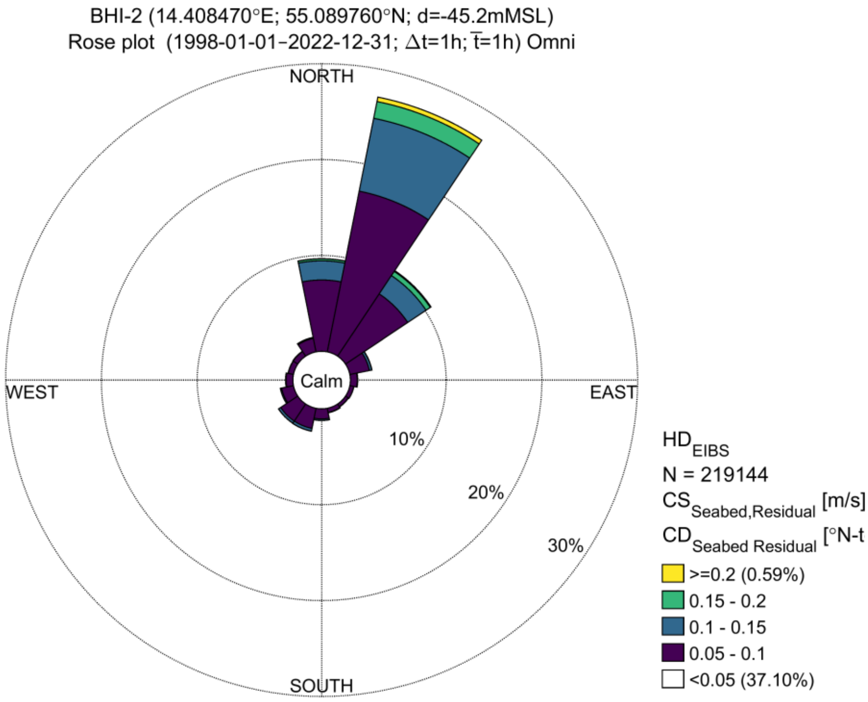

Figure 5.10 Near-seabed residual current rose at BHI-2

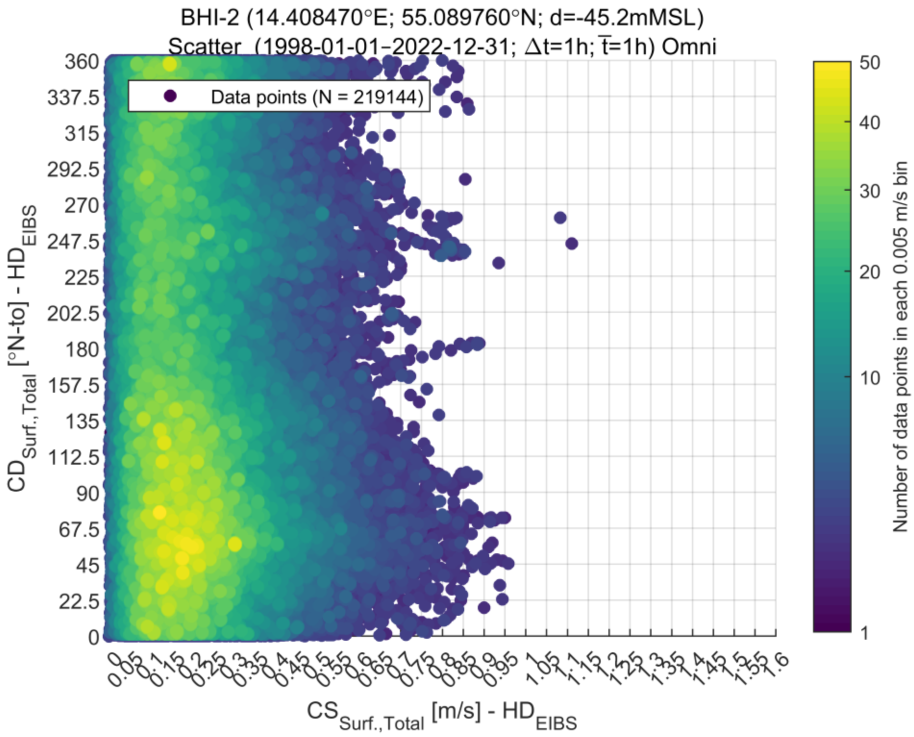

Figure 5.11 Scatter plot of near-surface total current at BHI-2

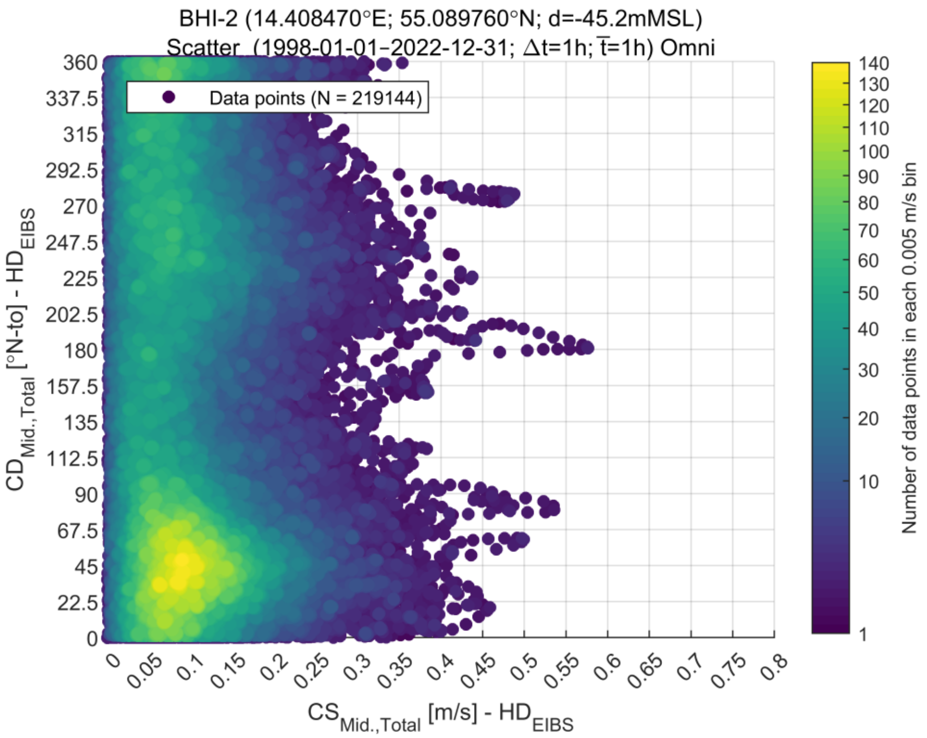

Figure 5.12 Scatter plot of mid-depth total current at BHI-2

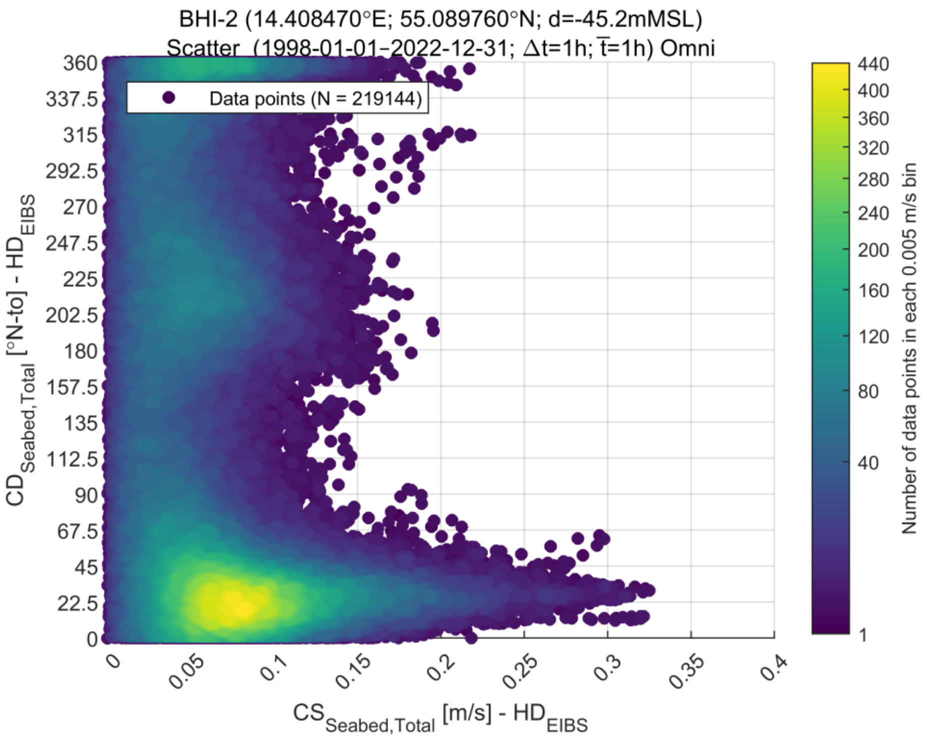

Figure 5.13 Scatter plot of near-seabed total current at BHI-2

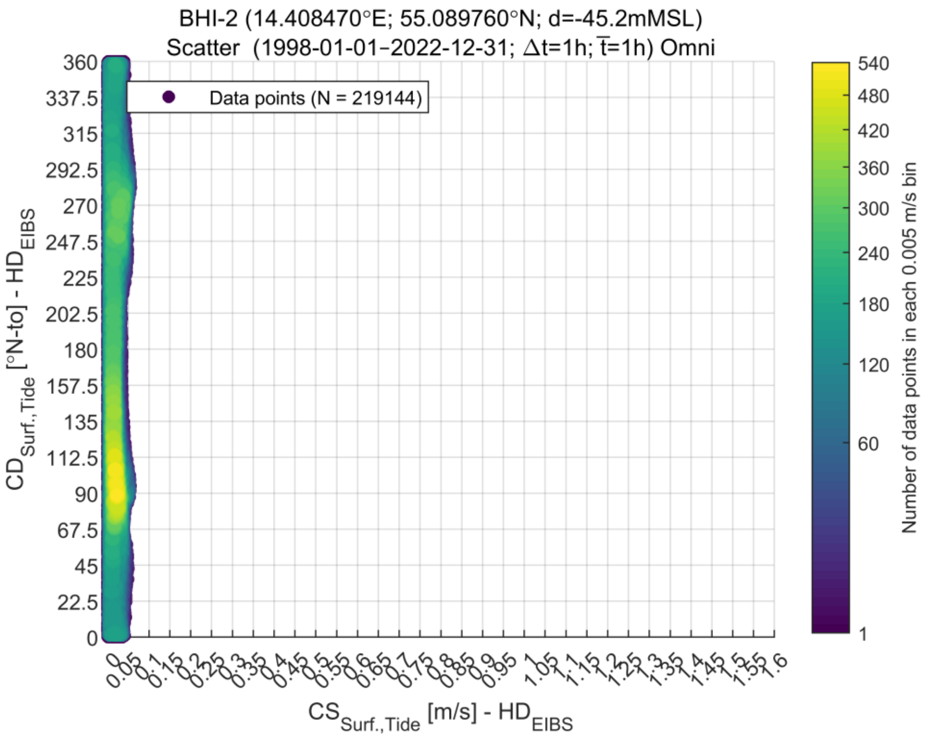

Figure 5.14 Scatter plot of near-surface tidal current at BHI-2

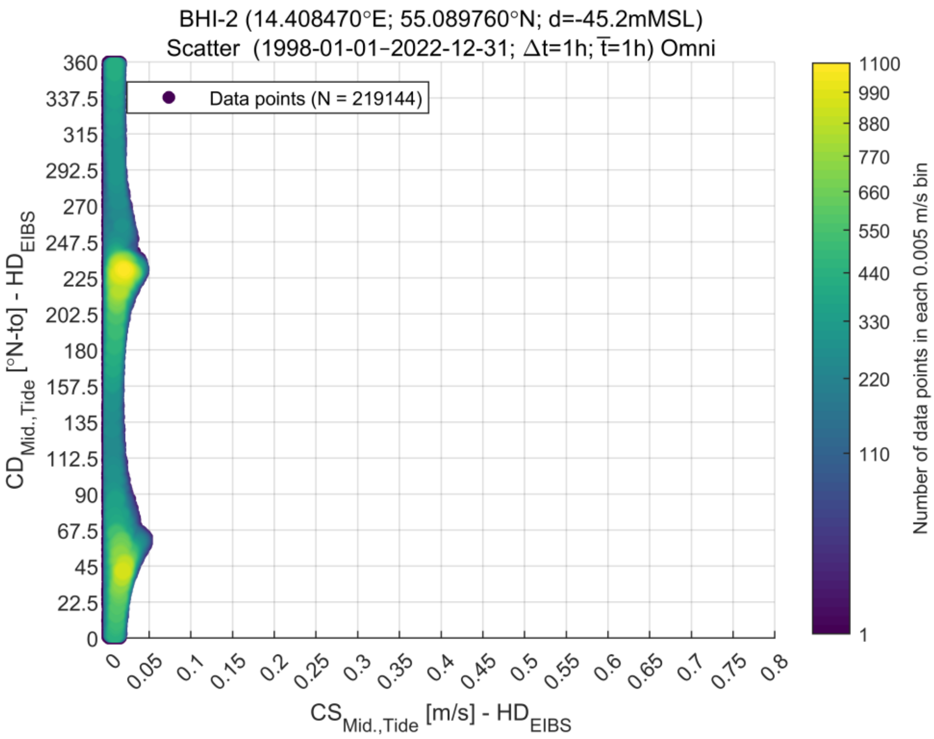

Figure 5.15 Scatter plot of mid-depth tidal current at BHI-2

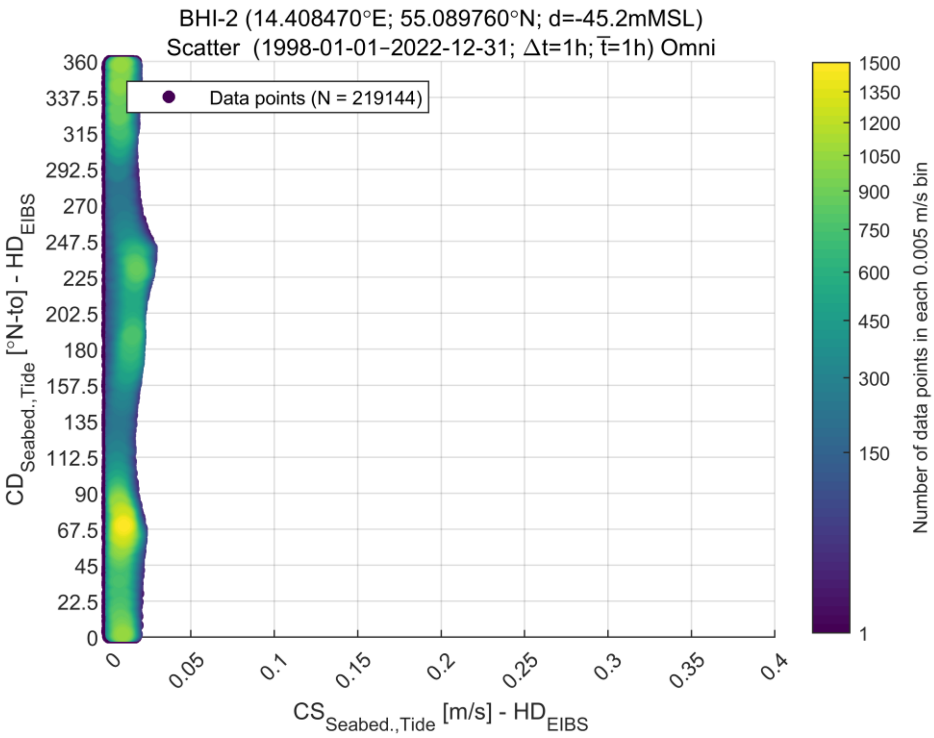

Figure 5.16 Scatter plot of near-seabed tidal current at BHI-2

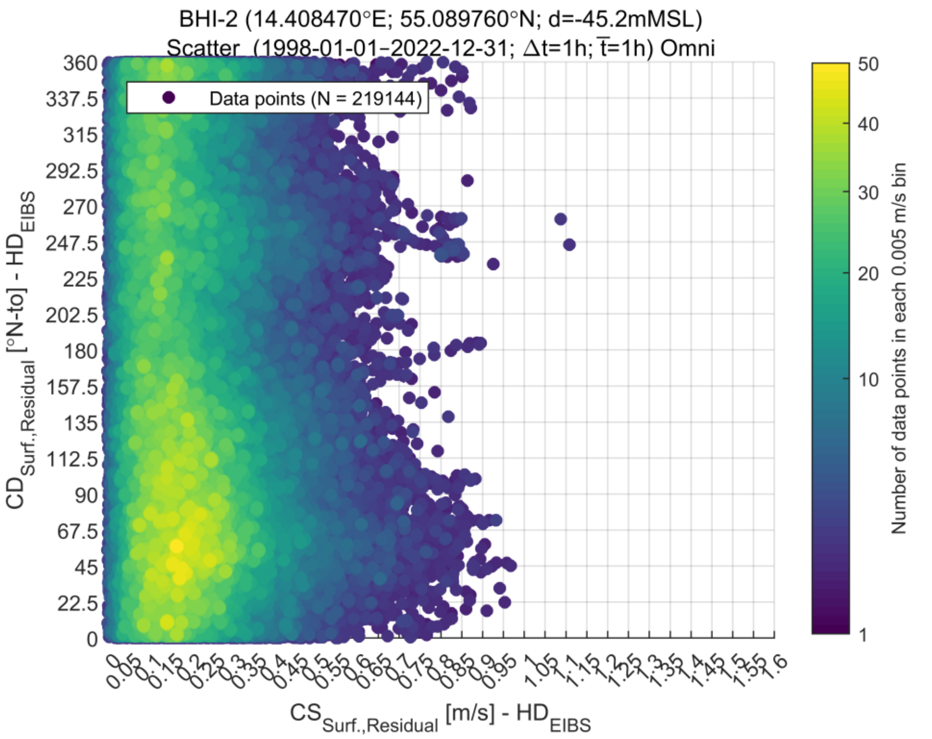

Figure 5.17 Scatter plot of near-surface residual current at BHI-2

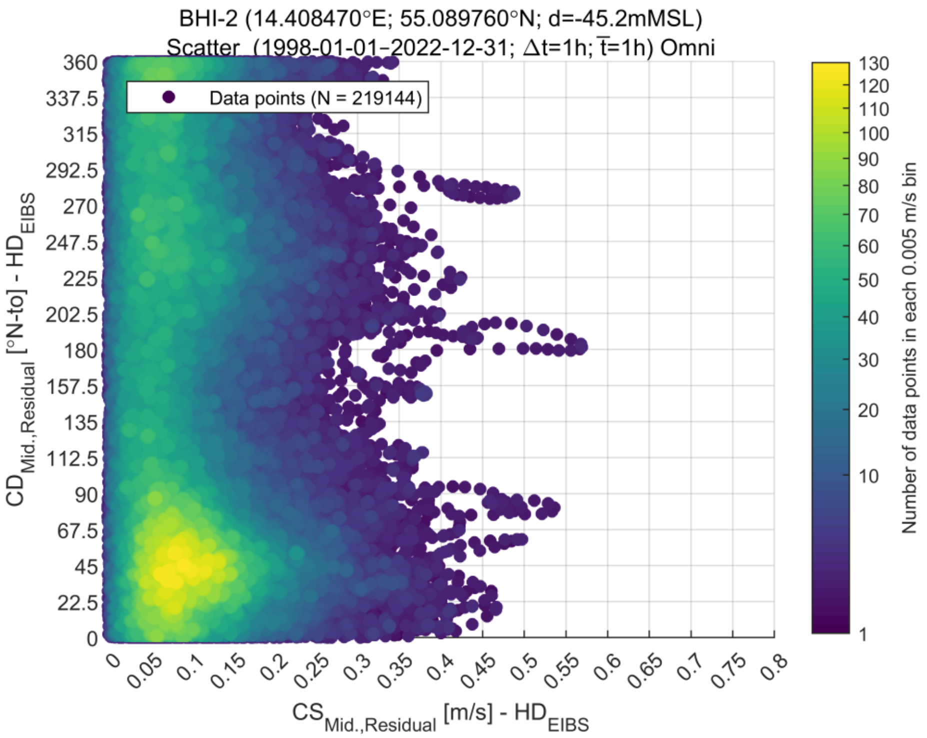

Figure 5.18 Scatter plot of mid-depth residual current at BHI-2

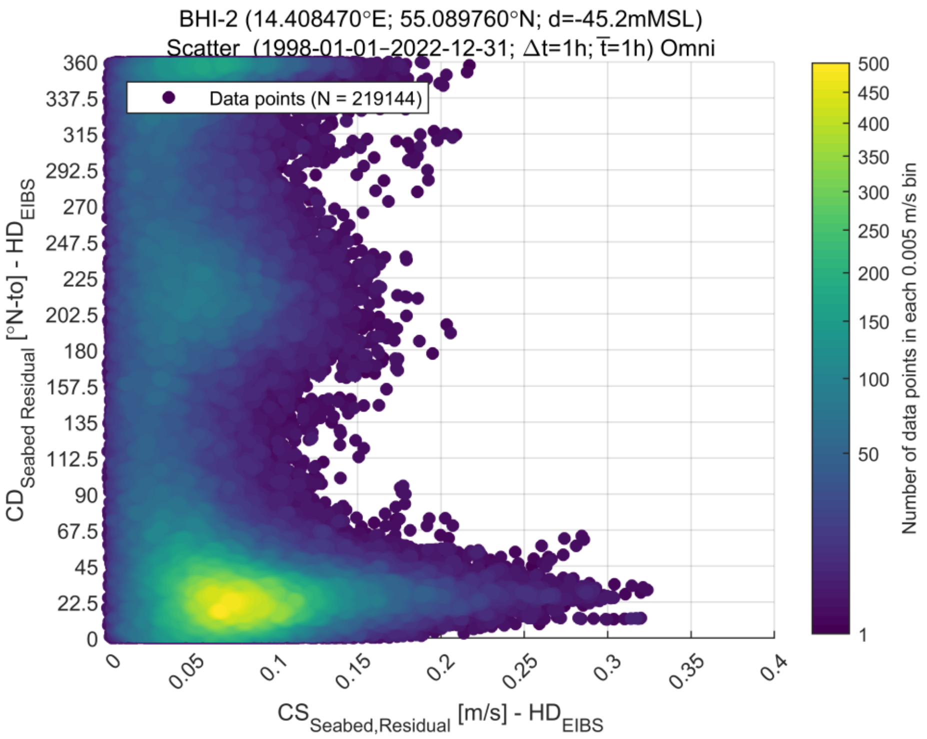

Figure 5.19 Scatter plot of near-seabed residual current at BHI-2

5.1.3 Histograms

Figure 5.20, Figure 5.21, and Figure 5.22 show histograms of current speeds at BHI-2, at near-surface, mid-depth, and near-seabed, respectively.

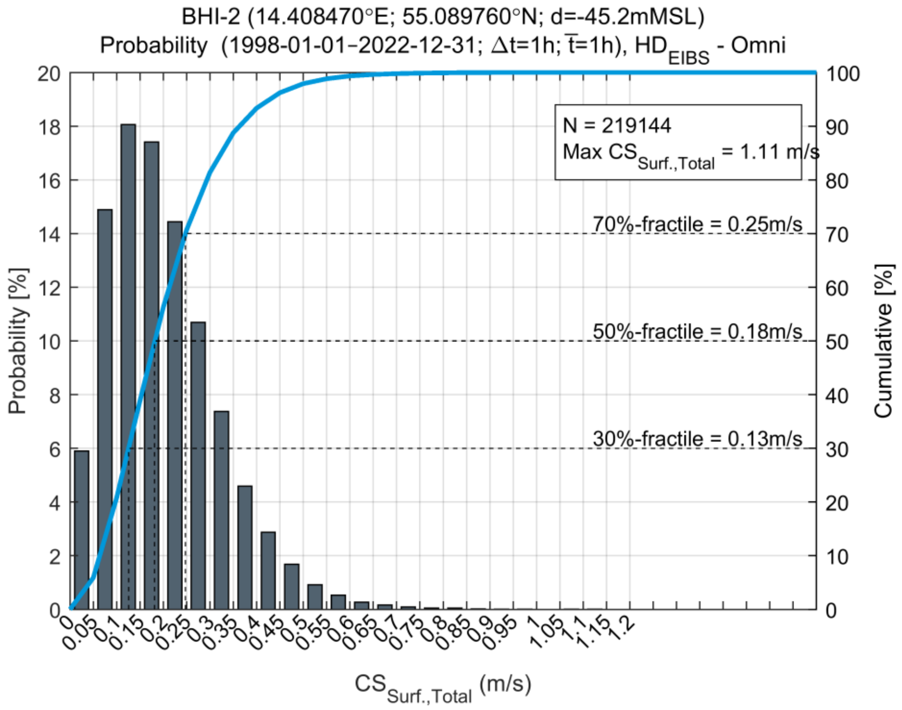

Figure 5.20 Histogram of near-surface current speed at BHI-2

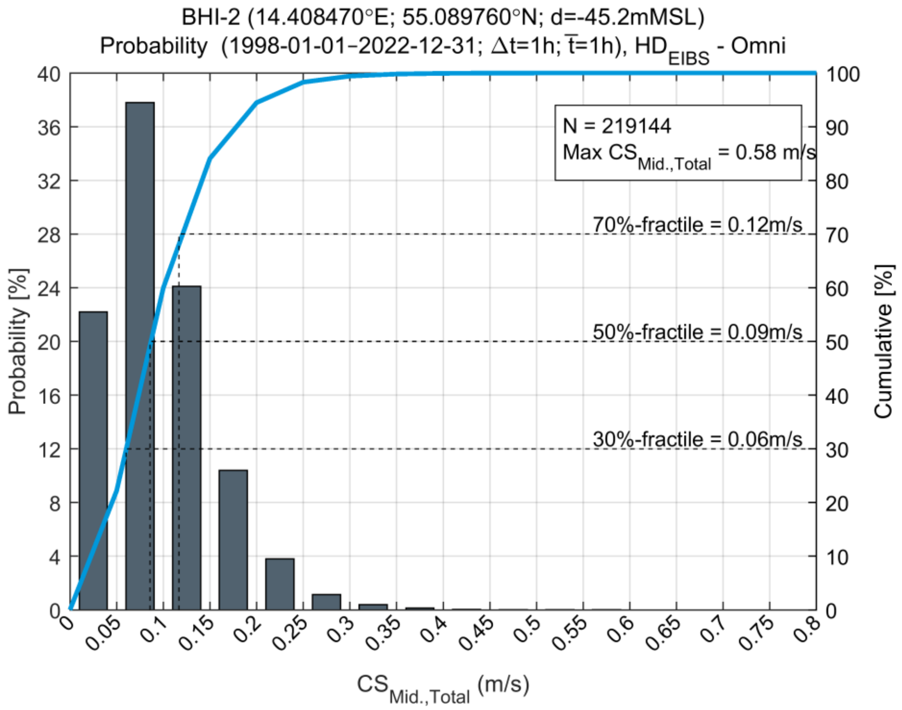

Figure 5.21 Histogram of mid-depth current speed at BHI-2

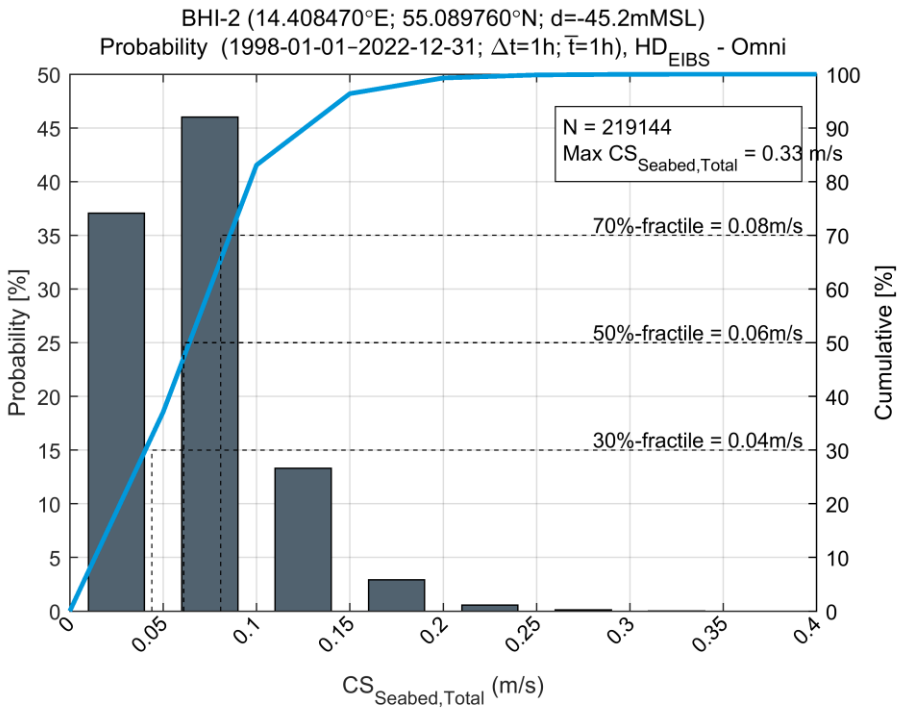

Figure 5.22 Histogram of near-seabed current speed at BHI-2

5.1.4 Monthly statistics

Figure 5.23 shows monthly statistics of current speeds at BHI-2. The mean current speed at near-surface, mid-depth and near-seabed are 0.2, 0.1, and 0.07 m/s, respectively. The strongest current speeds at near-surface (up to 1.11 m/s) occur during autumn - winter (October to February).

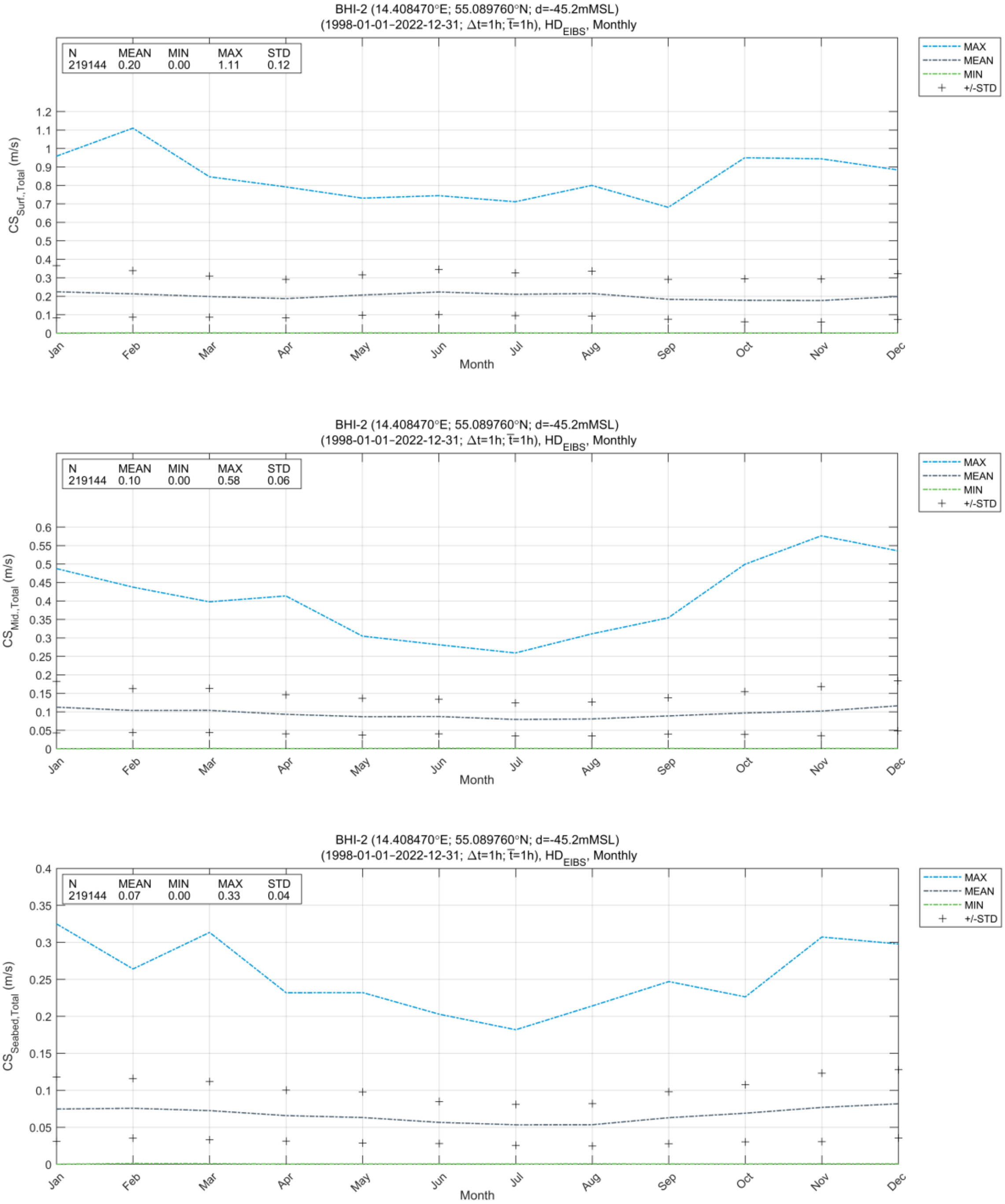

Figure 5.23 Monthly statistics of near-surface, mid-depth, and near-seabed current speed at BHI-2

5.1.5 Directional statistics

Figure 5.24 shows directional statistics of current speeds at BHI-2. The mean current speed at near-surface is strongest towards the east-northeast (67.5°N) of about 0.21 m/s. At near-seabed, the strongest mean current speed is about 0.07 m/s toward north-northeast.

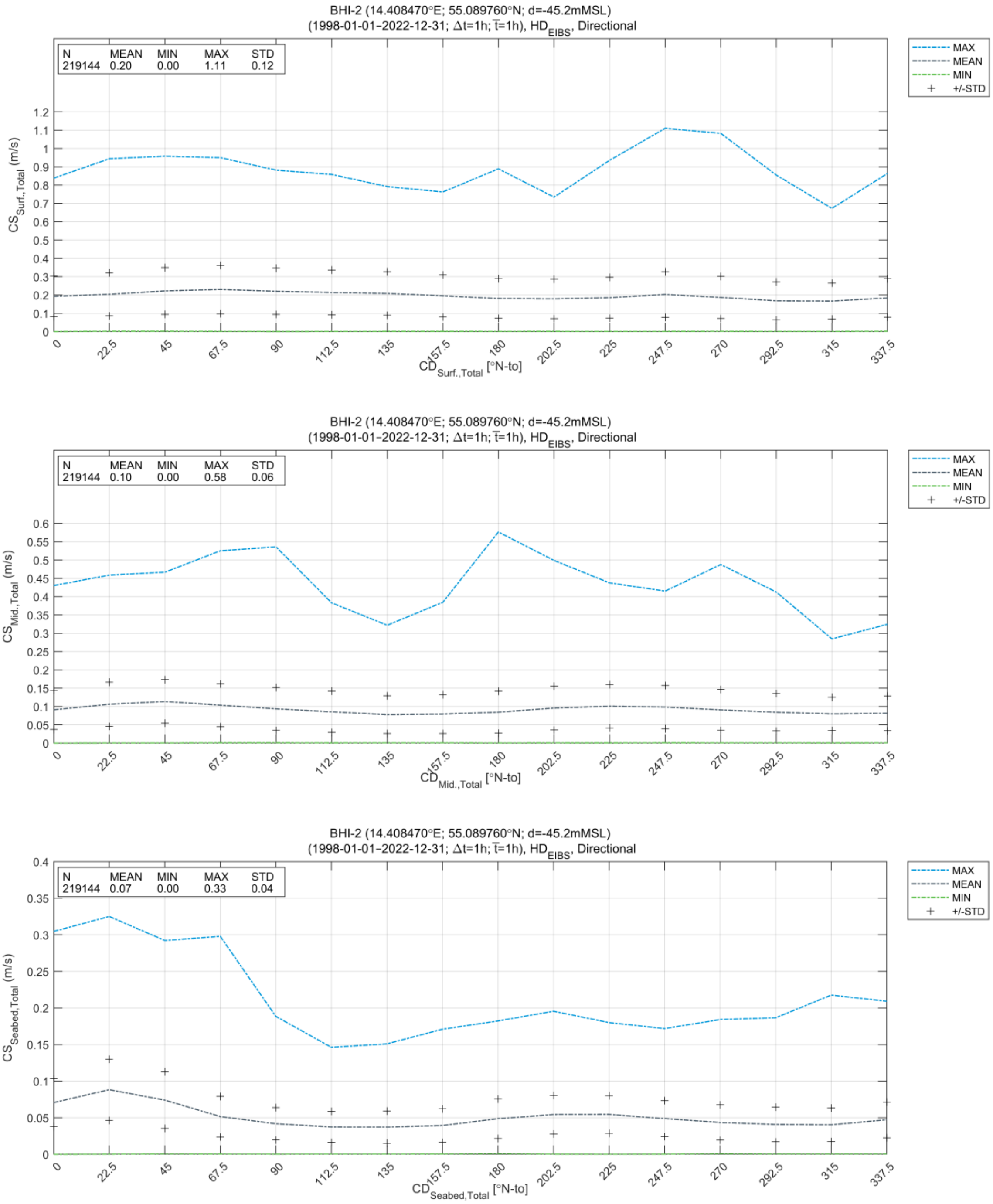

Figure 5.24 Directional statistics of near-surface, mid-depth, near-seabed current speed at BHI-2

5.1.6 Maps of mean current speed

Figure 5.25, Figure 5.26, and Figure 5.27 present the spatial variation across the EIBS OWFs area of the mean total near-surface, mid-depth, and near-seabed current speed, respectively. Mean values of CS_{tot} from the hindcast data at each mesh element are calculated and the variation is presented as contours.

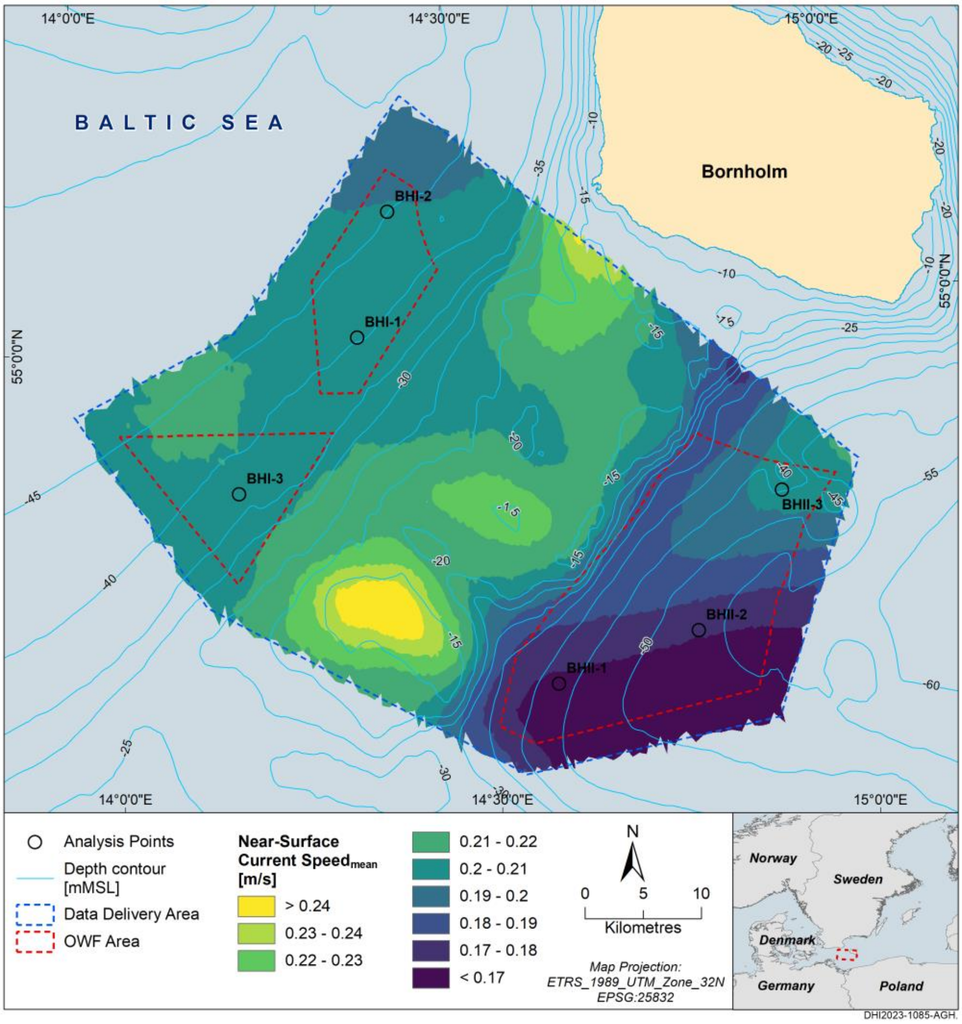

Figure 5.25 Spatial variation across EIBS OWF area of the mean total near-surface current speed

The colour map shows the current speed, and the contours show the water depth.

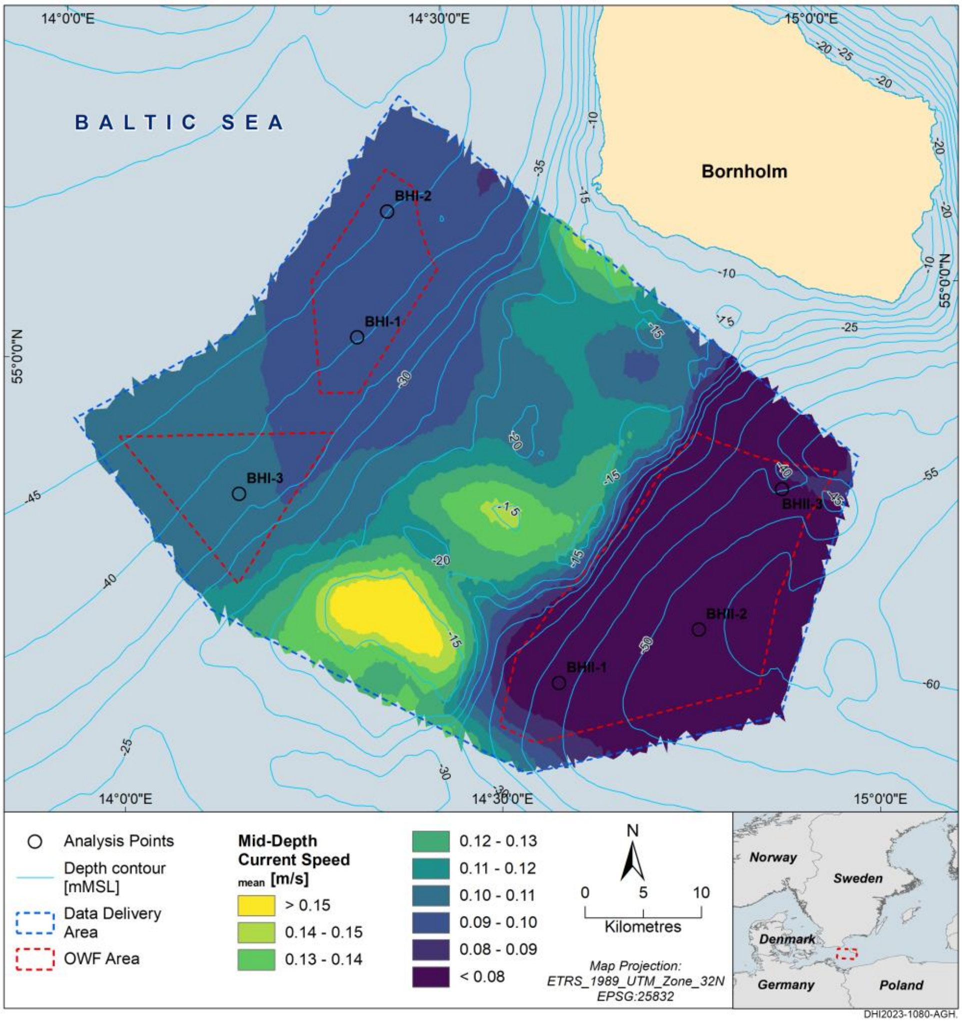

Figure 5.26 Spatial variation across EIBS OWF area of the mean total mid-depth current speed

The colour map shows the current speed, and the contours show the water depth.

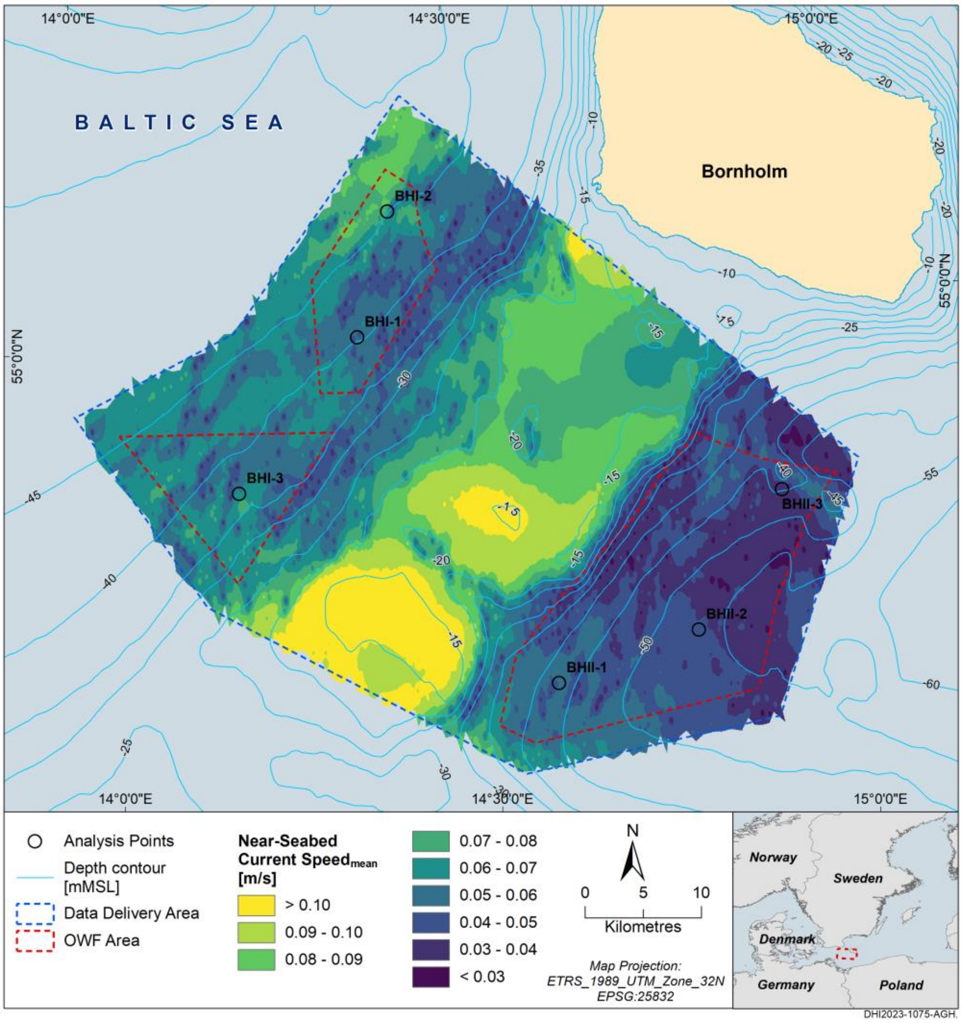

Figure 5.27 Spatial variation across EIBS OWF area of the mean total near-seabed current speed

The colour map shows the current speed, and the contours show the water depth.

5.1.7 Vertical profiles of current speed, temperature, and salinity

Figure 5.28 presents the seasonal variation of vertical profile of current speed, temperature, and salinity. The seasonal vertical variations in current speed and salinity are relatively small. In summer, the seasonal thermocline can occur at around a depth of -20 meters. Figure 5.29 to Figure 5.31 show seasonal current plots at different depth layers. The current direction at mid-depth and near-seabed is relatively consistent throughout the season.

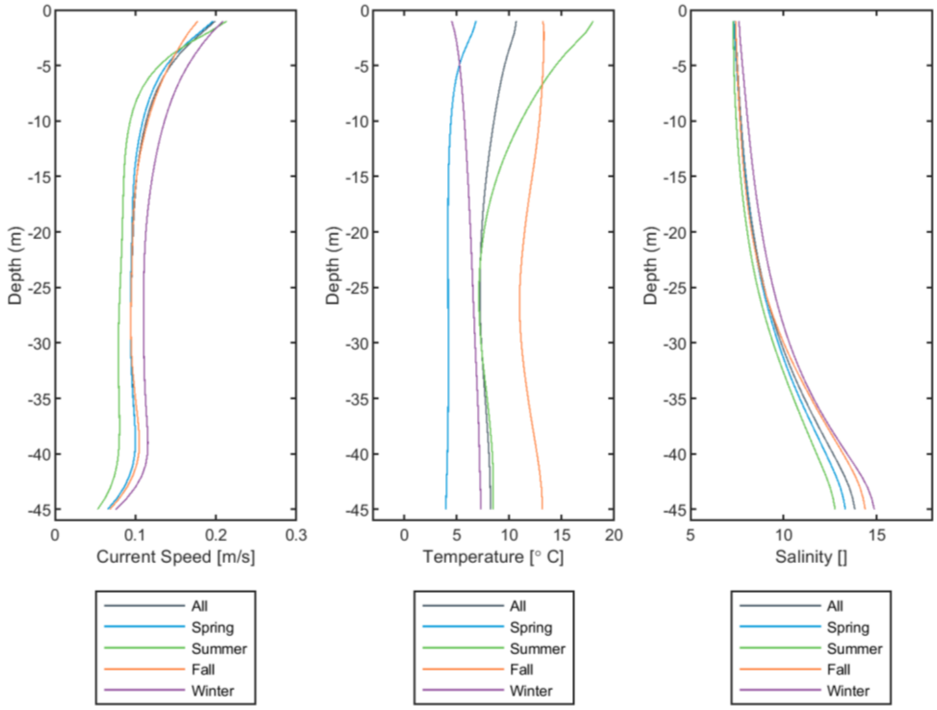

Figure 5.28 Seasonal mean vertical profile of total current speed, temperature, and salinity at BHI-2

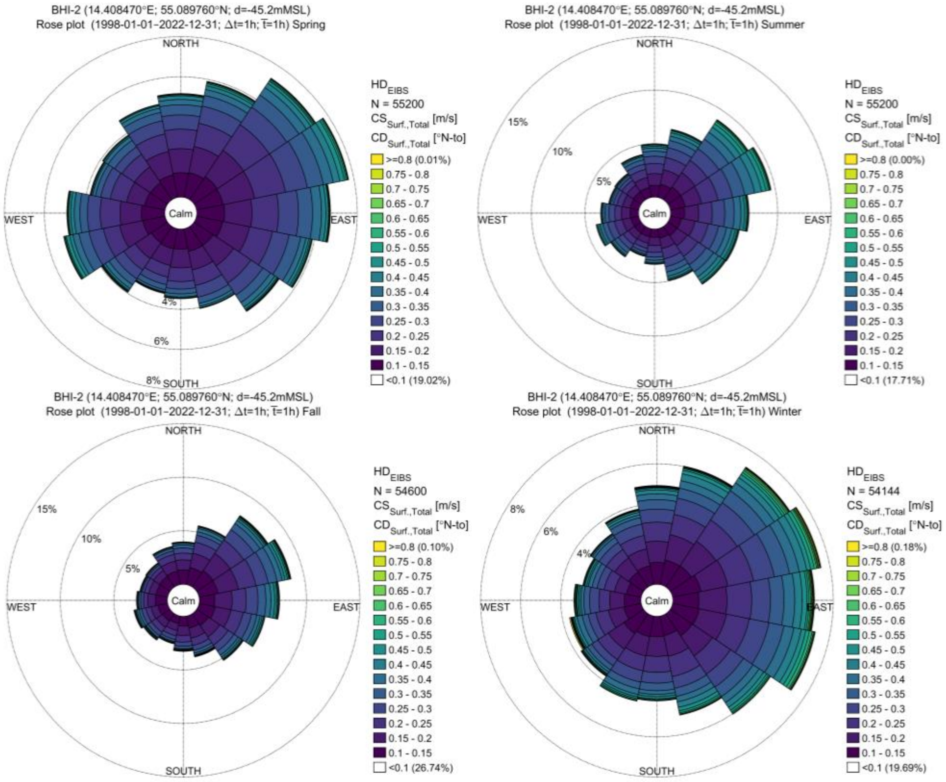

Figure 5.29 Seasonal near-surface current rose plots at BHI-2

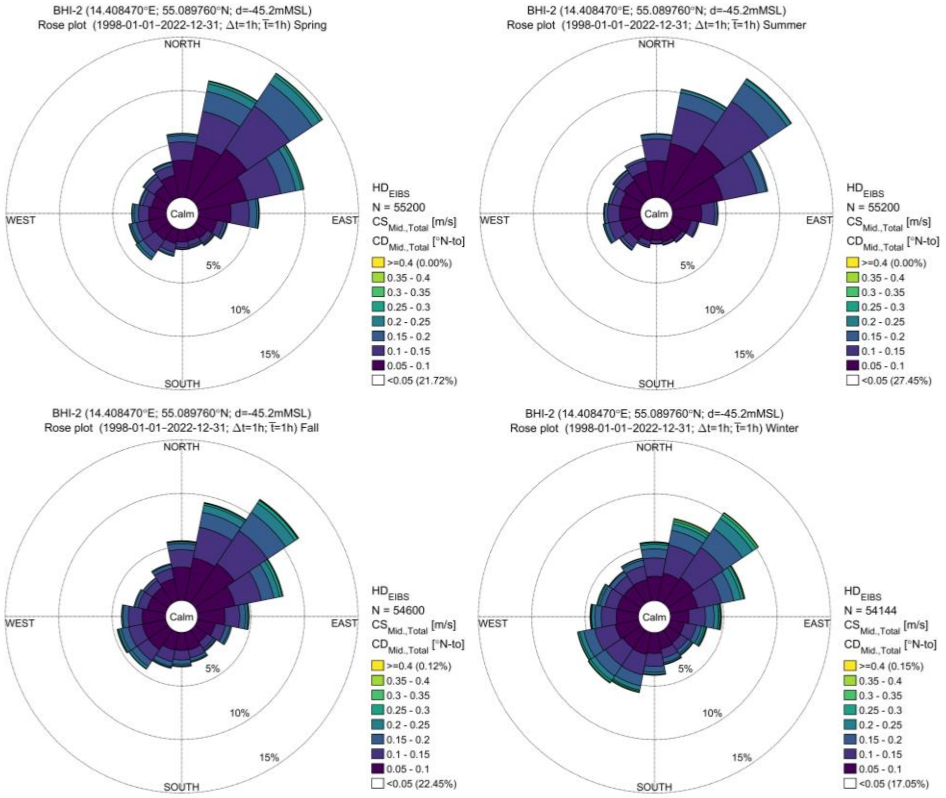

Figure 5.30 Seasonal mid-depth current rose plots at BHI-2

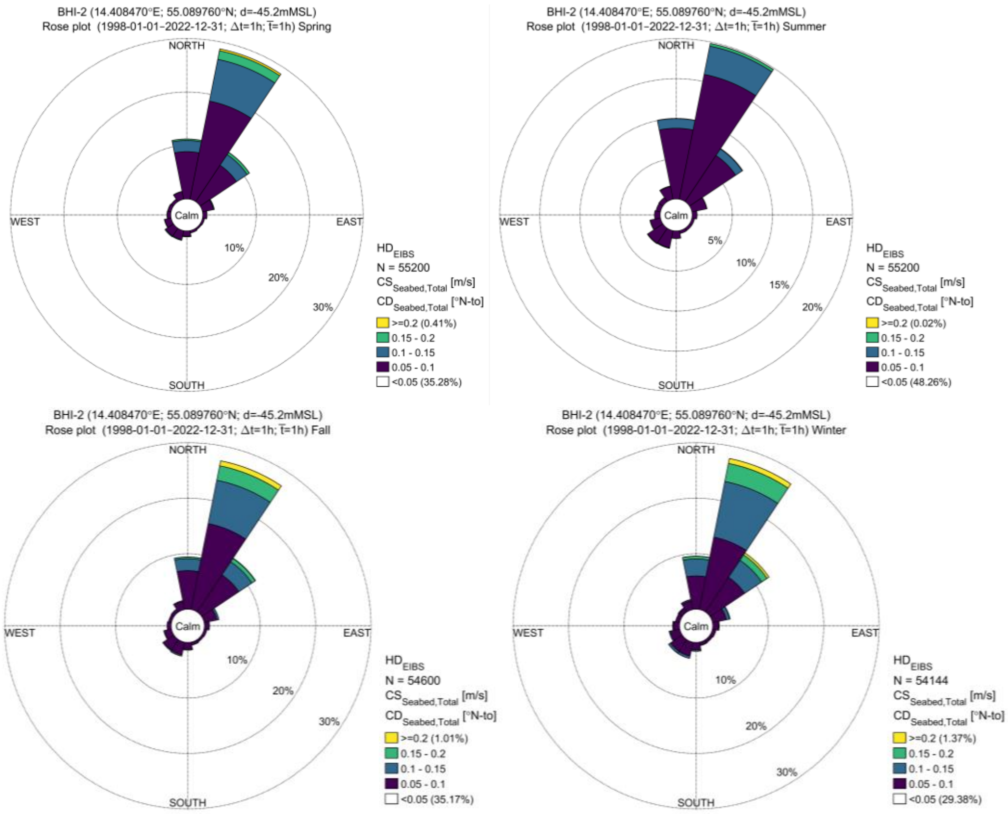

Figure 5.31 Seasonal near-seabed current rose plots at BHI-2

5.2 Extreme current conditions

Extreme current conditions were established using Traditional Extreme Value Analysis (T-EVA) following the methodology and settings derived and described in Appendix B Sensitivity of T-EVA to Distribution, Threshold, and Fitting.

For current speed, the 2-p Weibull distribution was fitted by the least square method to 75 peak events separated by at least 36 hours (annual average of 3 events).

5.2.1 Extreme total current speed

Table 5.3 and Figure 5.32 depict the directional extreme total near-surface current speed at BHI-2. Table 5.4 and Figure 5.33 illustrate the directional extreme total mid-depth current speed at BHI-2. Table 5.5 and Figure 5.34 present the directional extreme total near-seabed current speed at BHI-2.

The fitted distribution aligns very well to the hindcast data points, also at the tail, and all events are within the confidence levels. The 50-year total near-surface current speed is 1.1 ± 0.1 m/s (the 2.5- and 97.5%-tile confidence levels). The 50-year total mid-depth current speed is 0.6 ± 0.1 m/s (the 2.5- and 97.5%-tile confidence levels). The 50-year total near-seabed current speed is 0.35 ± 0.1 m/s (the 2.5- and 97.5%-tile confidence levels). The highest 50-year current speeds at the near-surface, mid-depth, and near-seabed are in the directions of 67.5°, 45°, and 22.5°, respectively.

Table 5.3 Extreme near-surface current speed, $CS_{surf.,tot}$, at BHI-2

Direction	$CS_{surf., Total}$ [m/s]			
	T_R 1 year	T_R 5 years	T_R 10 years	T_R 50 years
0°	0.70	0.82	0.87	0.99
22.5°	0.78	0.90	0.95	1.07
45°	0.78	0.91	0.97	1.09
67.5°	0.78	0.91	0.97	1.09
90°	0.78	0.91	0.96	1.06
112.5°	0.77	0.87	0.90	0.99
135°	0.72	0.79	0.82	0.89
157.5°	0.68	0.78	0.82	0.91
180°	0.68	0.80	0.85	0.97
202.5°	0.65	0.74	0.77	0.84
225°	0.69	0.81	0.87	0.99
247.5°	0.73	0.88	0.94	1.09
270°	0.73	0.88	0.95	1.09
292.5°	0.66	0.79	0.84	0.97
315°	0.60	0.69	0.72	0.80
337.5°	0.64	0.76	0.81	0.93
Omni	0.78	0.91	0.97	1.09

Table 5.4 Extreme mid-depth current speed, $CS_{mid.,tot}$, at BHI-2

Direction	$CS_{mid.,Total}$ [m/s]			
	T_R 1 year	T_R 5 years	T_R 10 years	T_R 50 years
0°	0.36	0.44	0.47	0.55
22.5°	0.38	0.46	0.49	0.55
45°	0.38	0.46	0.48	0.54
67.5°	0.38	0.46	0.49	0.57
90°	0.38	0.46	0.49	0.57
112.5°	0.34	0.41	0.44	0.51
135°	0.30	0.35	0.37	0.42
157.5°	0.31	0.37	0.40	0.46
180°	0.34	0.44	0.48	0.57
202.5°	0.37	0.46	0.49	0.57
225°	0.36	0.43	0.46	0.53
247.5°	0.36	0.42	0.45	0.50
270°	0.35	0.43	0.46	0.55
292.5°	0.31	0.37	0.40	0.45
315°	0.27	0.30	0.31	0.34
337.5°	0.29	0.34	0.36	0.42
Omni	0.38	0.46	0.49	0.57

Table 5.5 Extreme near-seabed current speed $CS_{seabed,tot}$, at BHI-2

Direction	$CS_{seabed.,Total}$ [m/s]			
	T_R 1 year	T_R 5 years	T_R 10 years	T_R 50 years
0°	0.24	0.27	0.29	0.33
22.5°	0.25	0.29	0.31	0.35
45°	0.25	0.29	0.31	0.35
67.5°	0.21	0.26	0.28	0.33
90°	0.14	0.17	0.19	0.22
112.5°	0.13	0.15	0.16	0.18
135°	0.14	0.16	0.18	0.20
157.5°	0.14	0.17	0.18	0.21
180°	0.16	0.18	0.19	0.21
202.5°	0.16	0.18	0.19	0.21
225°	0.16	0.18	0.19	0.22
247.5°	0.14	0.17	0.18	0.20
270°	0.14	0.17	0.18	0.21
292.5°	0.14	0.18	0.20	0.25
315°	0.15	0.20	0.22	0.27
337.5°	0.17	0.21	0.23	0.27
Omni	0.25	0.29	0.31	0.35

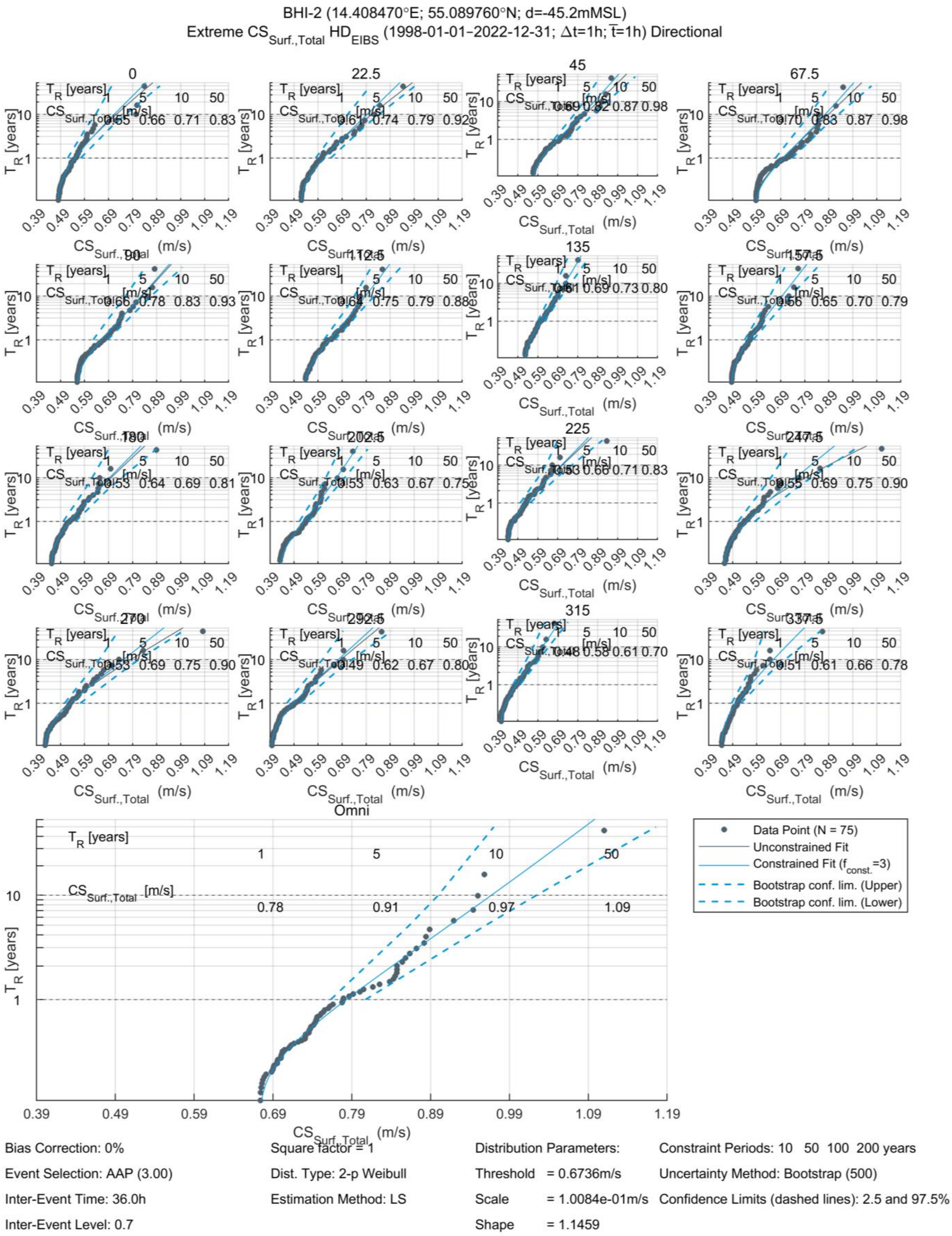

Figure 5.32 Extreme total near-surface current speed at BHI-2

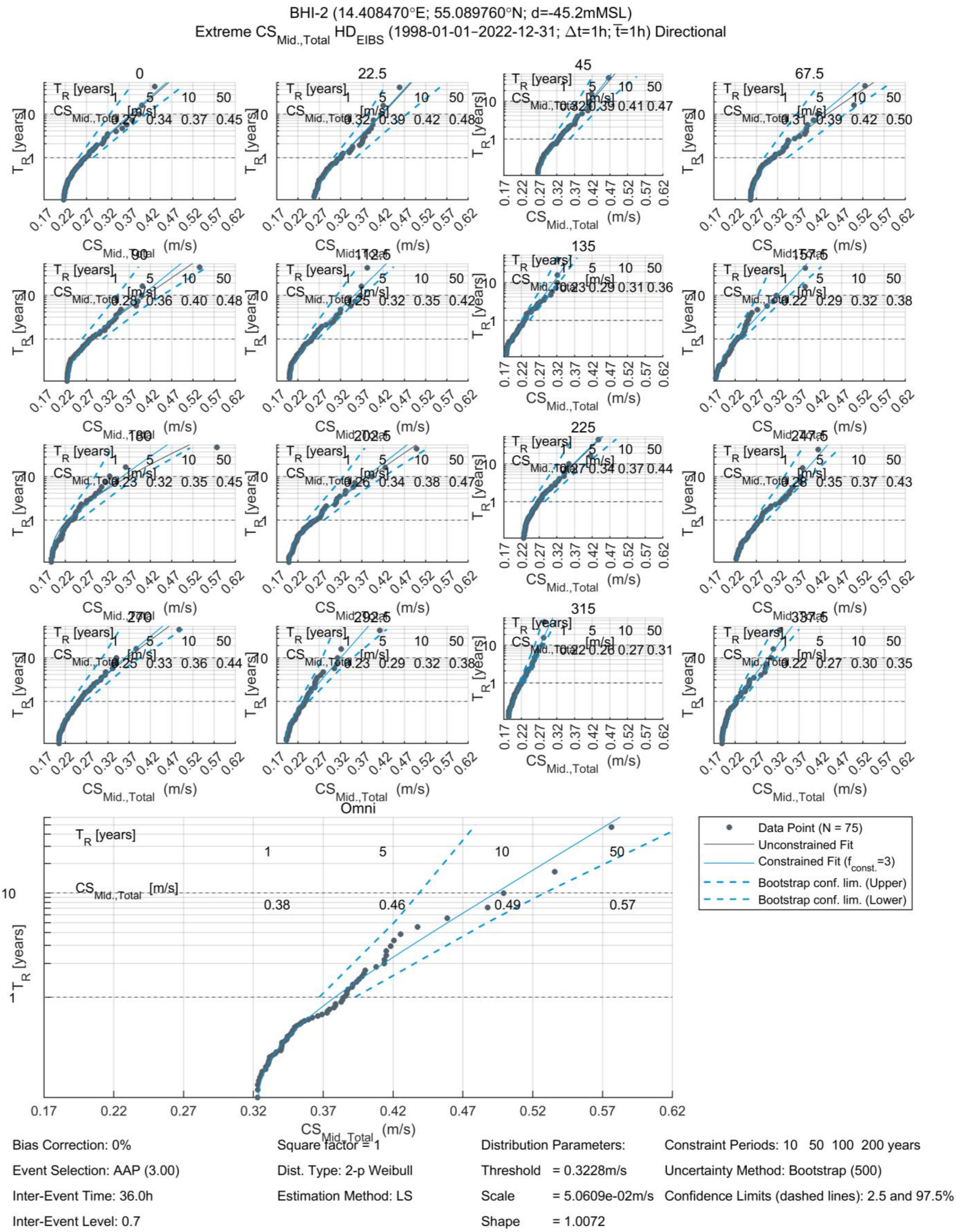

Figure 5.33 Extreme total mid-depth current speed at BHI-2

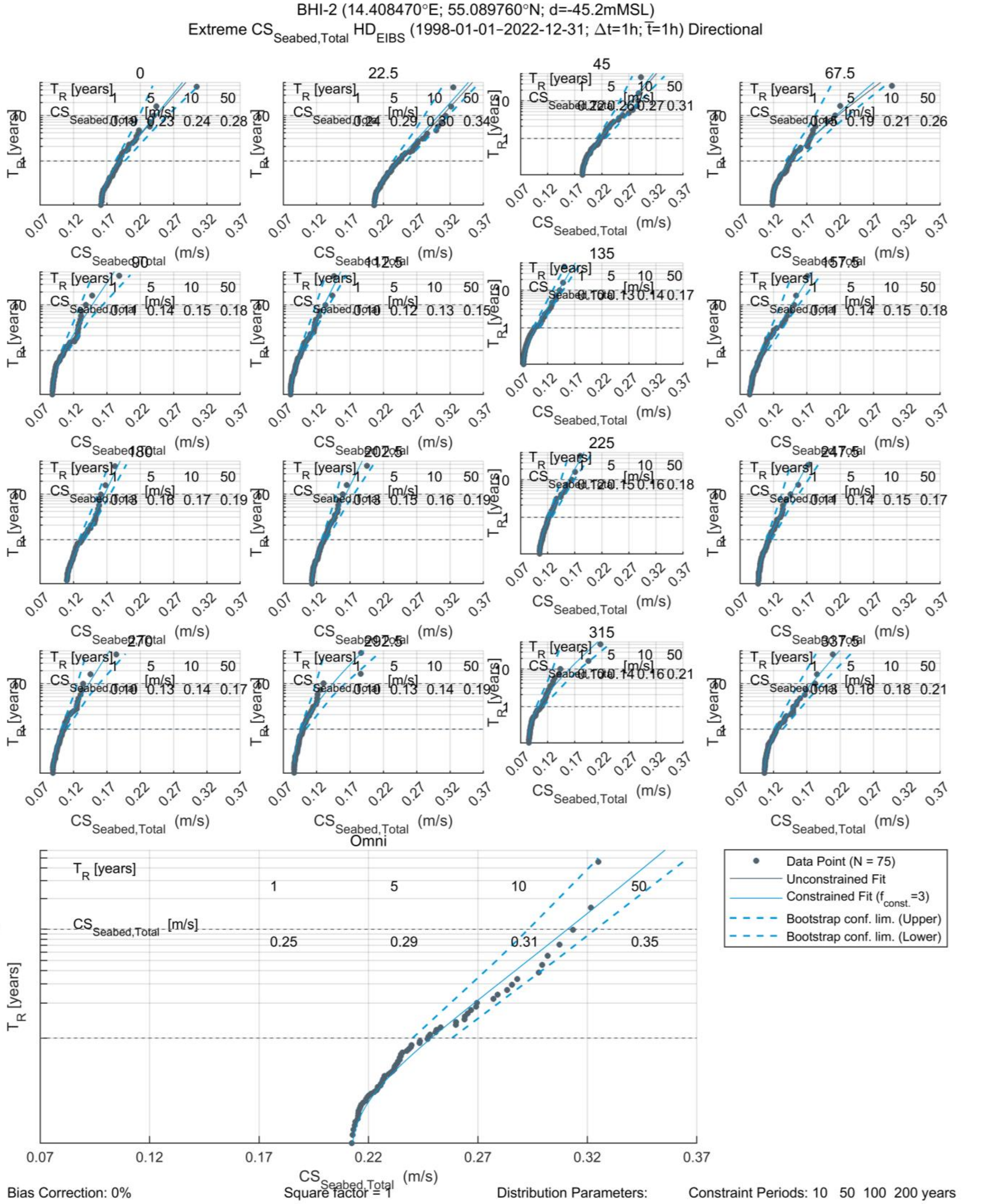

Bias Correction: 0%
Event Selection: AAP (3.00)
Inter-Event Time: 36.0h
Inter-Event Level: 0.7

Square factor = 1
Dist. Type: 2-p Weibull
Estimation Method: LS

Distribution Parameters:
Threshold = 0.2121m/s
Scale = 3.3675e-02m/s
Shape = 1.1370

Constraint Periods: 10 50 100 200 years
Uncertainty Method: Bootstrap (500)
Confidence Limits (dashed lines): 2.5 and 97.5%

Figure 5.34 Extreme total near-seabed current speed at BHI-2

5.2.2 Maps of extreme total current speed

Figure 5.35 to Figure 5.46 present the spatial variation in the omni-directional total current speed across the EIBS OWF areas (near-surface, mid-depth, and near-seabed) for return periods of 1, 5, 10, and 50-years based on traditional extreme value analysis at each mesh element.

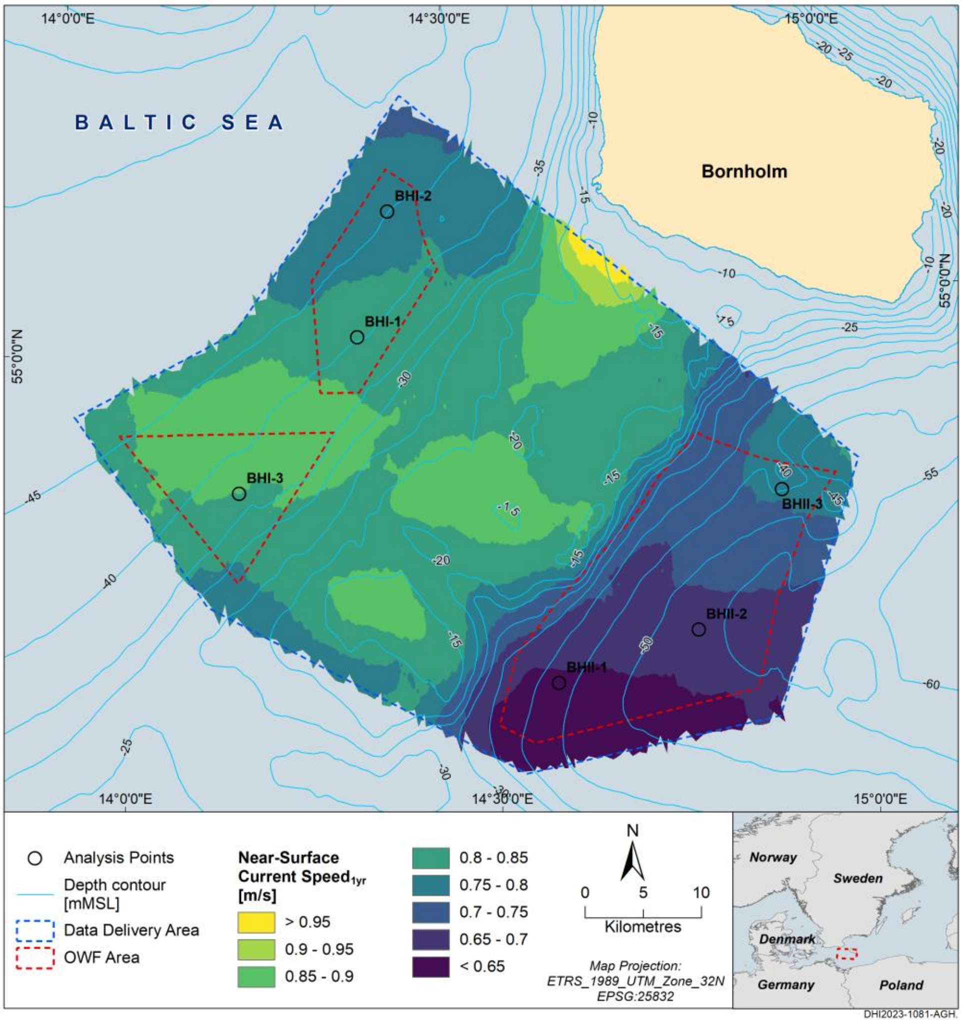

Figure 5.35 Spatial variation across EIBS OWF area of total near-surface current speed for return period of 1 year
The colour map shows the current speed, and the contours show water depth.

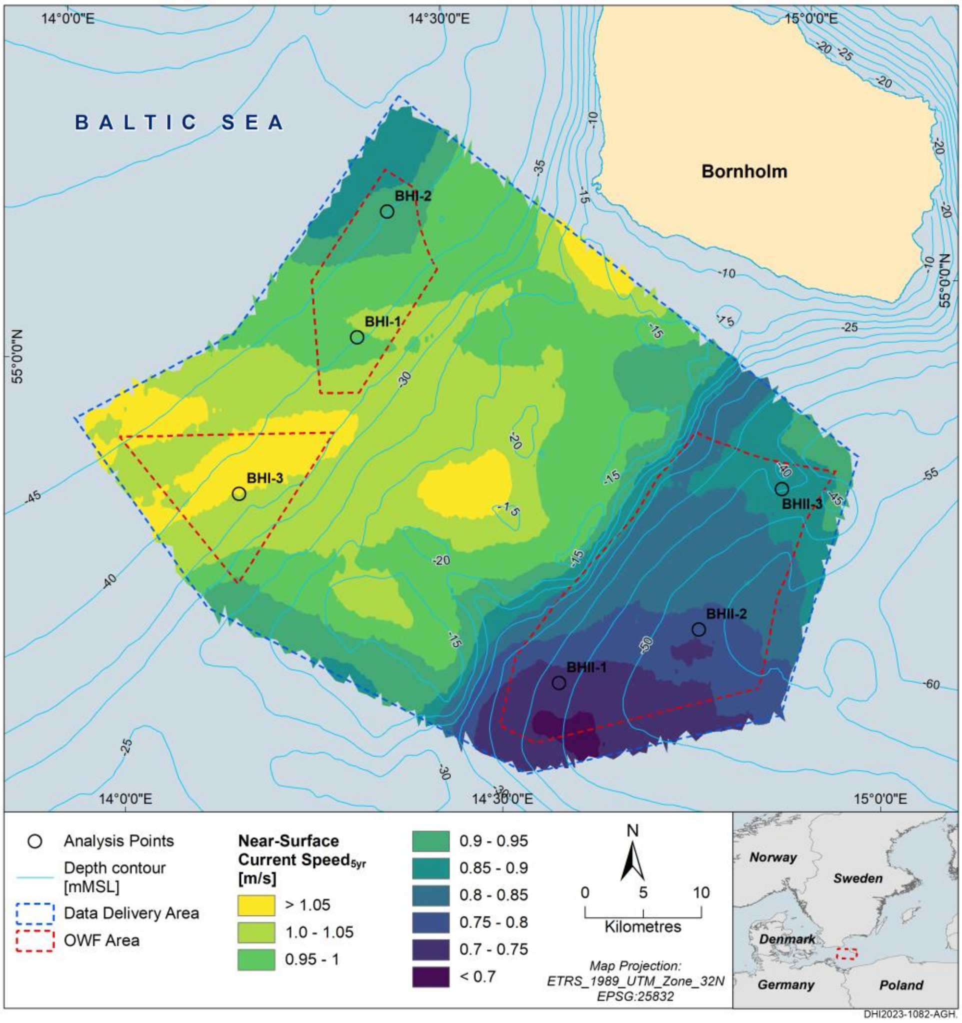

Figure 5.36 Spatial variation across EIBS OWF area of total near-surface current speed for return period of 5 years

The colour map shows the current speed, and the contours show water depth.

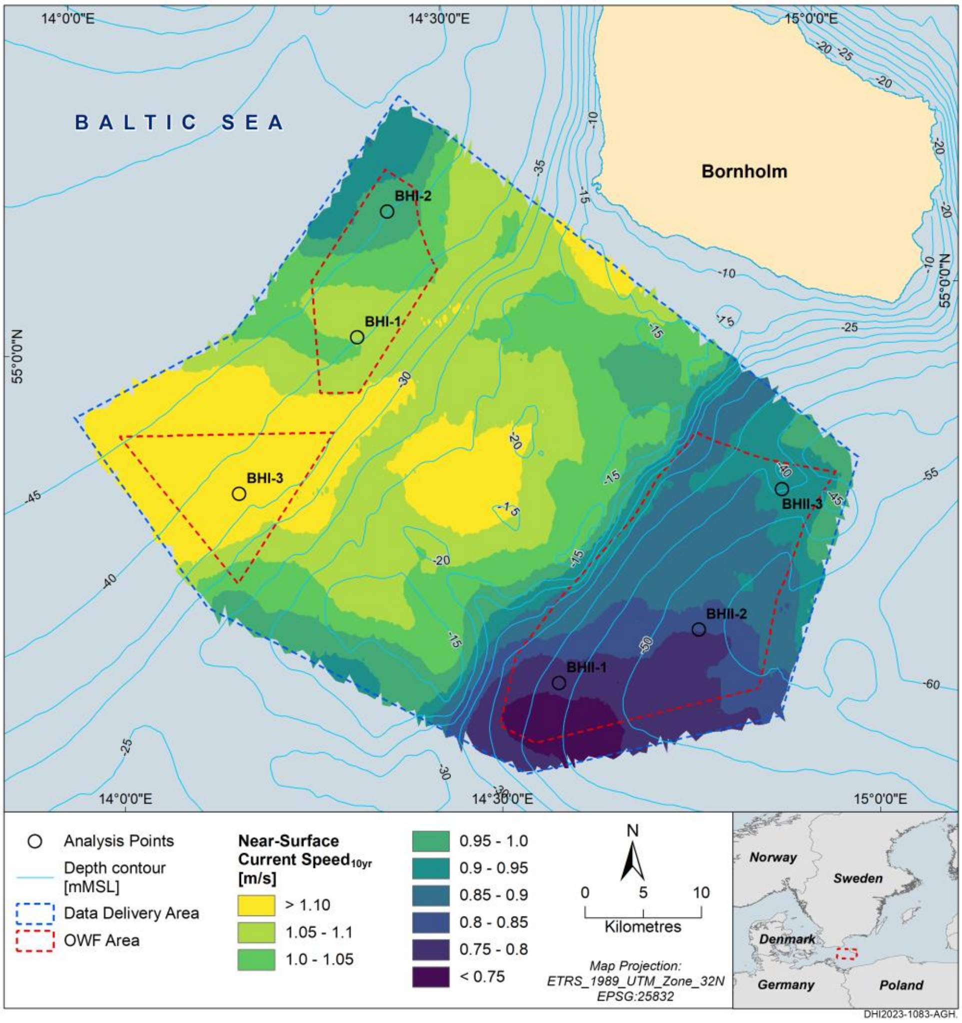

Figure 5.37 Spatial variation across EIBS OWF area of total near-surface current speed for return period of 10 years

The colour map shows the current speed, and the contours show water depth.

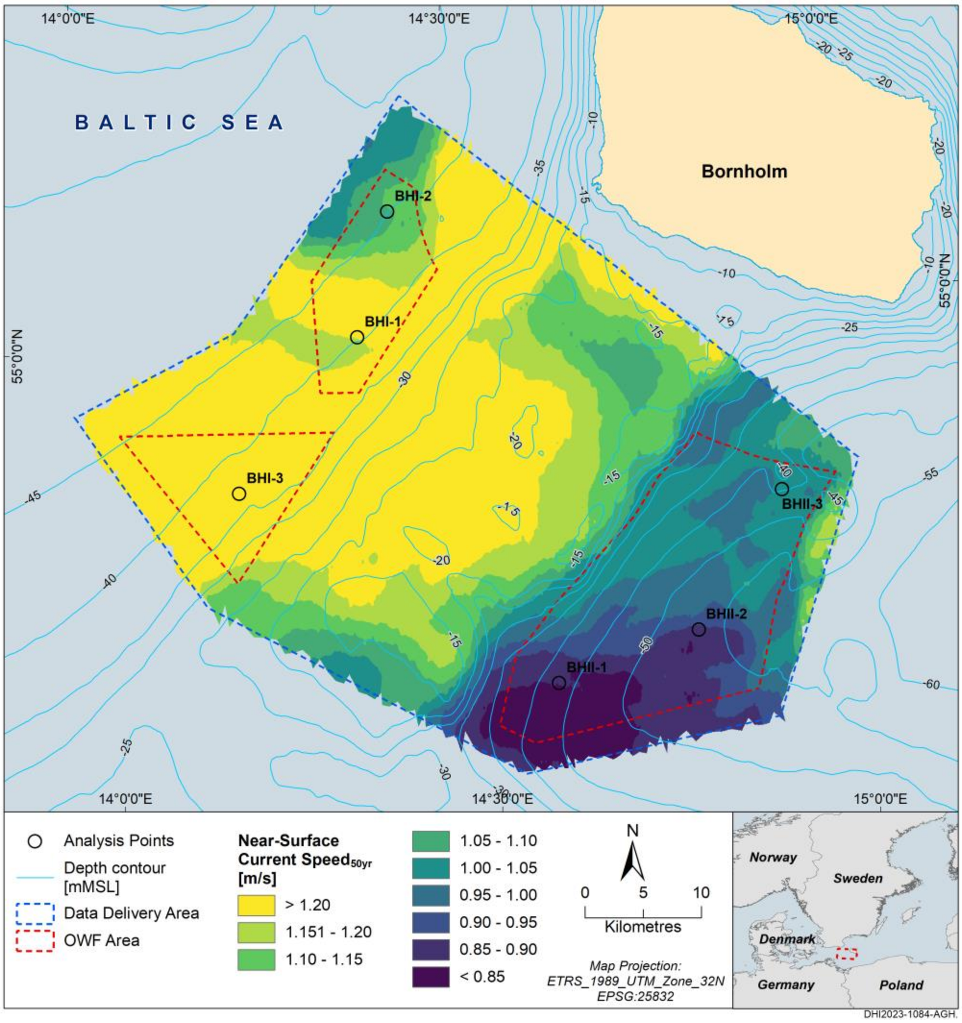

Figure 5.38 Spatial variation across EIBS OWF area of total near-surface current speed for return period of 50 years

The colour map shows the current speed, and the contours show water depth.

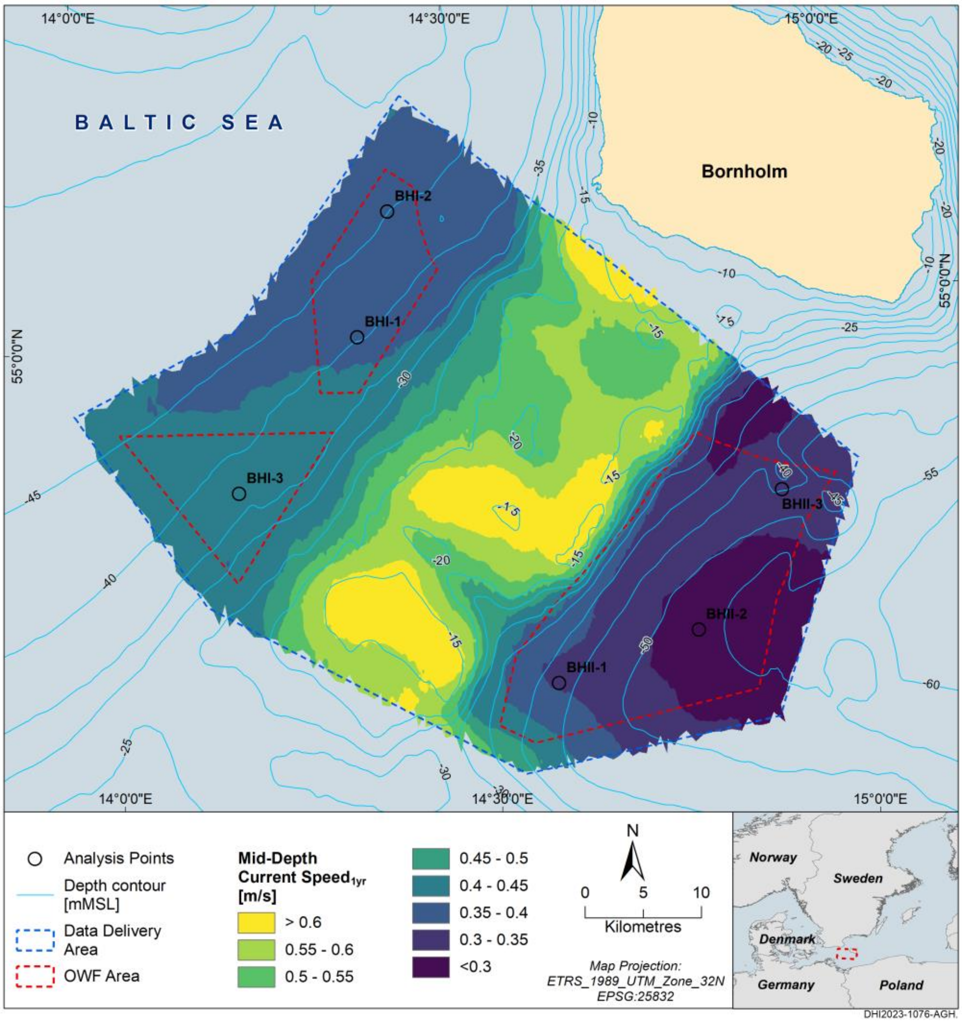

Figure 5.39 Spatial variation across EIBS OWF area of total mid-depth current speed for return period of 1 year

The colour map shows the current speed, and the contours show water depth.

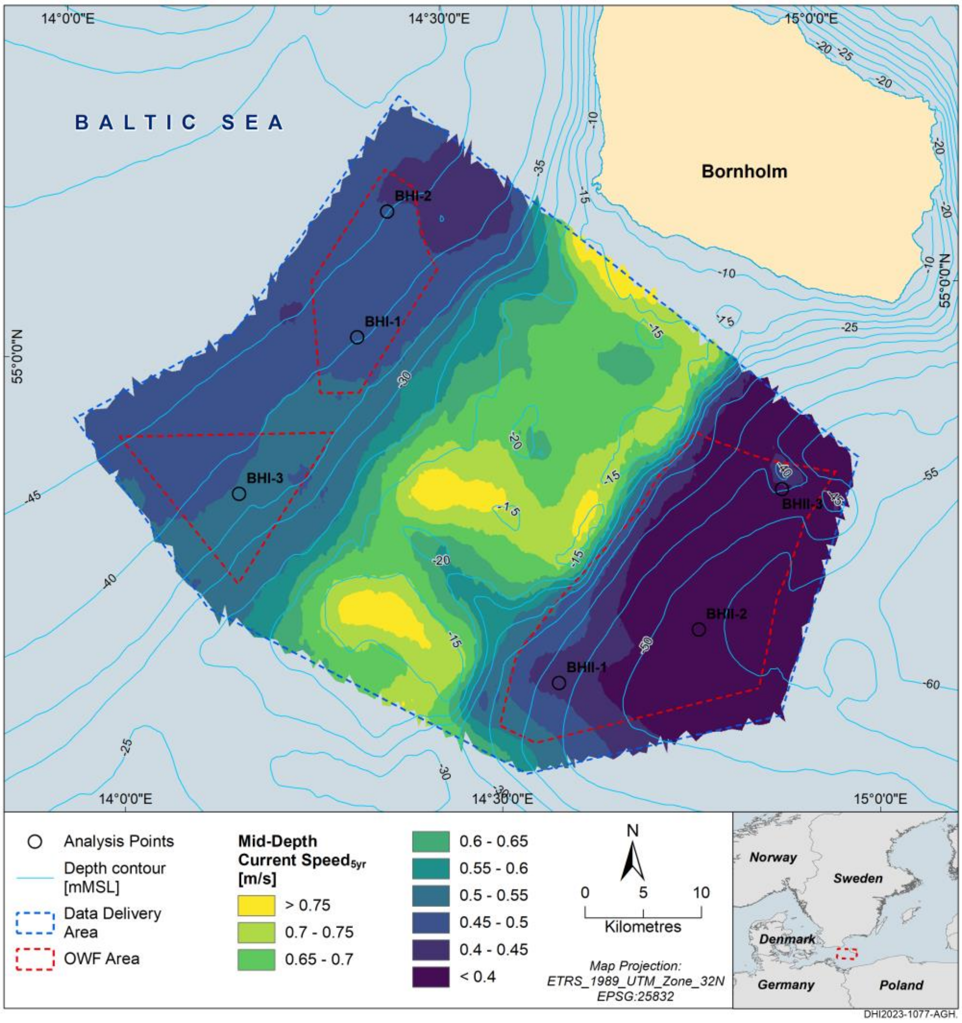

Figure 5.40 Spatial variation across EIBS OWF area of total mid-depth current speed for return period of 5 years

The colour map shows the current speed, and the contours show water depth.

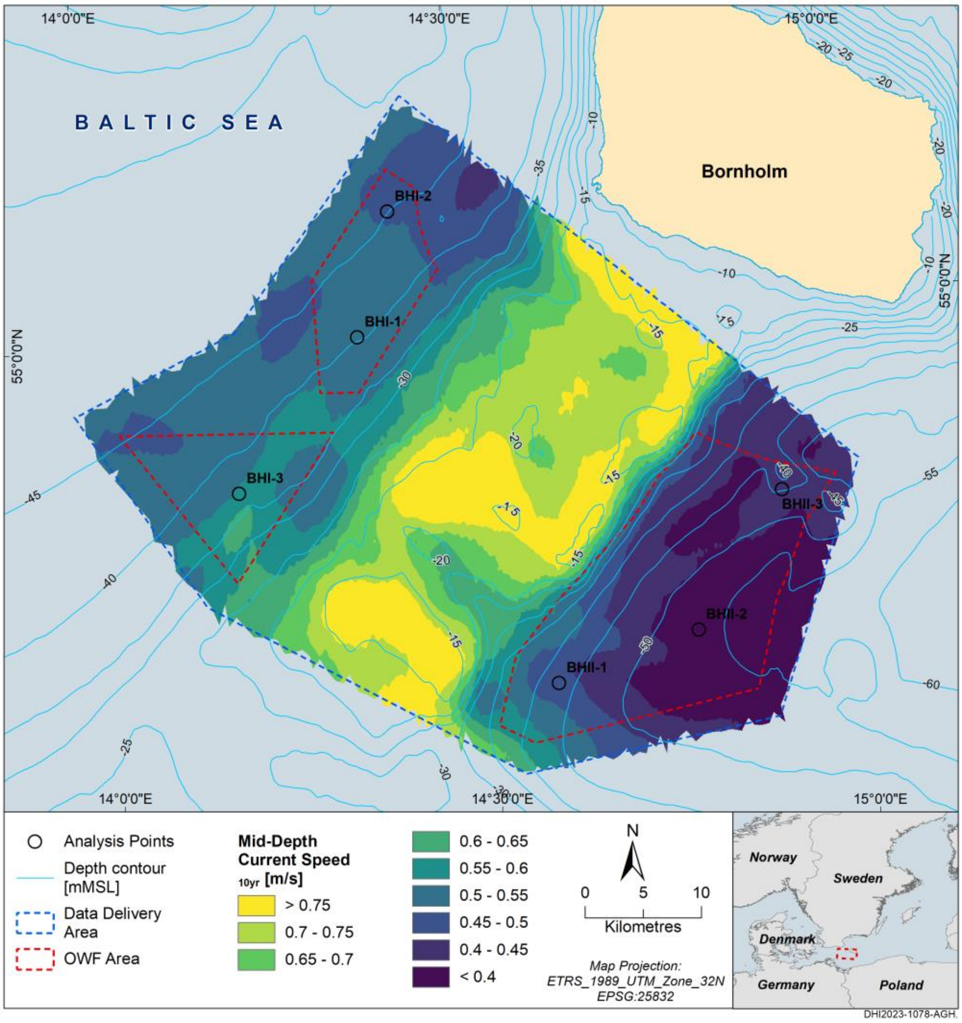

Figure 5.41 Spatial variation across EIBS OWF area of total mid-depth current speed for return period of 10 years

The colour map shows the current speed, and the contours show water depth.

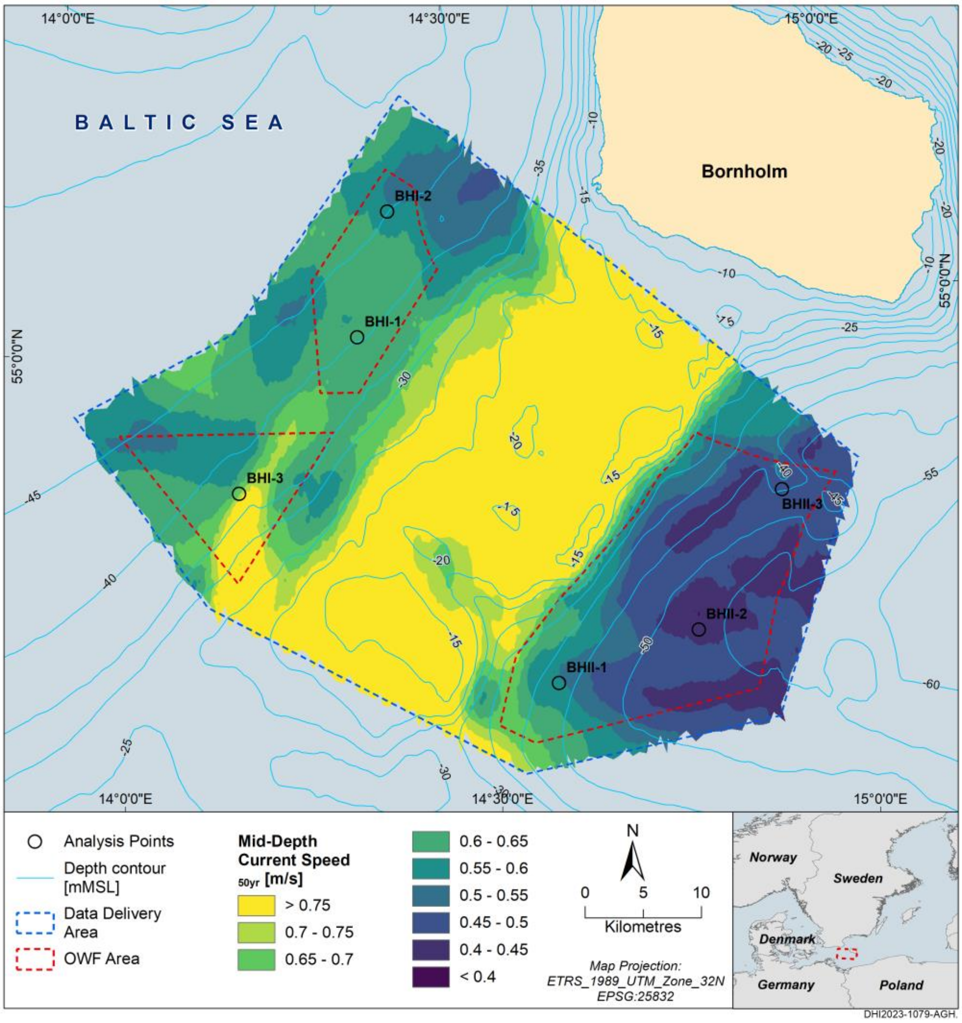

Figure 5.42 Spatial variation across EIBS OWF area of total mid-depth current speed for return period of 50 years

The colour map shows the current speed, and the contours show water depth.

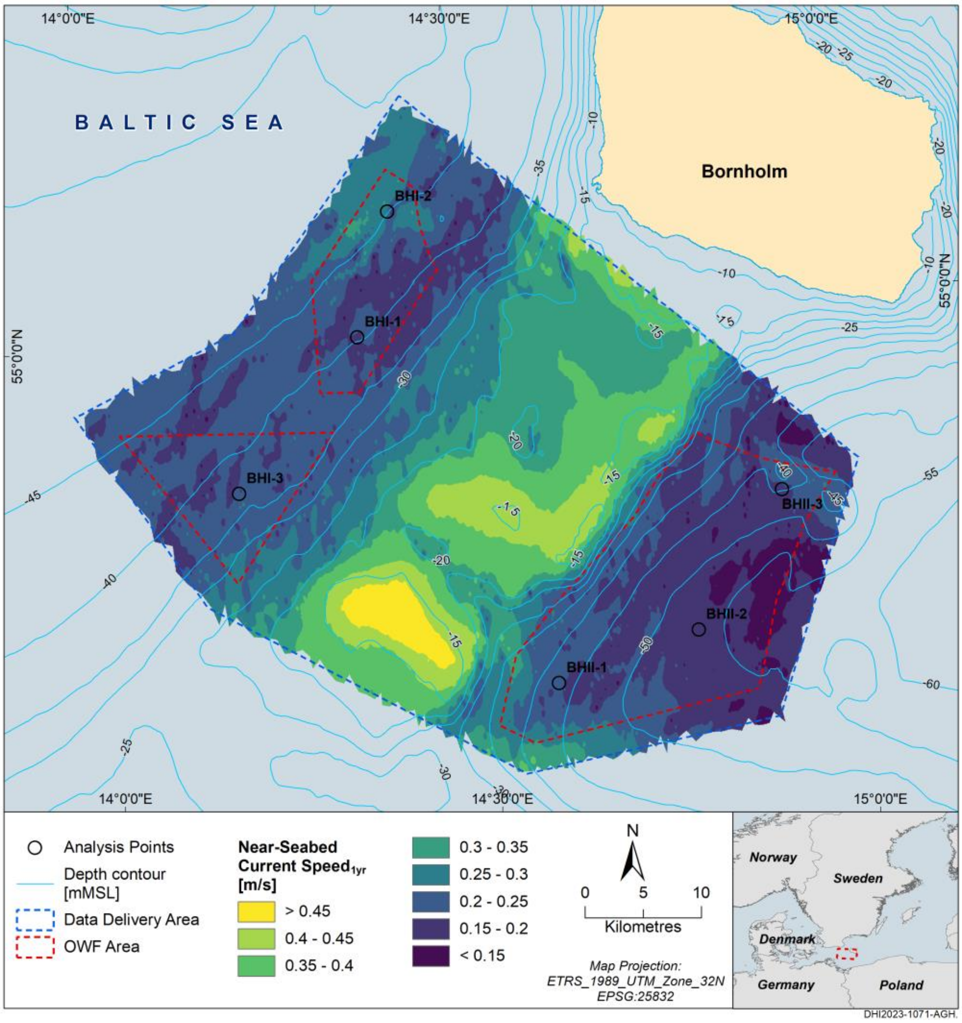

Figure 5.43 Spatial variation across EIBS OWF area of total near-seabed current speed for return period of 1 year

The colour map shows the current speed, and the contours show water depth.

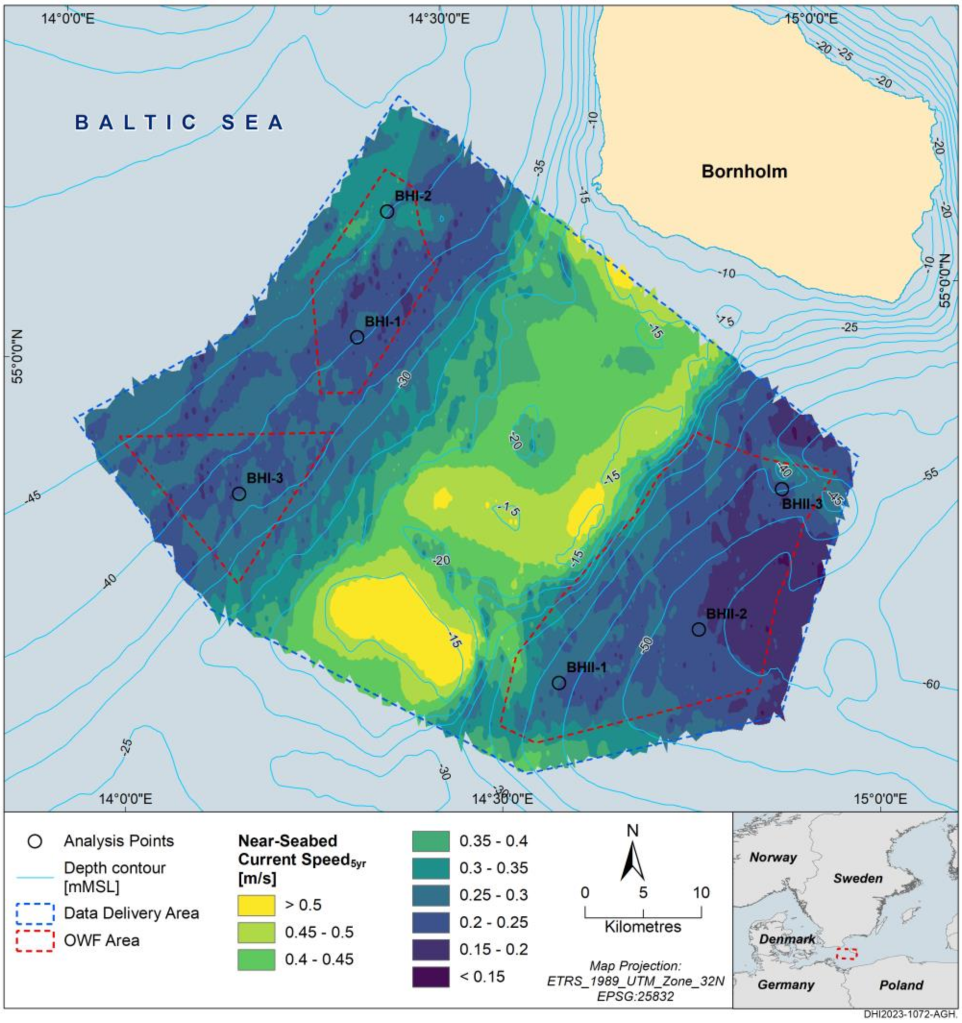

Figure 5.44 Spatial variation across EIBS OWF area of total near-seabed current speed for return period of 5 years

The colour map shows the current speed, and the contours show water depth.

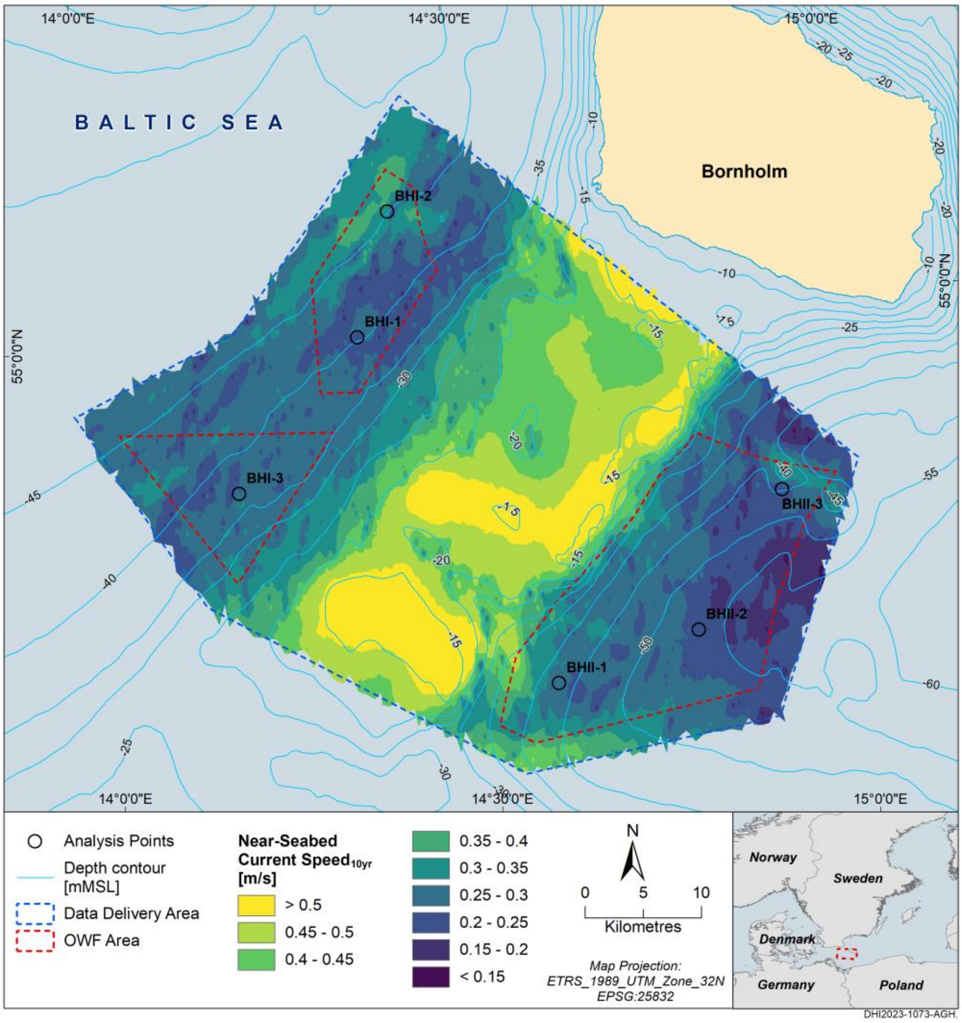

Figure 5.45 Spatial variation across EIBS OWF area of total near-seabed current speed for return period of 10 years

The colour map shows the current speed, and the contours show water depth.

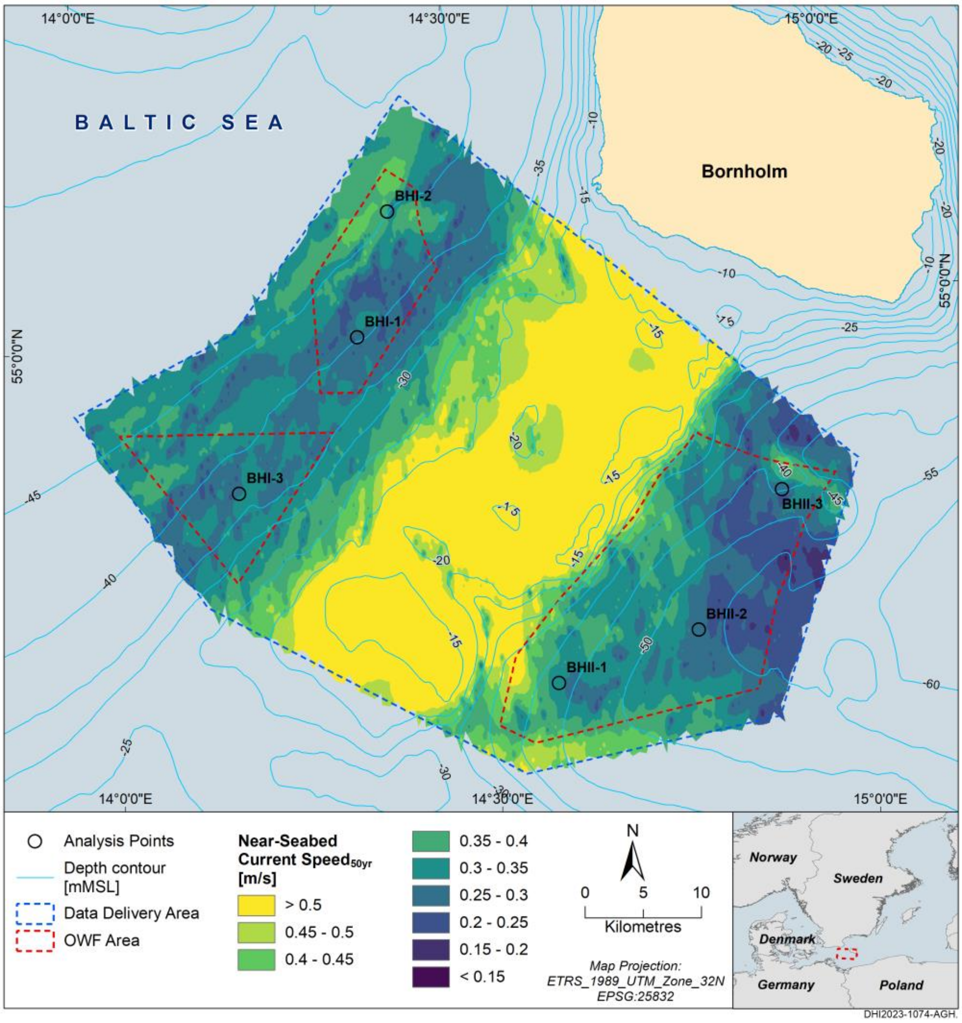

Figure 5.46 Spatial variation across EIBS OWF area of total near-seabed current speed for return period of 50 years
The colour map shows the current speed, and the contours show water depth.

5.3 Scaling of current speeds

Part A, Section 5.6 [1] includes a discussion of validation of the current profiles at stations LOT 3 and LOT 4. The recommendation is, where possible, to use the actual profile series or as a generic profile representative of the site, to use either a constant or the DNV recommended power-law profile.

The validation of the model indicates that there is uncertainty in the predicted current speeds and that there is a tendency for the current speeds in the deeper layers to be non-conservative i.e. underestimated.

To compensate for this uncertainty DHI recommends the post scaling factors shown in Table 5.6.

Table 5.6 Post-calibration scaling factors for current speeds

Depth	Factor
Surface	1.0
Mid-depth	1.25
Near-bed	1.1

6 Wave Conditions

This section presents a summary of the wave data basis established in [1], followed by a presentation of normal and extreme wave conditions at the EIBS OWF area.

The wave data is adopted from the spectral wave (MIKE 21 SW) model established for EIBS (SW_{EIBS}) in [2]. The generated wave data set, denoted EIBS-SW-NORA3, contains total, wind-sea, and swell partitions of the sea. Table 6.1 summarises the metadata of the EIBS-SW-NORA3 dataset.

Table 6.1 Metadata of the EIBS-SW-NORA3 dataset
Time series data is provided to Energinet (.dfs0).

Name	Value
Dataset ID:	EIBS-SW-NORA3
Start Date [UTC]:	1979-01-05 00:00:00
End Date [UTC]:	2022-12-31 23:00:00
Time Step [s]:	3600
Cell Size [m]:	~500 (OWF area)

The wave data is considered representative of 2-hour average sea state and is given at 1-hour interval. The wave analyses are presented in height bins of 0.5 m, period bins of 0.5 s, and directional bins of 22.5°.

Table 6.2 presents the variables of the EIBS-SW-NORA3 dataset, incl. the bin sizes applied in analyses throughout this report.

Table 6.2 Wave variables of the EIBS-SW-NORA3 wave dataset

Variable name	Abbrev.	Unit
Significant wave height	H_{m0}	m
Maximum wave height	H_{max}	m
Peak wave period	T_p	s
Mean wave period	T_{01}	s
Zero-crossing wave period	T_{02}	s
Mean energy period	T_{m10}	s
Peak wave direction	PWD	°N (clockwise from)
Mean wave direction	MWD	°N (clockwise from)
Direction standard deviation	DSD	°

The wave analyses cover the data period 1979-01-15 – 2022-12-31 (44 years). The main body of this report presents results at BHI-2, while results at all analysis points are given in the data reports (listed in Table A.1) which are attached to this report. The data reports contain all (scatter) tables and figures presented below.

6.1 Normal wave conditions

The normal wave conditions are presented in terms of:

- Time series
- Wave roses
- Histograms
- Monthly statistics
- Directional statistics
- Scatter diagrams (H_{m0})
- Wind-wave misalignment
- Wave spectra
- Maps of mean H_{m0}

6.1.1 Time series

Figure 6.1 shows time series of the total, wind-sea, and swell partition of H_{m0}, and T_p, and T_{02} at BHI-2 during the 44-year hindcast period. The mean of H_{m0} is 0.96 m, and the maximum is 7.18 m.

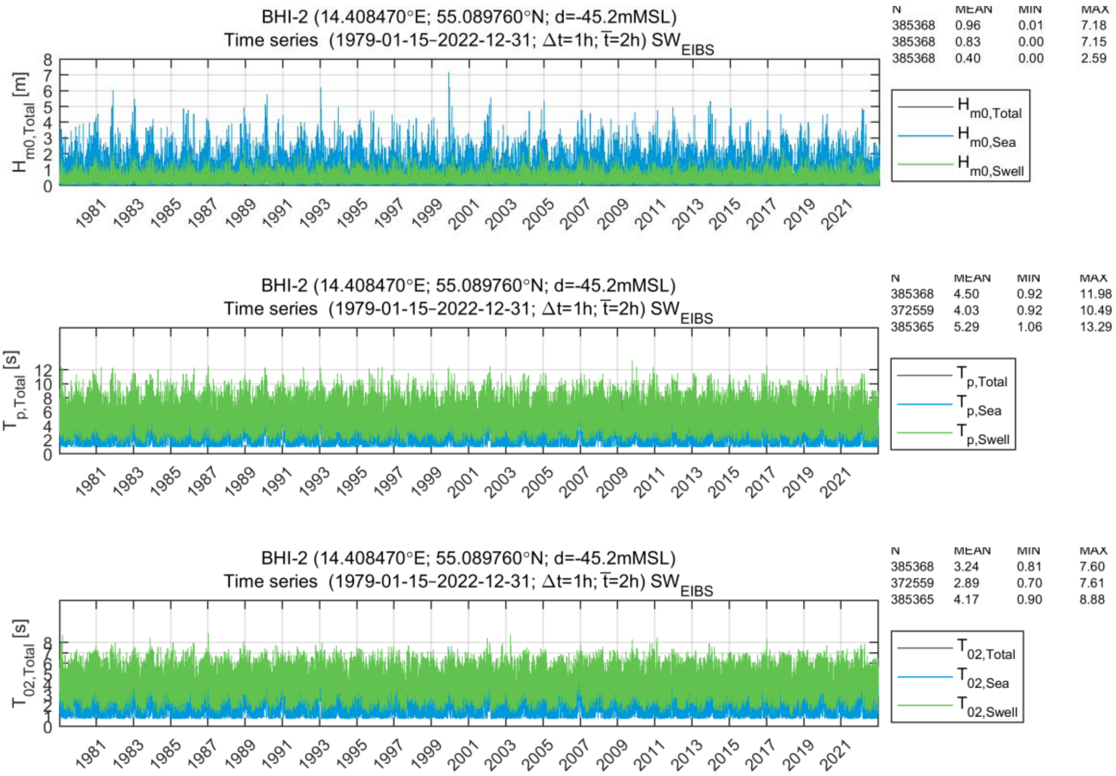

Figure 6.1 Time series of H_{m0}, T_p and T_{02} at BHI-2

6.1.2 Wave roses

Figure 6.2 - Figure 6.4 show wave roses at BHI-2 based on H_{m0} and MWD for total, wind-sea and swell respectively. The wave rose indicate the predominance of waves coming from westerly sectors (W-WSW The wind-driven waves mainly originate from the W-WSW direction, with calm (H_{m0} < 0.5) swell conditions occurring approximately 73% of the time. Wave roses based on T_p-MWD, and T_{02}-MWD are depicted in Figure 6.5 to Figure 6.7, and Figure 6.8 to Figure 6.10, respectively.

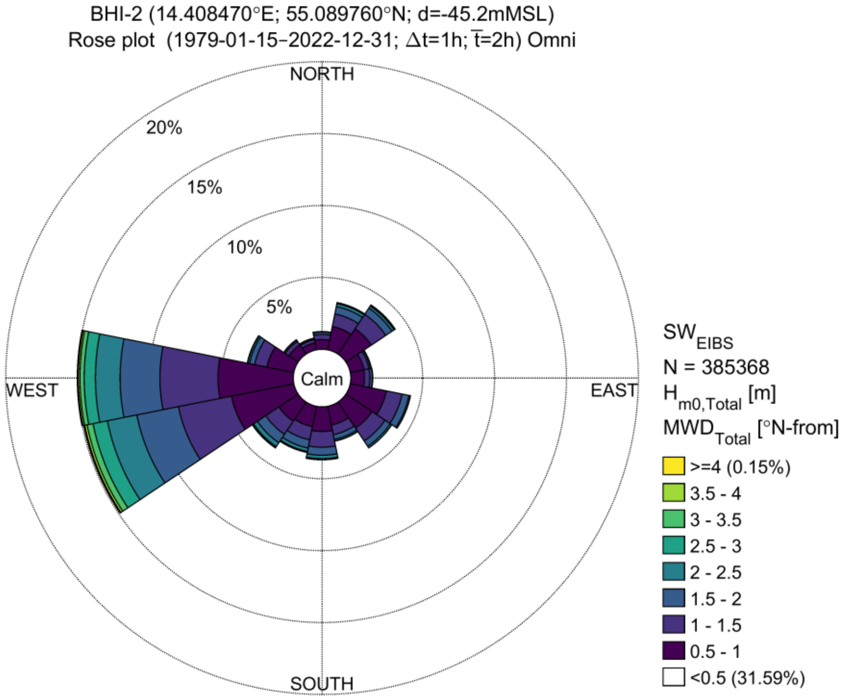

Figure 6.2 Wave rose at BHI-2; H_{m0} vs MWD – Total

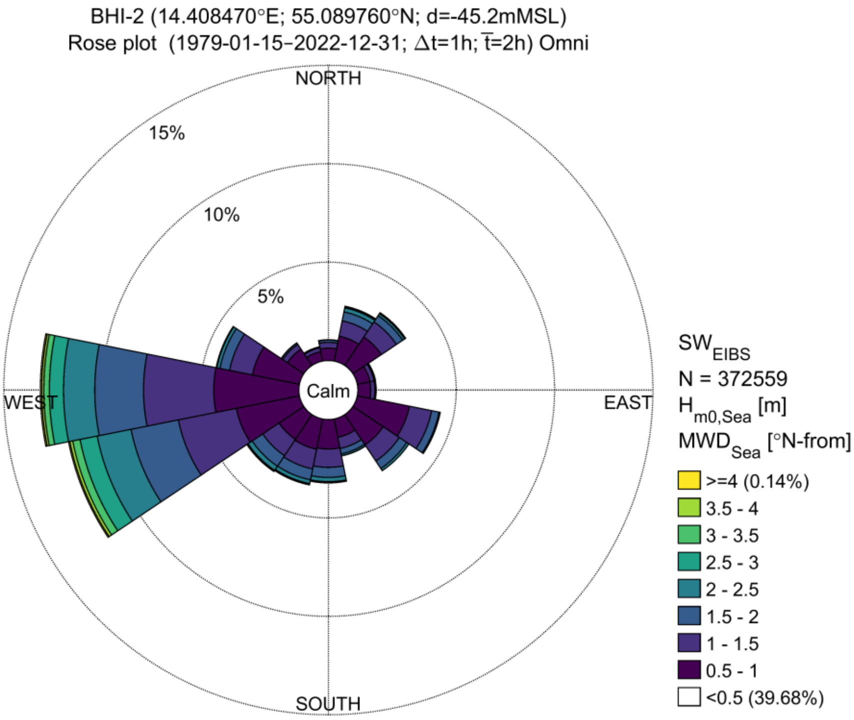

Figure 6.3 Wave rose at BHI-2; H_{m0} vs MWD – Wind-Sea

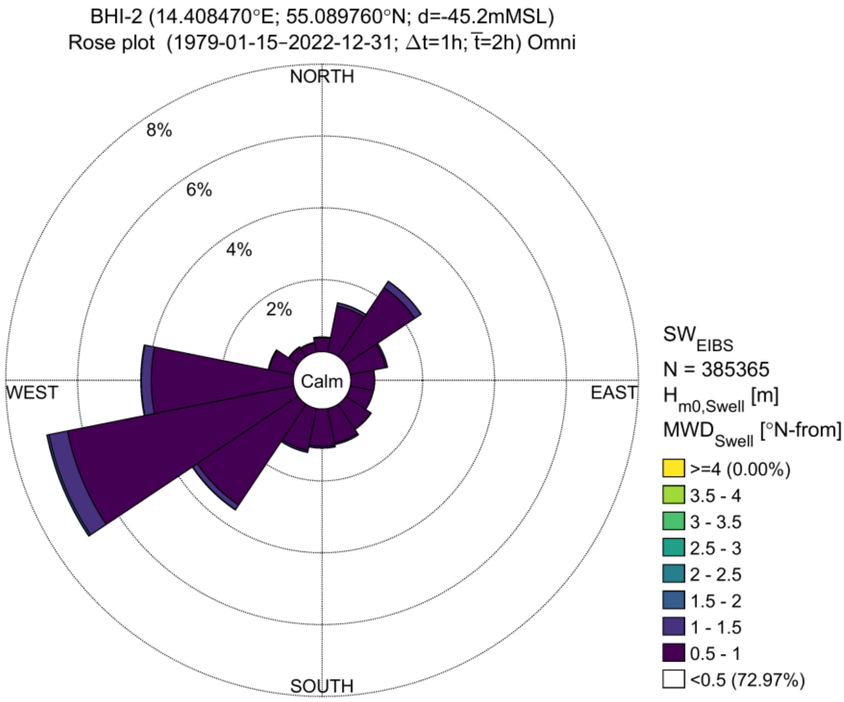

Figure 6.4 Wave rose at BHI-2; H_{m0} vs MWD – Swell

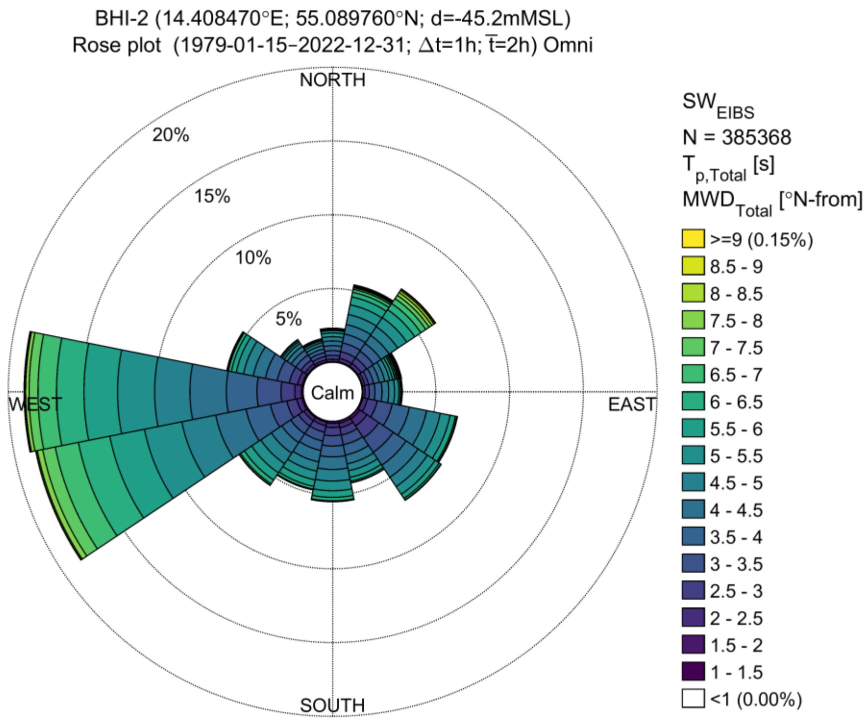

Figure 6.5 Wave rose at BHI-2; T_p vs MWD – Total

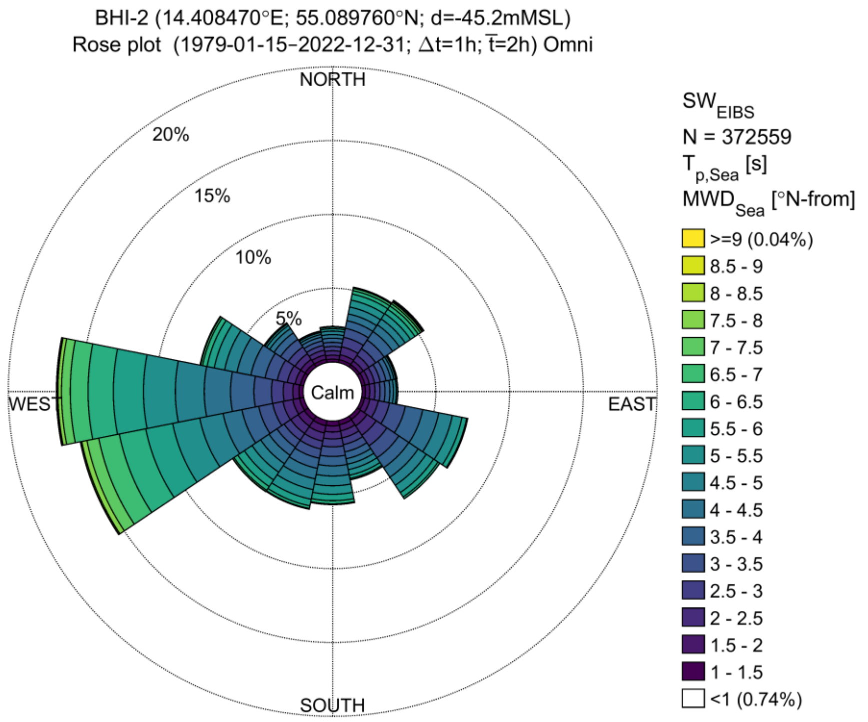

Figure 6.6 Wave rose at BHI-2; T_p vs MWD – Wind-Sea

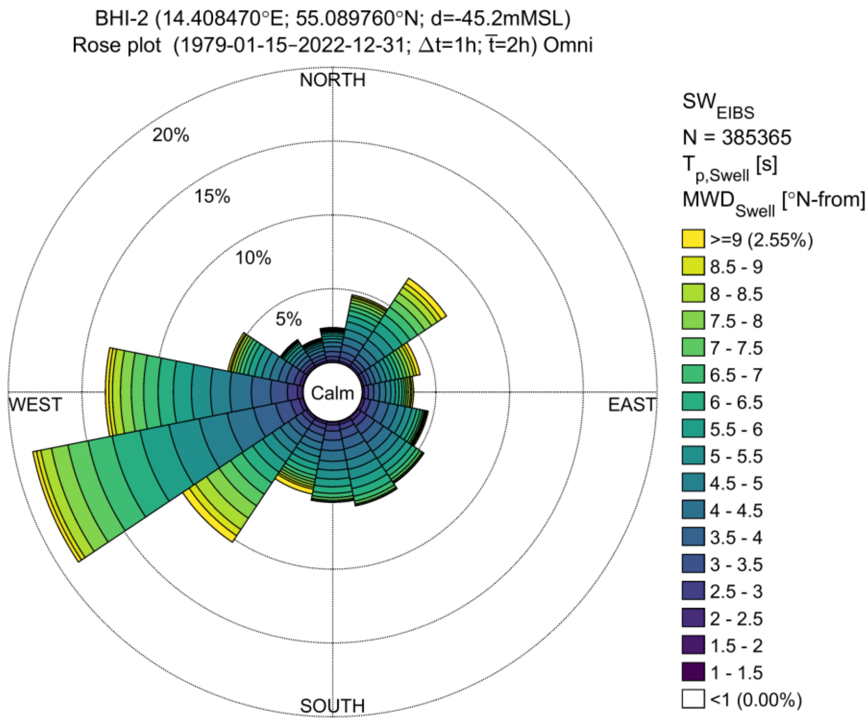

Figure 6.7 Wave rose at BHI-2; T_p vs MWD – Swell

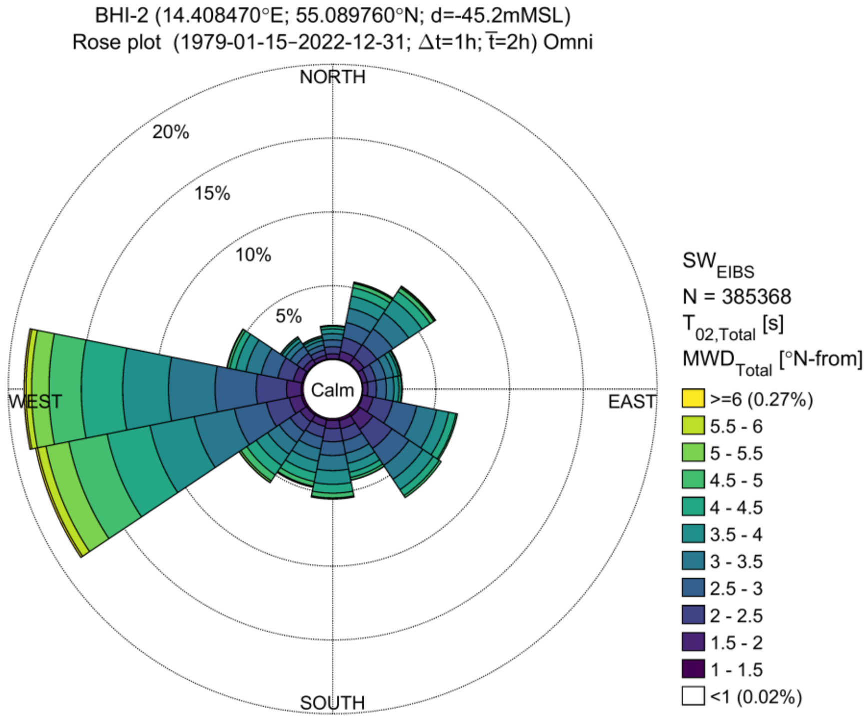

Figure 6.8 Wave rose at BHI-2; T_{02} vs MWD – Total

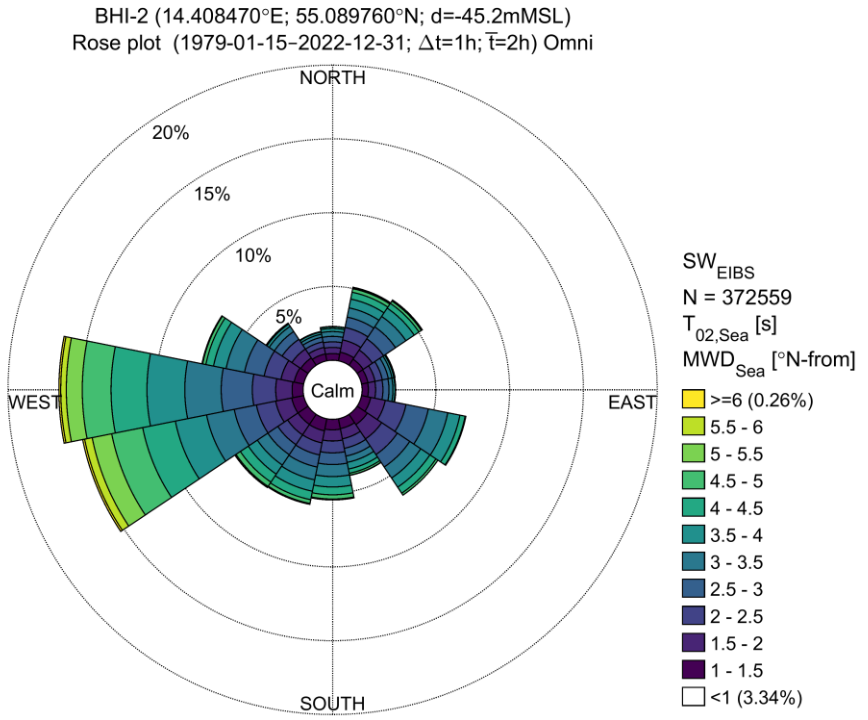

Figure 6.9 Wave rose at BHI-2; T_{02} vs MWD – Wind-Sea

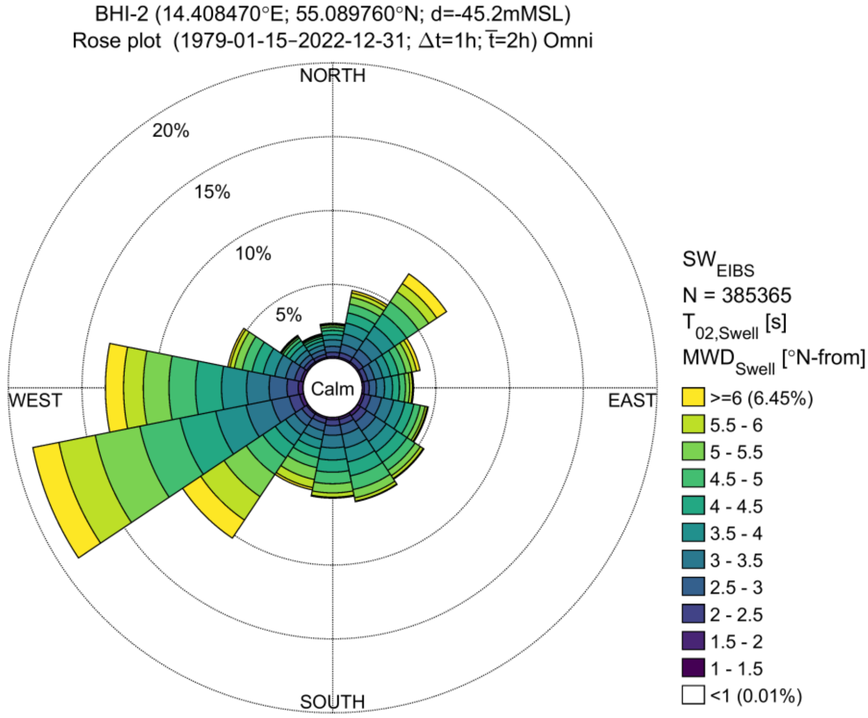

Figure 6.10 Wave rose at BHI-2; T_{02} vs MWD – Swell

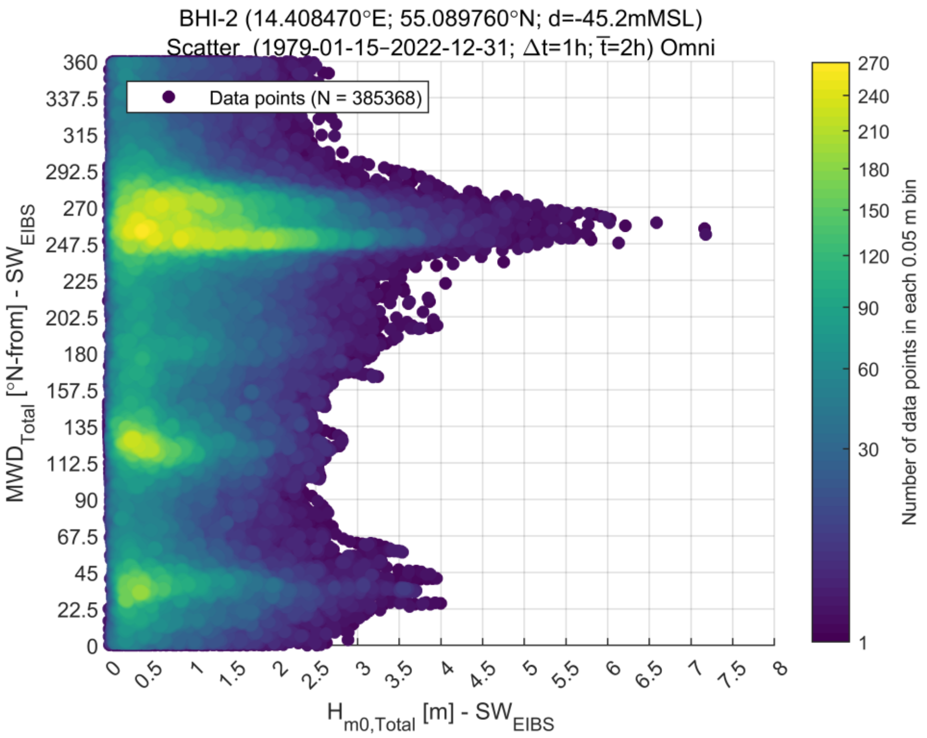

Figure 6.11 Scatter plot at BHI-2; H_{m0} vs MWD – Total

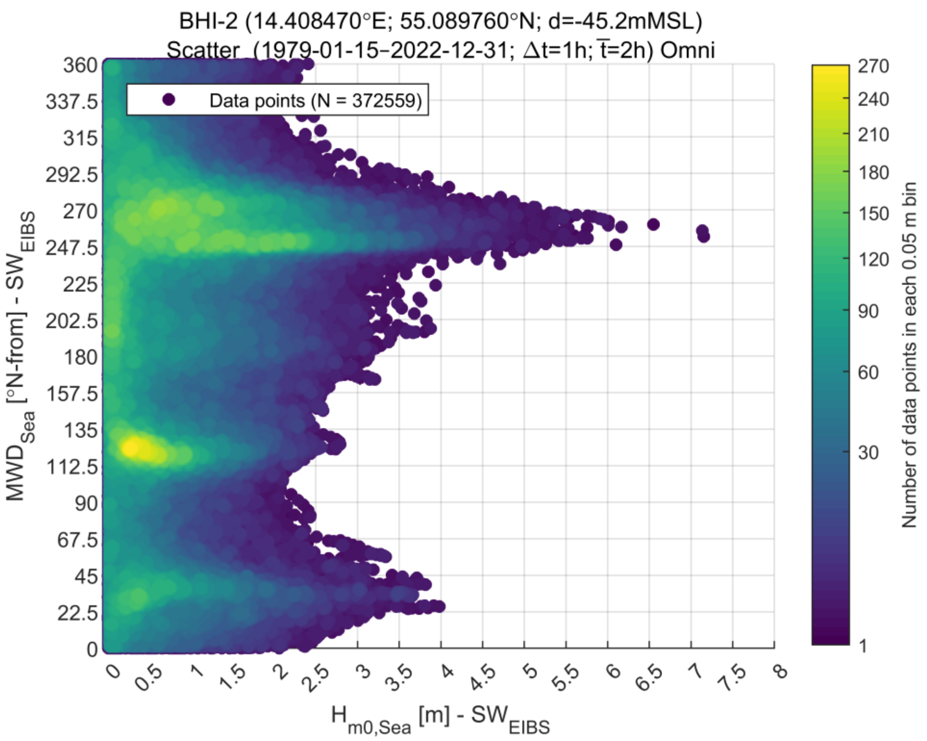

Figure 6.12 Scatter plot at BHI-2; H_{m0} vs MWD – Wind-Sea

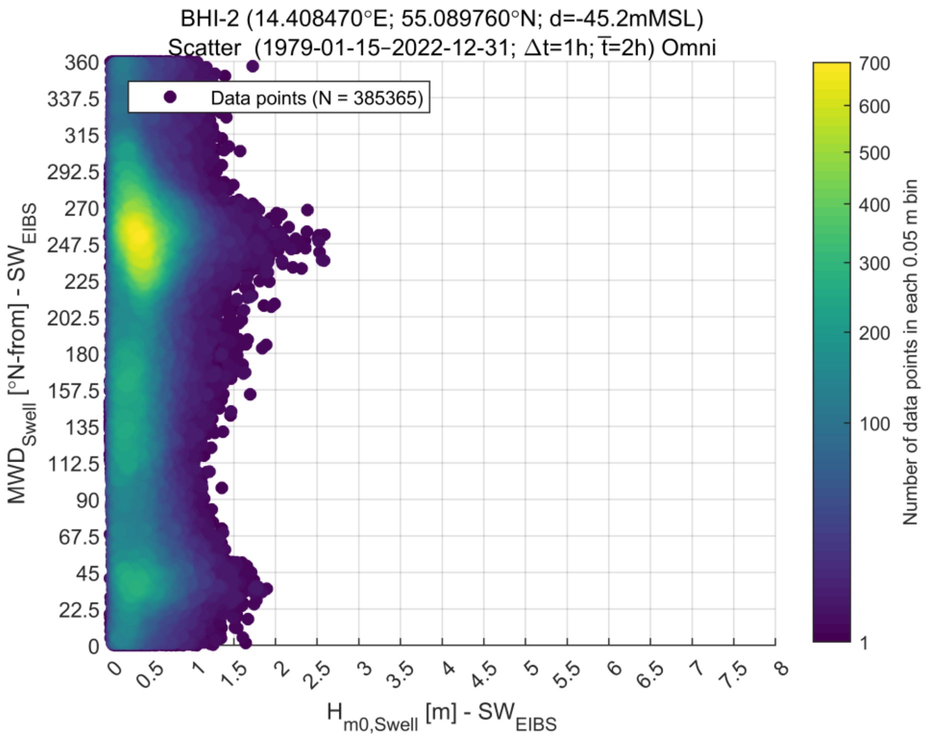

Figure 6.13 Scatter plot at BHI-2; H_{m0} vs MWD – Swell

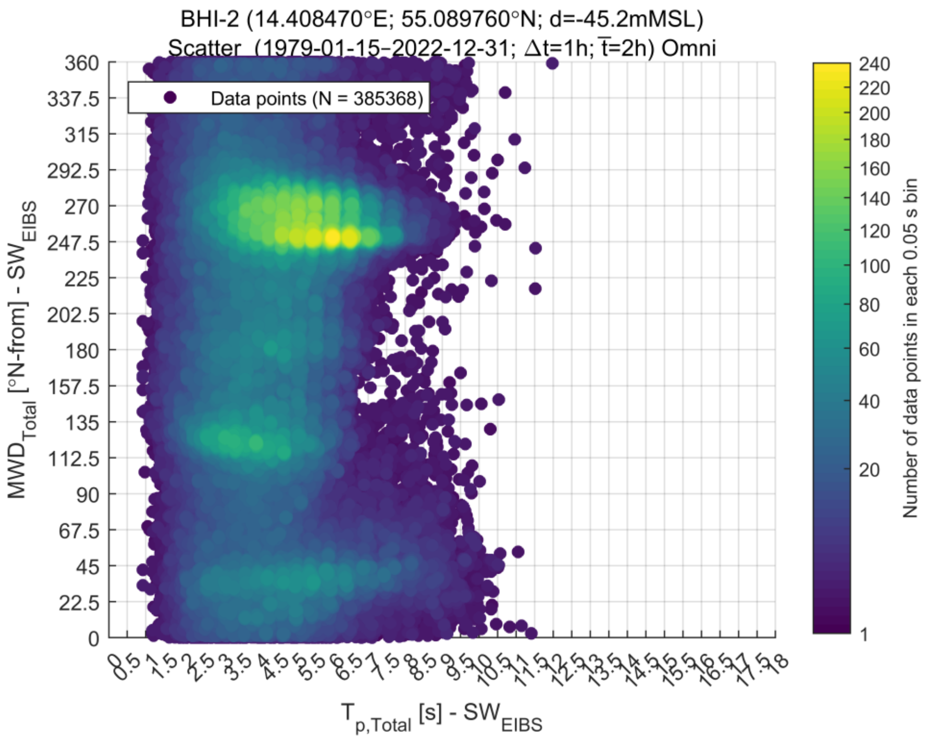

Figure 6.14 Scatter plot at BHI-2; T_p vs MWD – Total

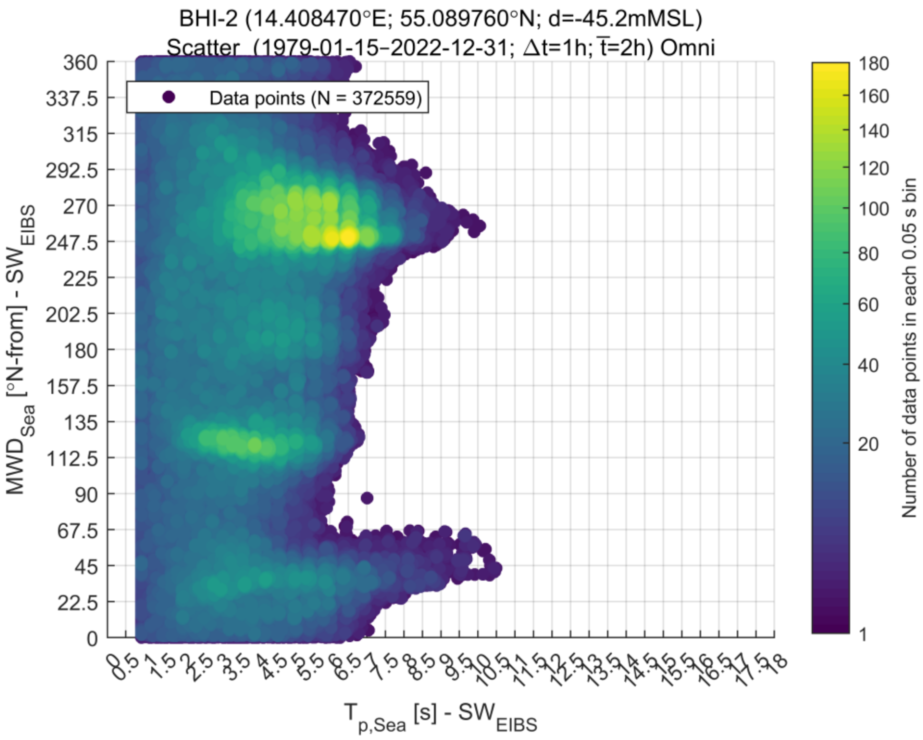

Figure 6.15 Scatter plot at BHI-2; T_p vs MWD – Wind-Sea

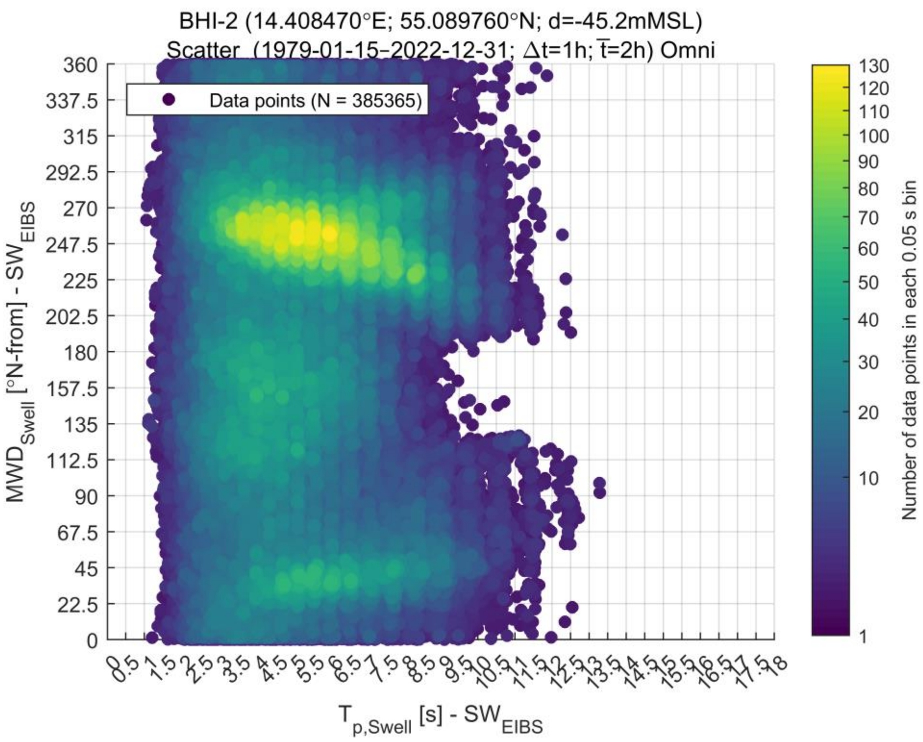

Figure 6.16 Scatter plot at BHI-2; T_p vs MWD – Swell

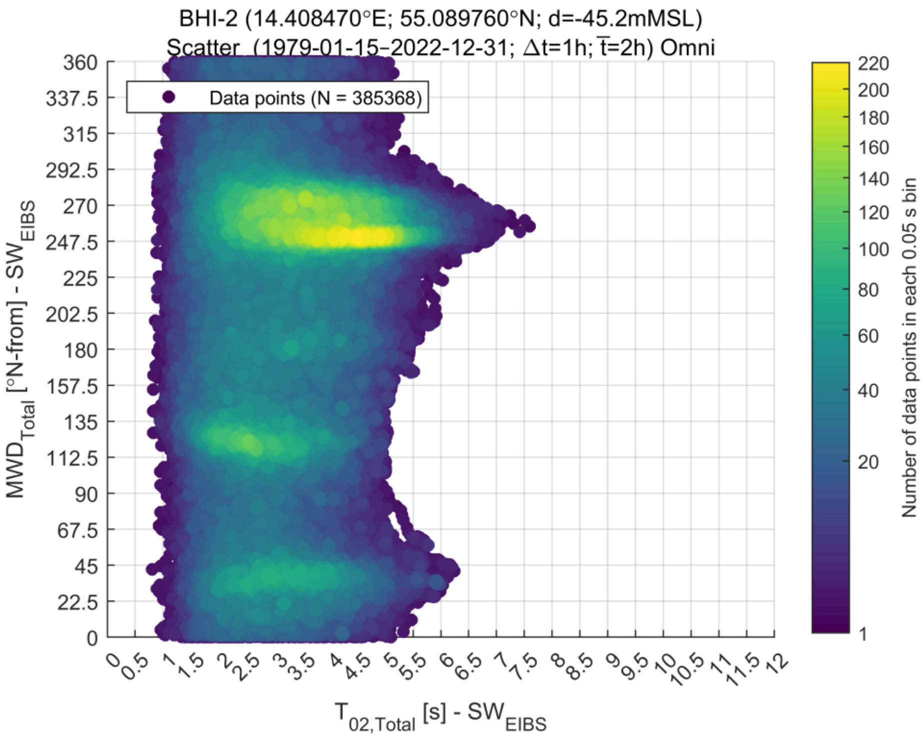

Figure 6.17 Scatter plot at BHI-2; T_{02} vs MWD – Total

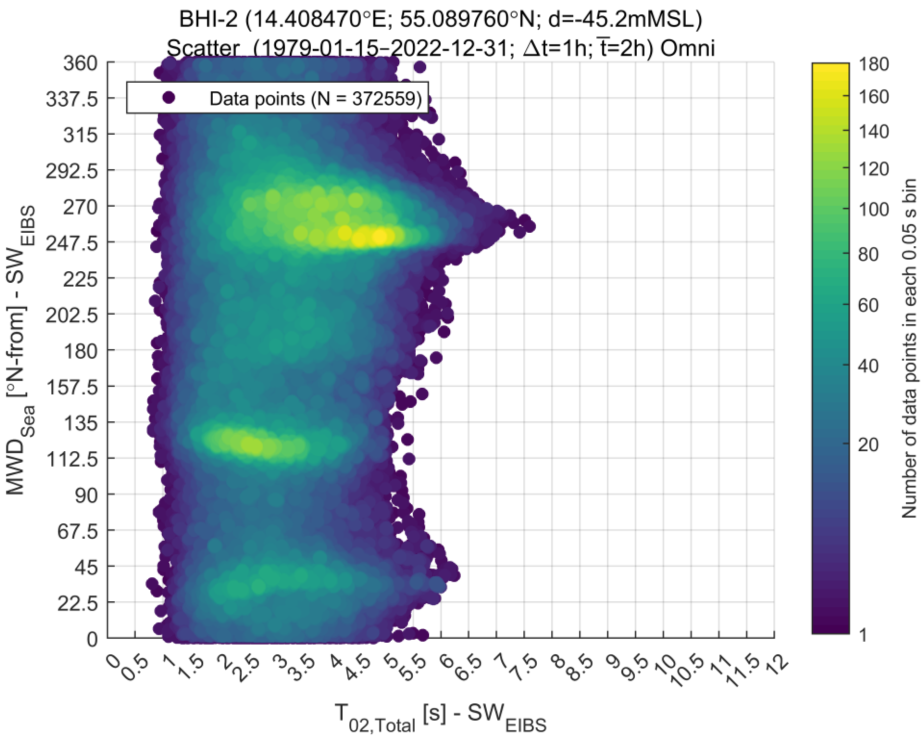

Figure 6.18 Scatter plot at BHI-2; T_{02} vs MWD – Wind-Sea

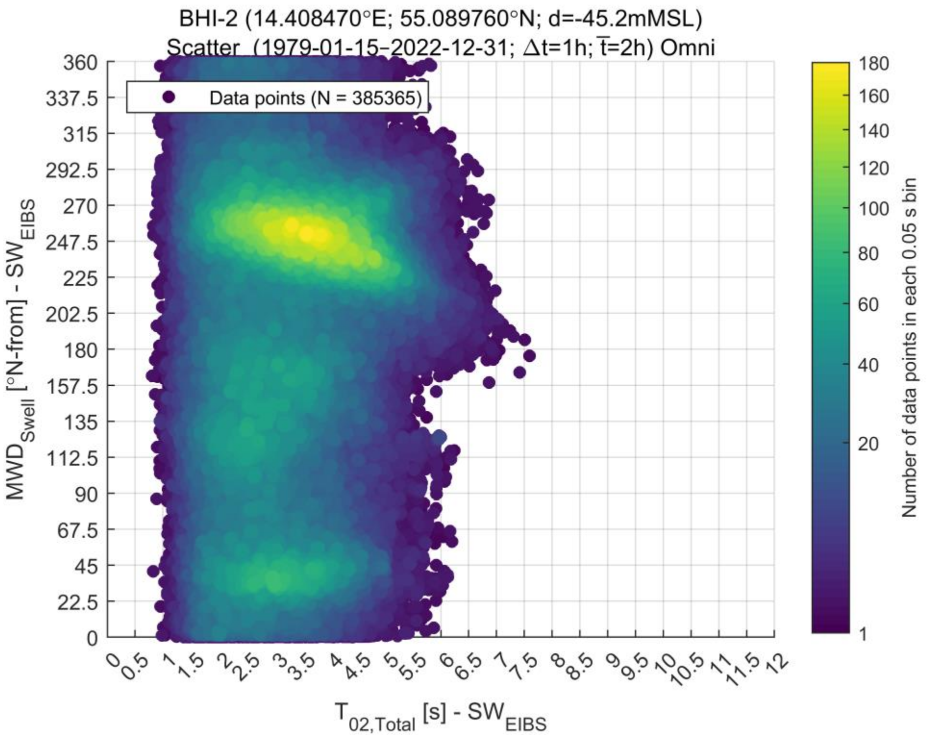

Figure 6.19 Scatter plot at BHI-2; T_{02} vs MWD – Swell

6.1.3 Histogram

Figure 6.20, Figure 6.21, and Figure 6.22 show histogram of H_{m0}, T_p, and T_{02} at BHI-2, respectively.

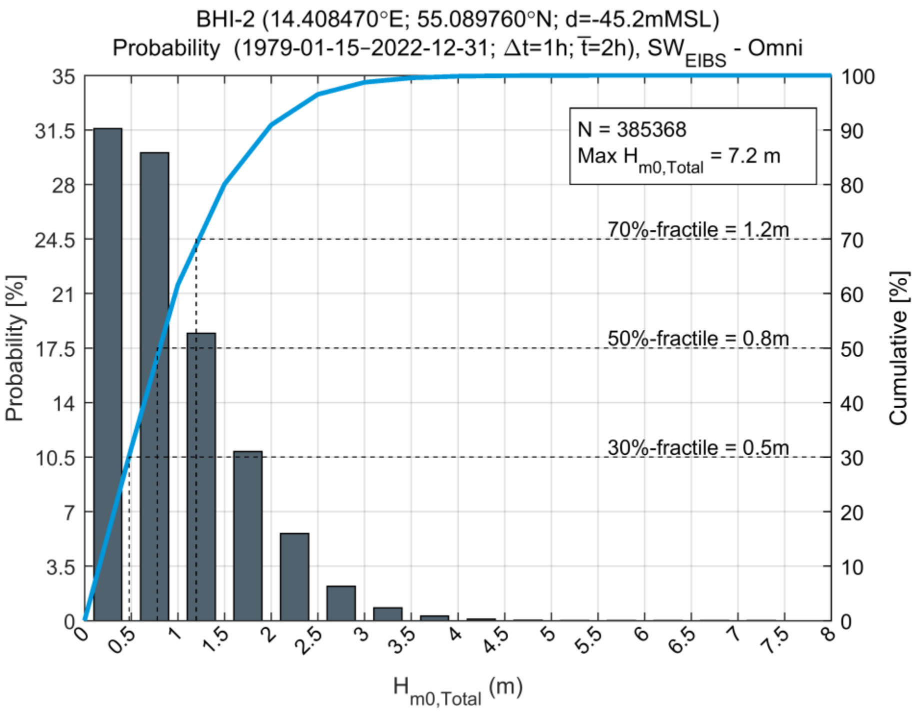

Figure 6.20 Histogram of H_{m0} at BHI-2

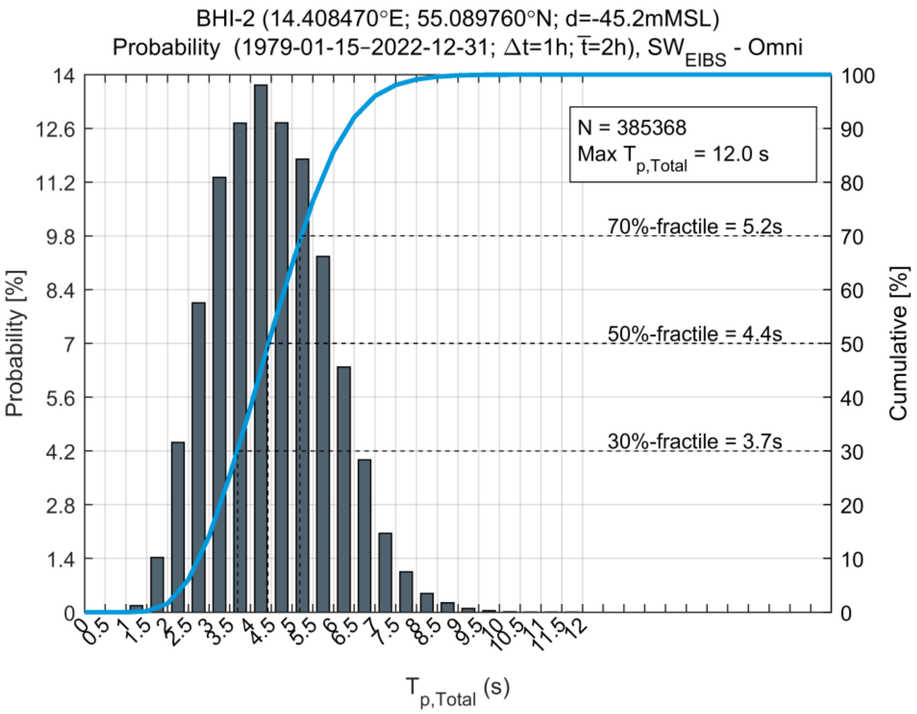

Figure 6.21 Histogram of T_p at BHI-2

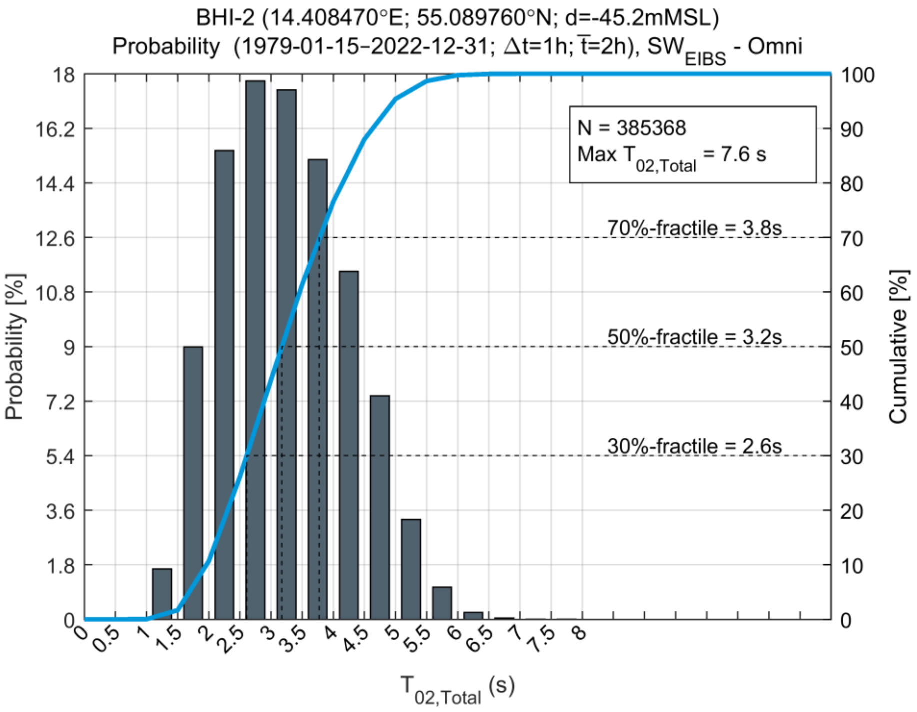

Figure 6.22 Histogram of T_{02} at BHI-2

6.1.4 Monthly statistics

Figure 6.23 shows monthly statistics of significant wave height, H_{m0}, at BHI-2. The mean varies from 0.6 m during summer to 1.4 m during winter. The highest waves occurred during the months of November to February. Figure 6.24 and Figure 6.25 display monthly statistics of T_p and T_{02}, respectively.

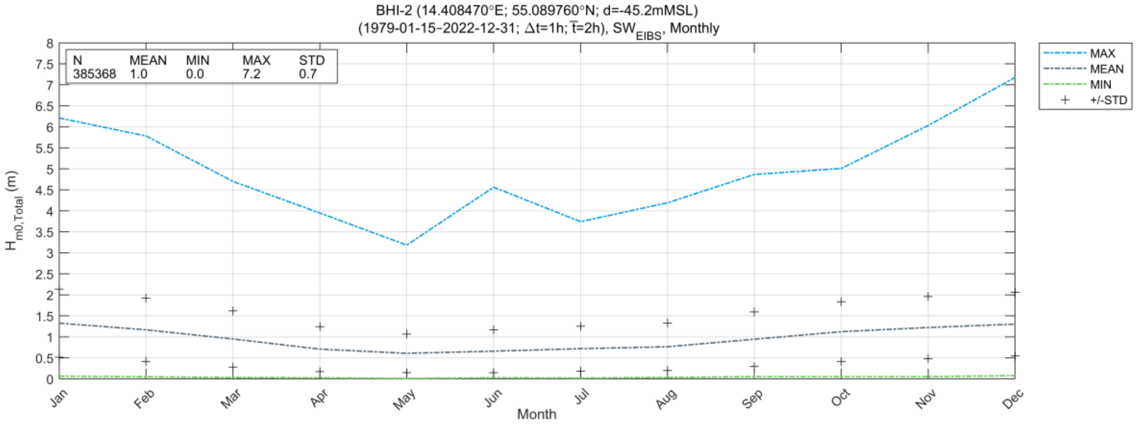

Figure 6.23 Monthly statistics of H_{m0} at BHI-2

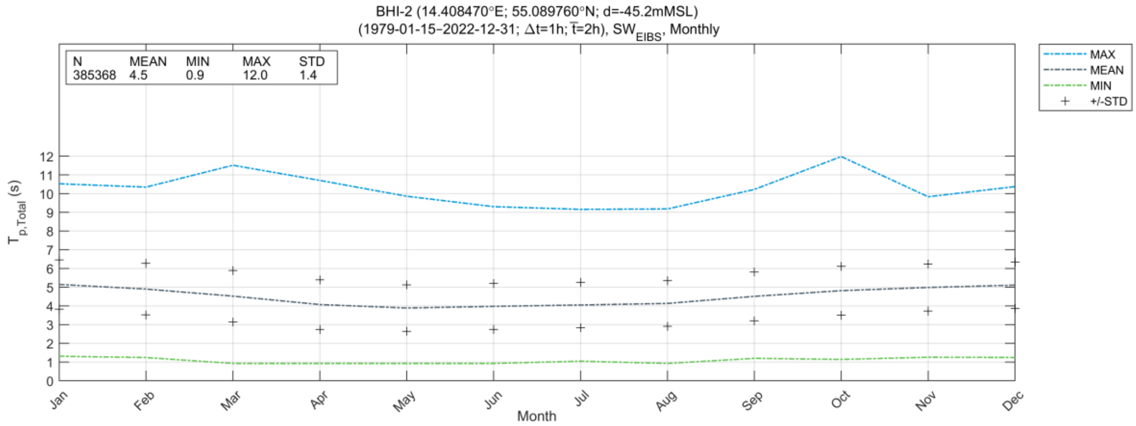

Figure 6.24 Monthly statistics of T_p at BHI-2

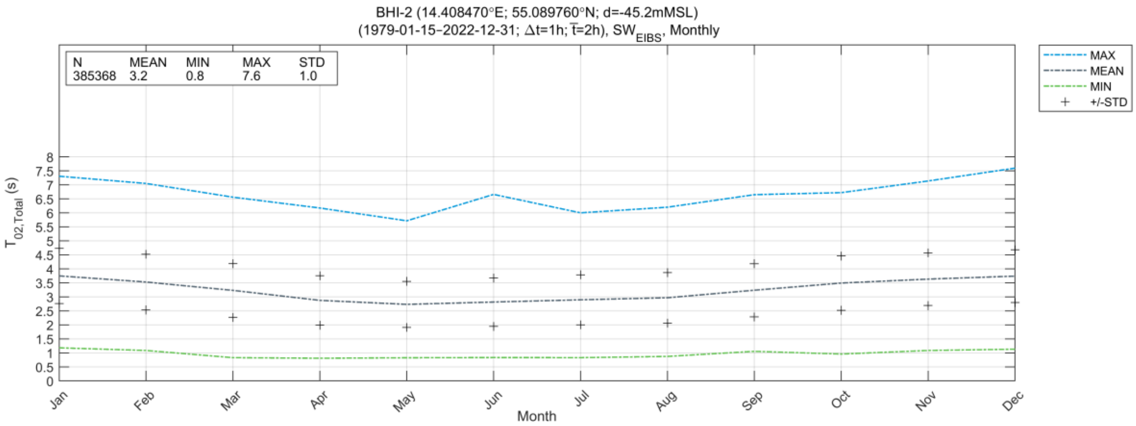

Figure 6.25 Monthly statistics of T_{02} at BHI-2

6.1.5 Directional statistics

Figure 6.26 shows directional statistics of significant wave height at BHI-2. The mean is highest from the south-southwest of about 1.3 m. The highest waves occur from the south-southwest sector with height of 7.2m. Figure 6.26 and Figure 6.28 display directional statistics of T_p and T_{02}, respectively.

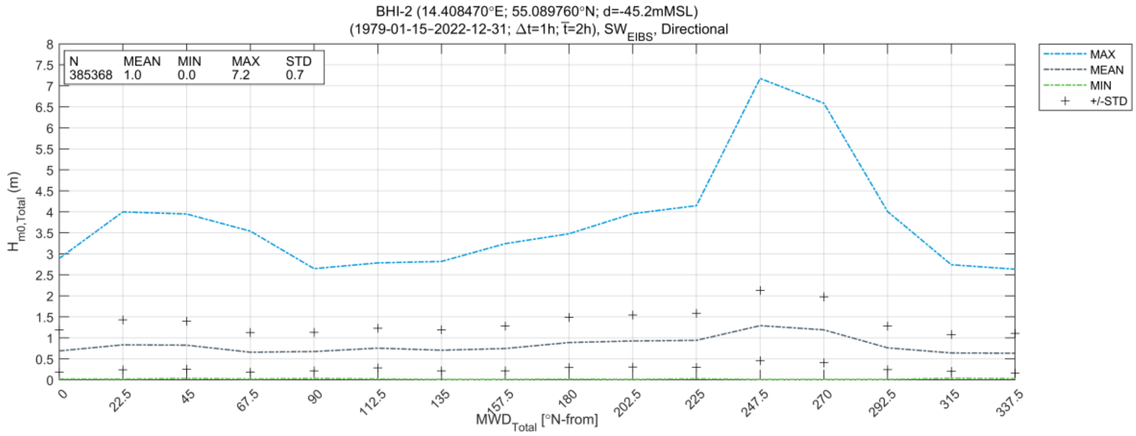

Figure 6.26 Directional statistics of H_{m0} at BHI-2

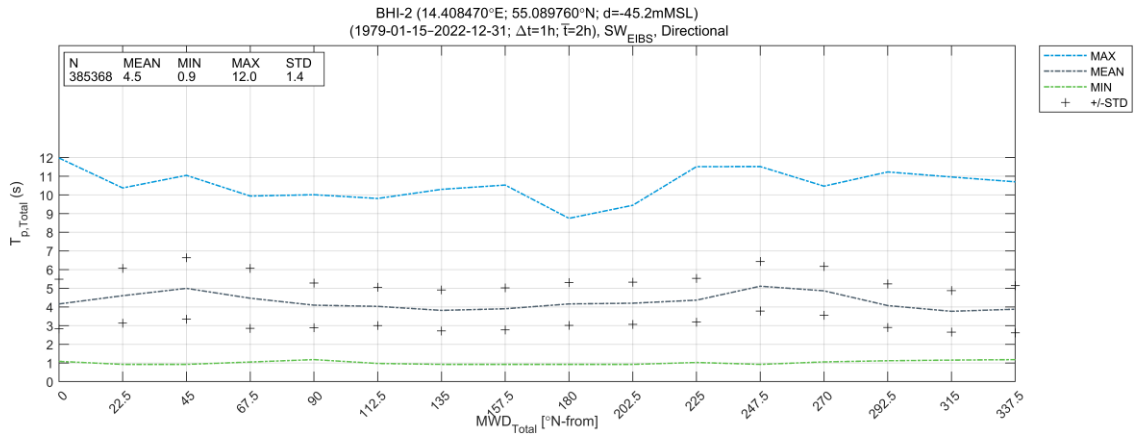

Figure 6.27 Directional statistics of T_p at BHI-2

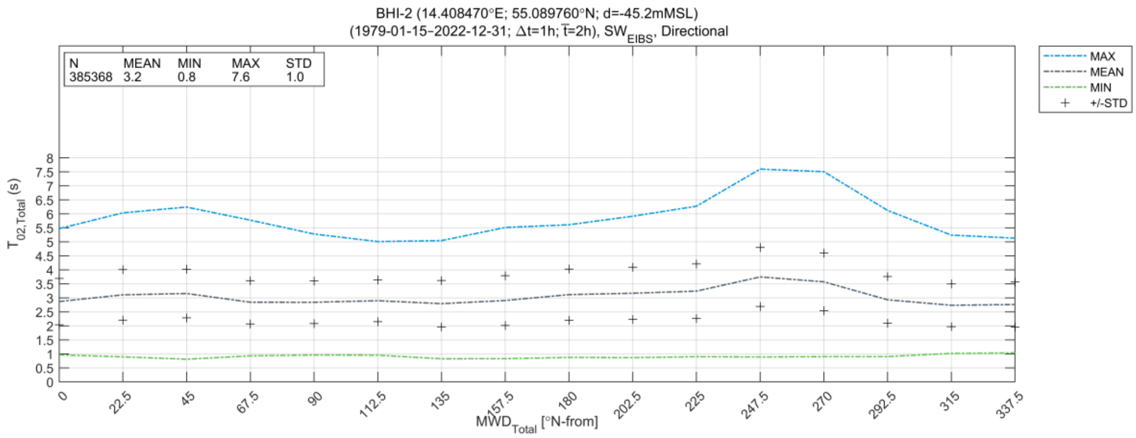

Figure 6.28 Directional statistics of T_{02} at BHI-2

6.1.6 Scatter diagrams (H_{m0})

This section presents scatter diagrams of H_{m0} against the following other metocean parameters at BHI-2:

- Figure 6.29 WS_{10} vs. H_{m0}
- Figure 6.30 H_{m0} vs. T_p
- Figure 6.31 H_{m0} vs. T_{02}
- Figure 6.32 H_{m0} vs. WL
- Figure 6.33 H_{m0} vs. CS

Each scatter diagram includes quantiles and power law fits to the 95%-tile highest data (except for WL and CS).

The scatter of WS_{10} vs H_{m0} shows a reasonable correlation, especially at windspeed higher than 7 m/s.

The wave periods (T_p and T_{02}) are very well correlated with $H_{m0,}$ especially for the high waves that are dominated by local wind.

There is weak correlation between WL (total) and H_{m0}.

The total current speed (CS) is almost entirely uncorrelated with H_{m0}, albeit there is a weak trend of stronger currents during high waves, but with significant scatter.

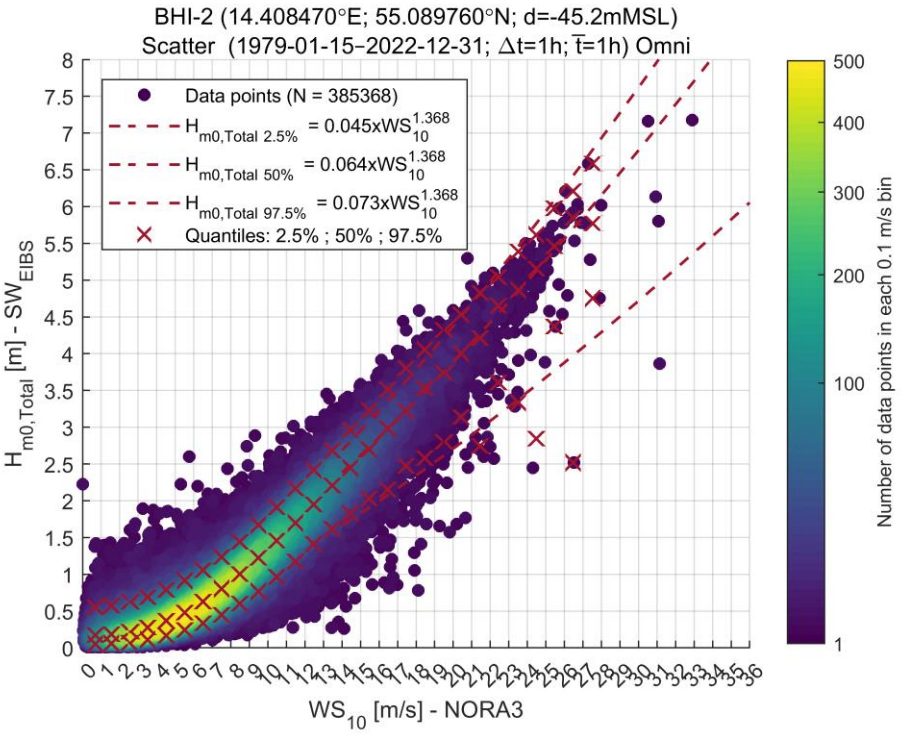

Figure 6.29 Scatter diagram of WS_{10} vs H_{m0} at BHI-2

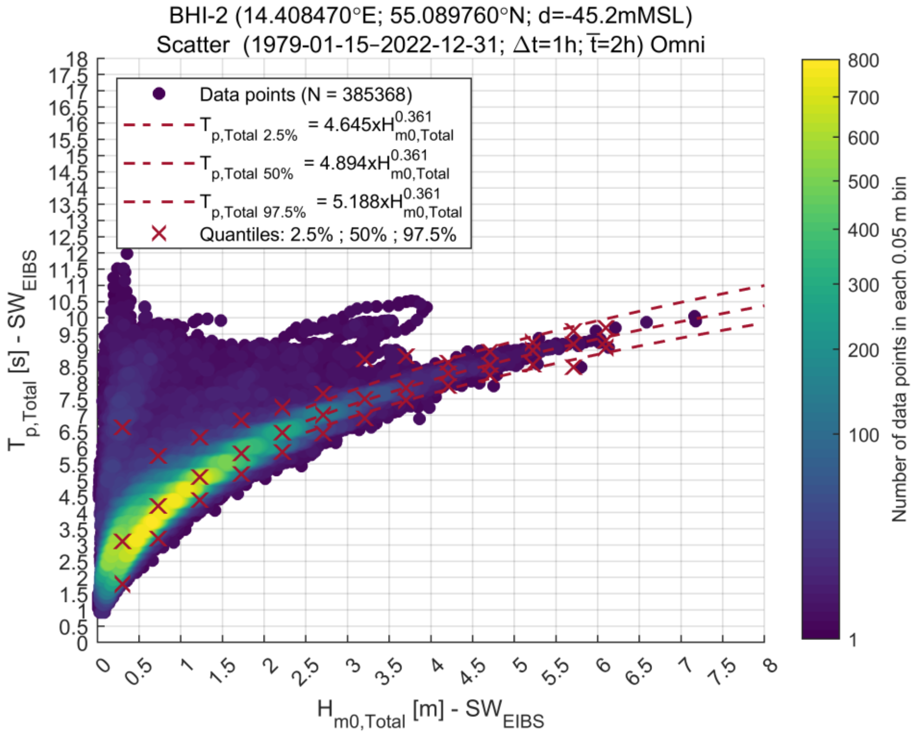

Figure 6.30 Scatter diagram of H_{m0} vs T_p at BHI-2

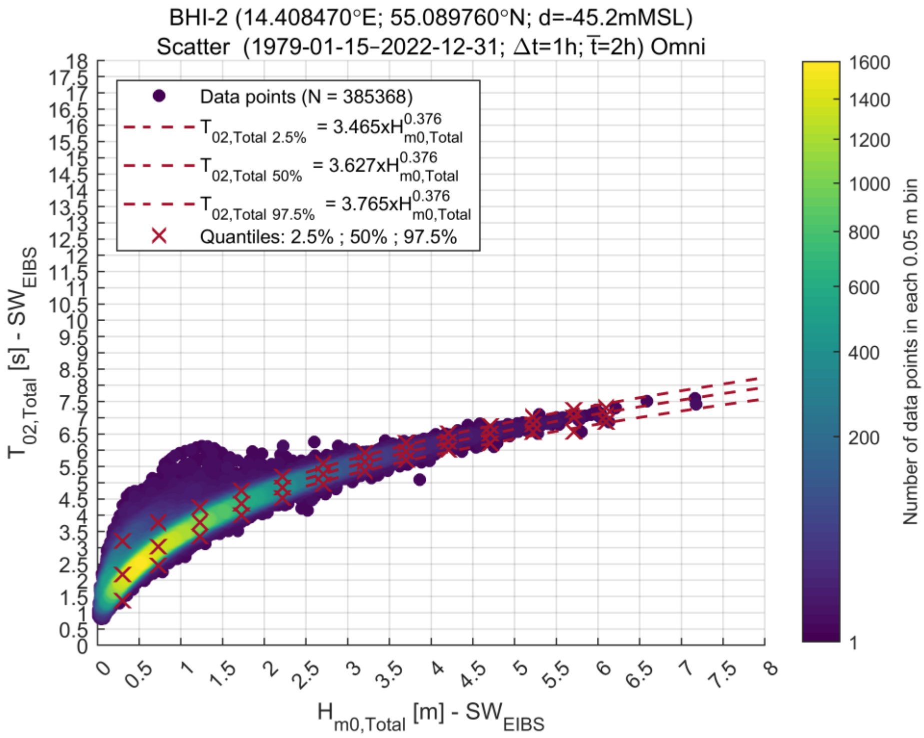

Figure 6.31 Scatter diagram of H_{m0} vs T_{02} at BHI-2

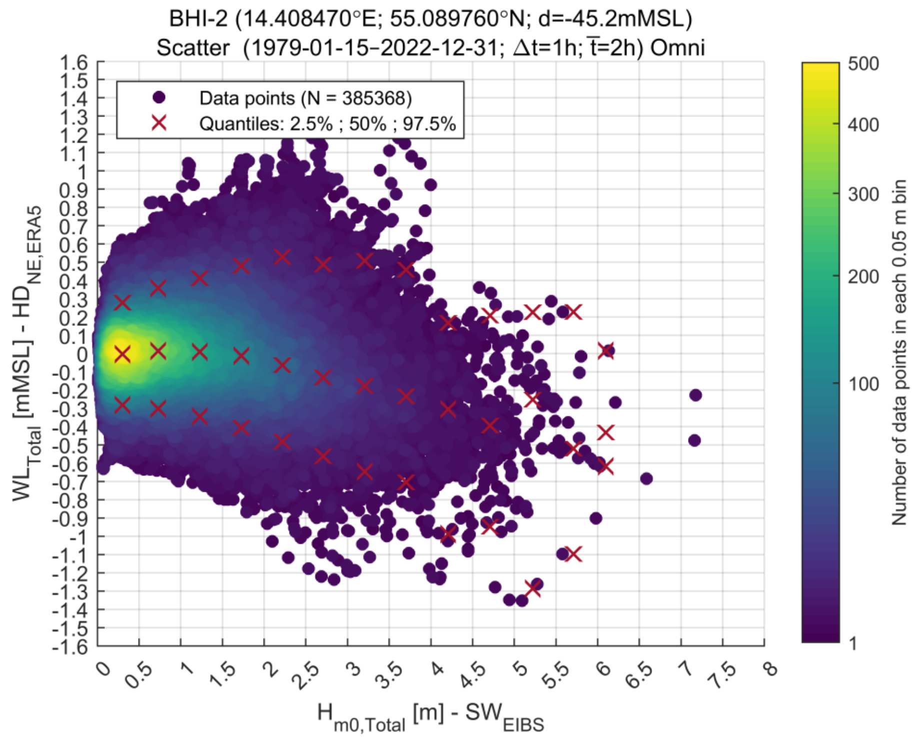

Figure 6.32 Scatter diagram of H_{m0} vs WL at BHI-2

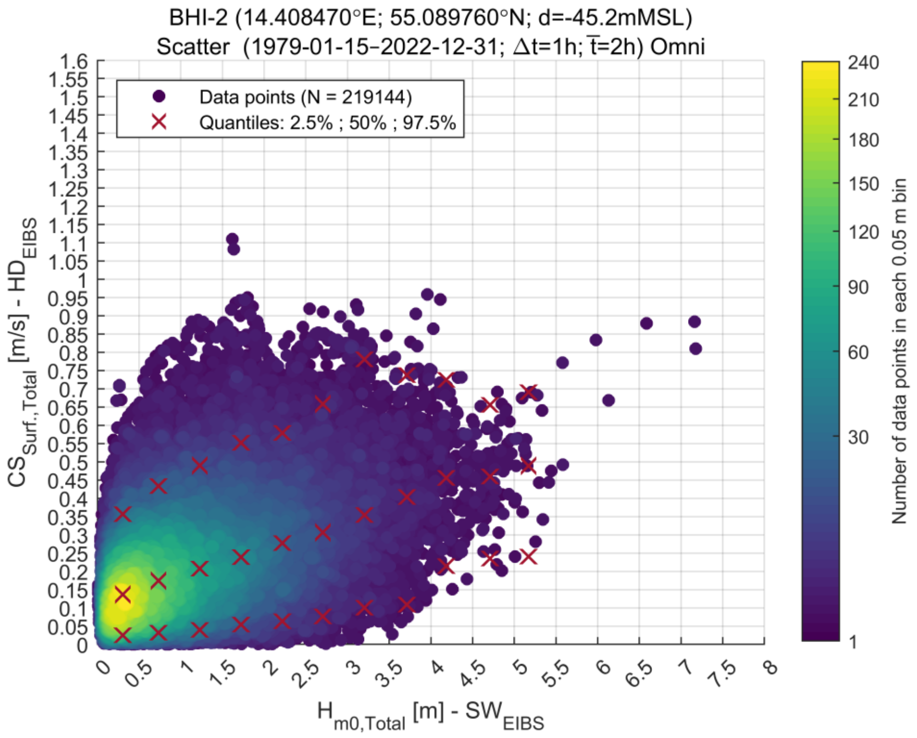

Figure 6.33 Scatter diagram of H_{m0} vs CS at BHI-2

6.1.7 Wind-wave misalignment

The wind-wave misalignment is calculated as WD_{10} minus the MWD. Figure 6.34 presents the misalignment vs. H_{m0} at BHI-2. The curves indicate the mean misalignment for each wind direction sector. The misalignment shows a high scatter for wave height less than ~1 m, while the scatter (misalignment) is relatively low for higher waves when the wind starts to pick up.

Figure 6.35 shows a trend of most frequent misalignment between 0 – 22.5°. For omni and almost all directions, the main probability of misalignment is within ±45°.

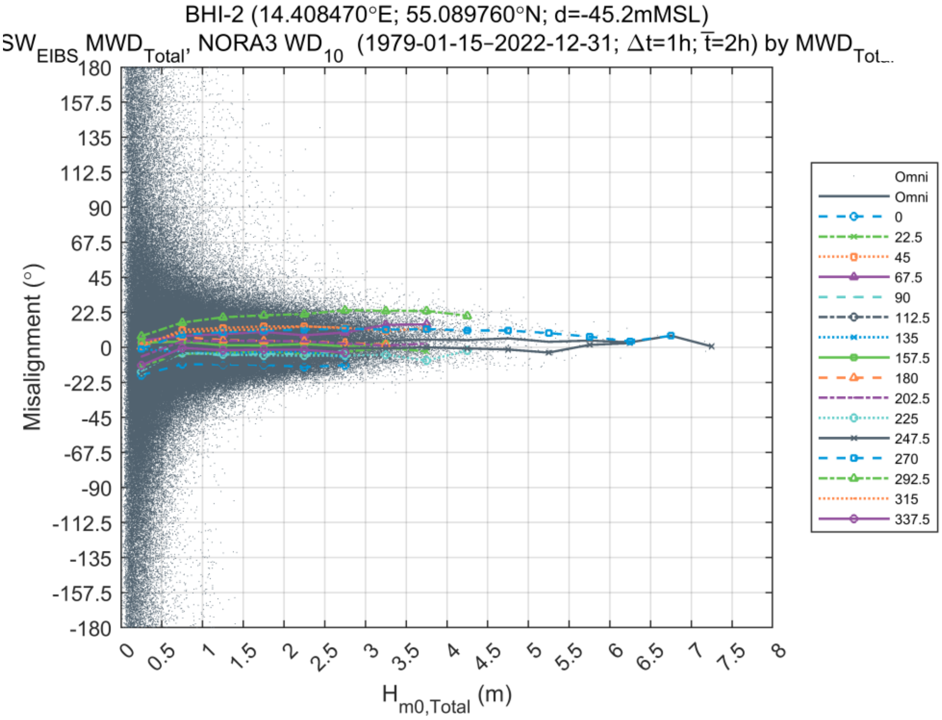

Figure 6.34 Wind-wave misalignment vs. H_{m0} at BHI-2

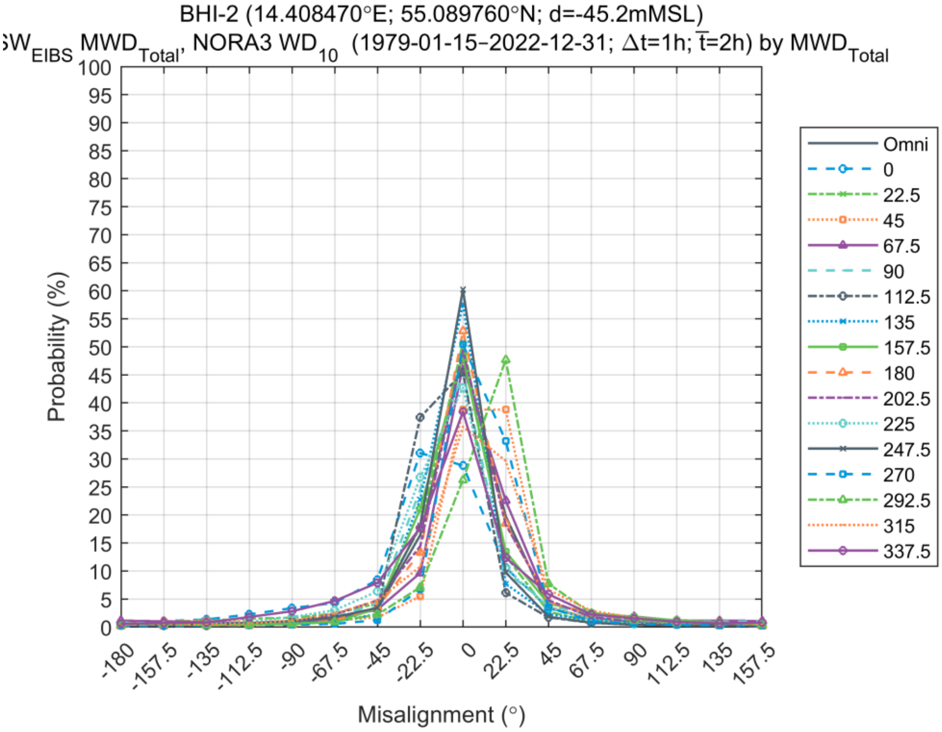

Figure 6.35 Probability of wind-wave misalignment per direction at BHI-2

6.1.8 Maps of mean H_{m0}

Figure 6.36, Figure 6.37, and Figure 6.38 present maps across the EIBS OWF area of the normalised moment of significant wave height, $\overline{H_{m0}}$, calculated as follows.

$$\overline{H_{m0}} = \left[\frac{1}{N}\sum_{i=1}^{N} H_{m0_i}{}^{m}\right]^{\frac{1}{m}} \tag{6.1}$$

where $m = (1,2)$ is the power coefficient, and N is the total number of hindcast data points (m = 1 is the mean H_{m0}, while m = 2 is the root-mean-square wave energy).

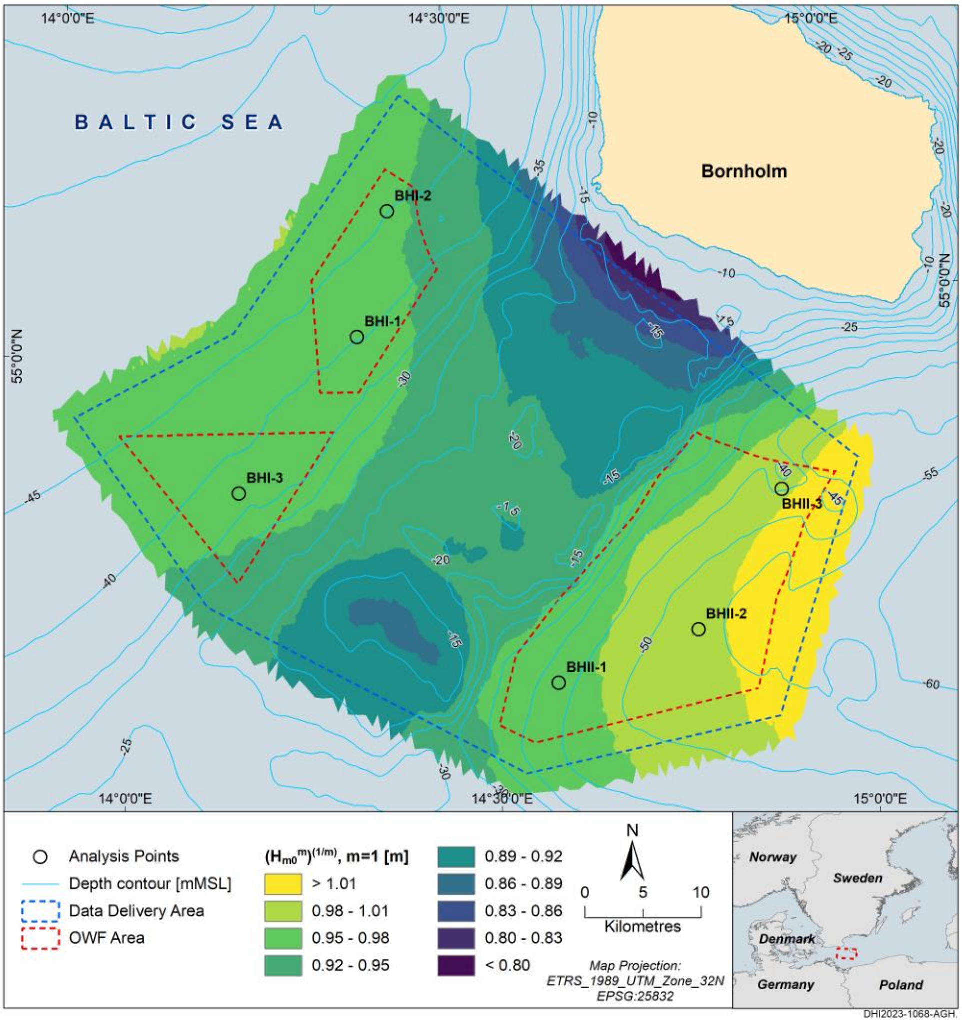

Figure 6.36 Spatial variation of $\overline{H_{m0}}$ across the EIBS OWFs area

The colour map shows the wave height, and the contours show water depth.

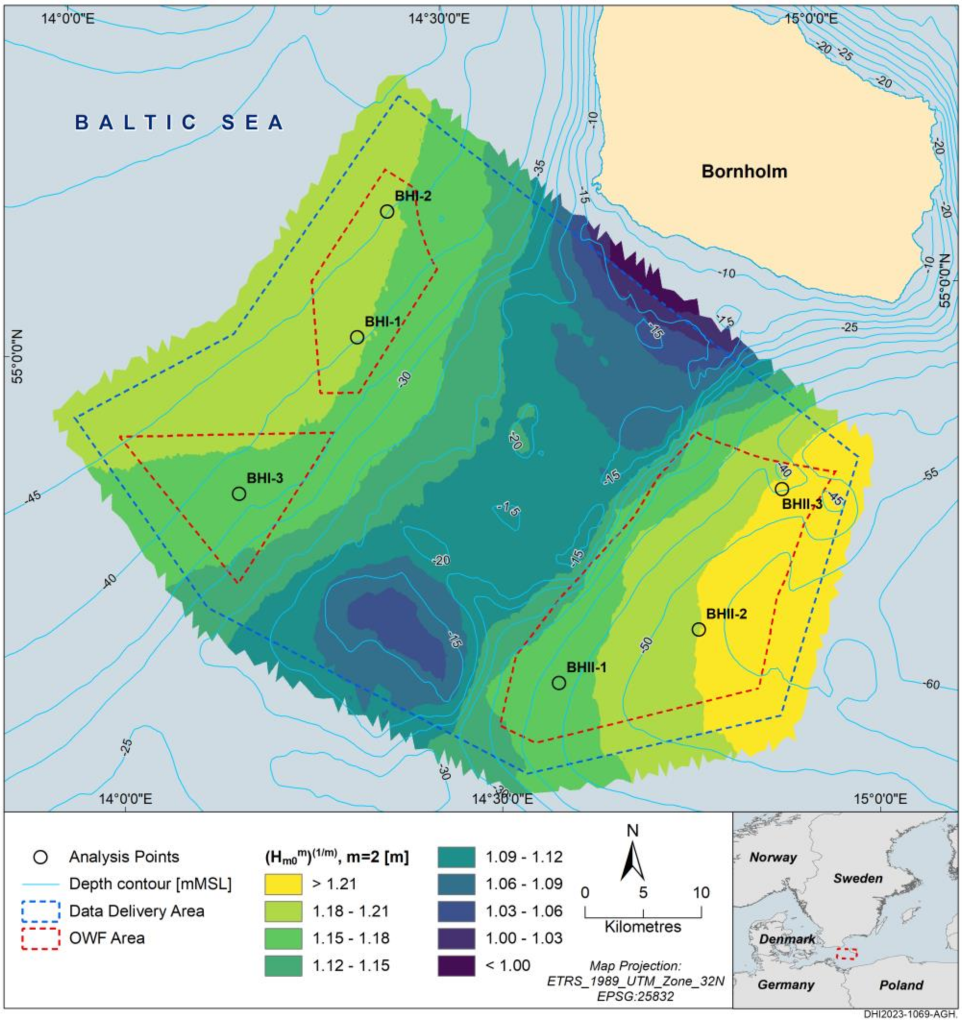

Figure 6.37 Spatial variation of $\sqrt{Hm0^2}$ across the EIBS OWFs area

The colour map shows the wave energy, and the contours show water depth.

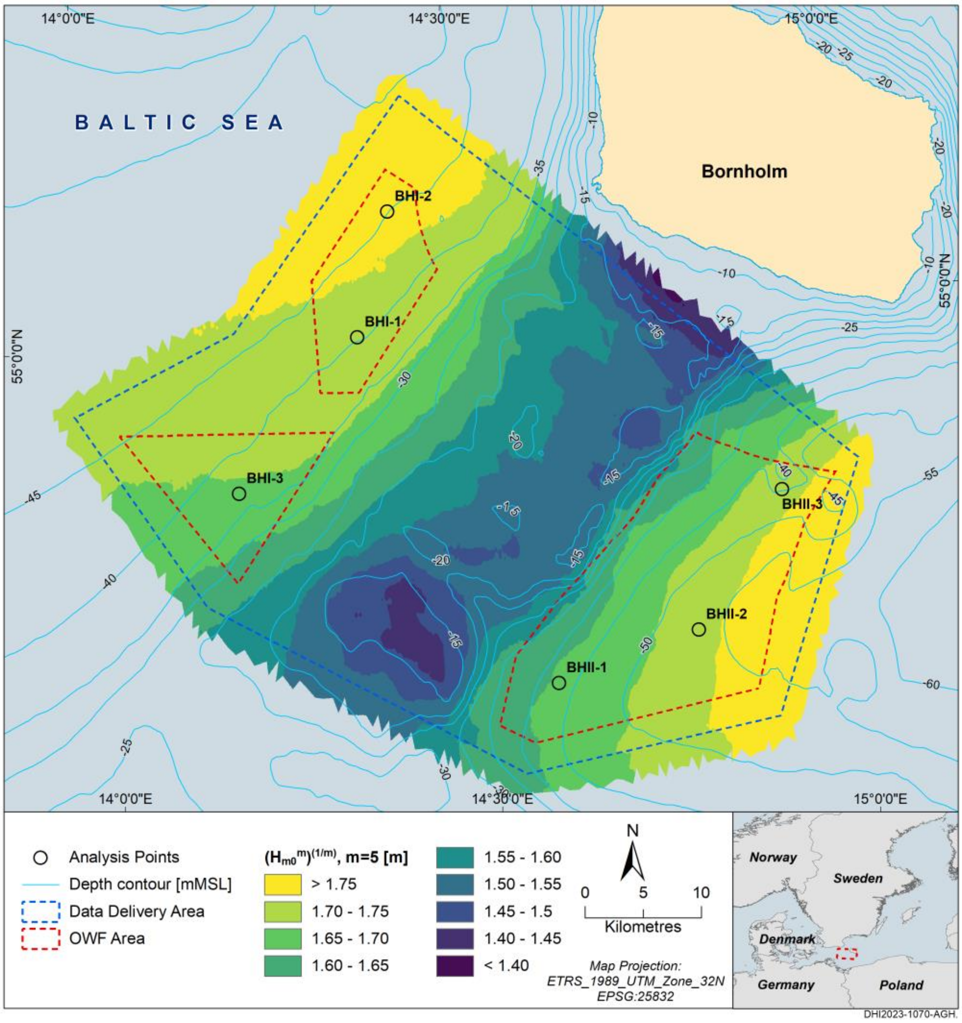

Figure 6.38 Spatial variation of $\sqrt[5]{Hm0^5}$ across the EIBS OWFs area
The colour map shows the wave energy, and the contours show water depth.

6.2 Extreme wave conditions

Extreme wave conditions were established using Traditional Extreme Value Analysis (T-EVA) following the methodology and settings derived and described in Appendix B Sensitivity of T-EVA to Distribution, Threshold, and Fitting.

For waves, the 2-p Weibull distribution was fitted by the least square method to 88 peak events separated by at least 36 hours (annual average of 2 events).

For H_{max}, the Glukhovskiy short-term distribution is used, whereas for C_{max}, the Forristall distribution is used.

$C_{max,MSL}$ is derived by convoluting the short-term distribution with the simultaneous (residual) water level.

6.2.1 Extreme H_{m0} and conditioned $T_p|H_{m0}$

Table 6.3 and Figure 6.39 present the directional extreme significant wave height, H_{m0}, at BHI-2. The fitted distribution aligns very well to the hindcast data points, also at the tail, and all events are within the confidence levels, which gives confidence in the derived values. The directional extreme values are constrained to the omni-directional extreme values.

The conditioned $T_p|H_{m0}$ is estimated by fits to the upper 95%-tile of scatter plot given in Figure 6.30.

Table 6.3 Extreme total significant wave height, H_{m0}, at BHI-2

Direction	$H_{m0, Total}$ [m]			
	T_R 1 year	T_R 5 years	T_R 10 years	T_R 50 years
0°	2.6	3.0	3.1	3.4
22.5°	3.2	3.7	3.9	4.4
45°	3.2	3.9	4.1	4.8
67.5°	2.5	3.1	3.3	3.9
90°	2.3	2.6	2.7	3.0
112.5°	2.4	2.8	3.0	3.3
135°	2.5	2.7	2.8	3.0
157.5°	2.7	3.0	3.1	3.5
180°	3.1	3.4	3.5	3.8
202.5°	3.4	3.9	4.1	4.5
225°	3.6	4.0	4.2	4.6
247.5°	4.4	5.3	5.7	6.6
270°	4.4	5.3	5.7	6.6
292.5°	3.4	4.1	4.4	5.1
315°	2.4	2.7	2.9	3.2
337.5°	2.4	2.7	2.9	3.2
Omni	4.4	5.3	5.7	6.6

Table 6.4 Conditioned peak wave period, $T_{p|Hm0}$, at BHI-2

Direction	$T_{p\|Hm0}$ [s]			
	T_R 1 year	T_R 5 years	T_R 10 years	T_R 50 years
0°	6.7	7.1	7.2	7.5
22.5°	7.8	8.4	8.6	9.1
45°	8.6	9.3	9.6	10.1
67.5°	8.5	9.4	9.8	10.7
90°	5.8	6.1	6.1	6.3
112.5°	6.4	6.7	6.8	7.1
135°	6.4	6.6	6.7	6.9
157.5°	6.6	6.9	7.0	7.3
180°	6.9	7.1	7.2	7.5
202.5°	7.0	7.4	7.5	7.8
225°	7.4	7.7	7.8	8.1
247.5°	8.4	9.0	9.2	9.7
270°	8.4	9.0	9.2	9.7
292.5°	7.7	8.4	8.6	9.2
315°	6.3	6.6	6.7	7.0
337.5°	6.4	6.7	6.8	7.1
Omni	8.4	8.9	9.2	9.7

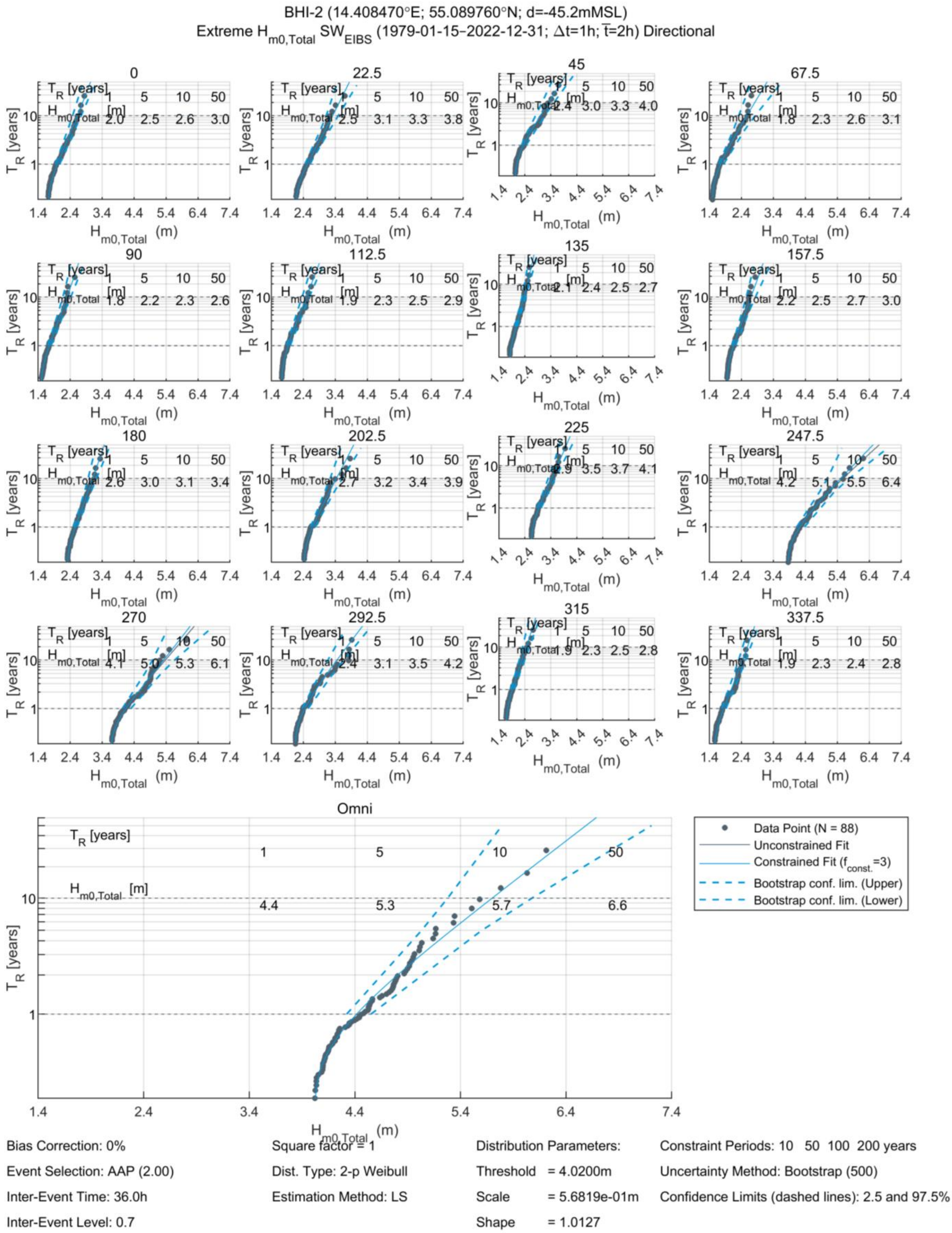

Figure 6.39 Extreme significant wave height, H_{m0} at BHI-2

6.2.2

6.2.2 Extreme H_{max} and conditioned T_{Hmax}

Table 6.5 and Figure 6.40 present the extreme maximum wave height, H_{max}, at BHI-2, while Table 6.6 gives the conditioned wave period, T_{Hmax}.

T_{Hmax} is taken as 0.9 x T_p as suggested in [3].

Table 6.5 Extreme maximum wave height, H_{max}, at BHI-2

Direction	H_{max} [m]			
	T_R 1 year	T_R 5 years	T_R 10 years	T_R 50 years
0°	5.0	5.8	6.1	6.8
22.5°	6.6	7.6	8.1	9.1
45°	6.6	8.0	8.6	10.0
67.5°	5.1	6.4	7.0	8.4
90°	4.6	5.3	5.6	6.2
112.5°	5.1	5.9	6.3	7.0
135°	5.3	5.9	6.1	6.7
157.5°	5.5	6.3	6.6	7.4
180°	6.3	7.1	7.4	8.1
202.5°	6.6	7.7	8.2	9.2
225°	6.9	7.7	8.0	8.8
247.5°	8.6	10.4	11.1	12.7
270°	8.6	10.4	11.1	12.7
292.5°	6.4	7.7	8.2	9.5
315°	4.5	5.3	5.6	6.4
337.5°	4.5	5.5	5.8	6.7
Omni	8.6	10.4	11.1	12.7

Table 6.6 Extreme conditioned wave period, T_{Hmax}, at BHI-2

Direction	T_{Hmax} [s]			
	T_R 1 year	T_R 5 years	T_R 10 years	T_R 50 years
0°	6.1	6.3	6.5	6.7
22.5°	7.1	7.6	7.8	8.2
45°	7.8	8.4	8.6	9.1
67.5°	7.6	8.5	8.9	9.6
90°	5.3	5.5	5.5	5.7
112.5°	5.7	6.0	6.1	6.4
135°	5.8	6.0	6.0	6.2
157.5°	5.9	6.2	6.3	6.5
180°	6.2	6.4	6.5	6.7
202.5°	6.3	6.6	6.8	7.0
225°	6.6	6.9	7.1	7.3
247.5°	7.6	8.1	8.3	8.8
270°	7.5	8.1	8.3	8.7
292.5°	7.0	7.5	7.8	8.3
315°	5.7	6.0	6.0	6.3
337.5°	5.7	6.0	6.1	6.4
Omni	7.5	8.1	8.3	8.7

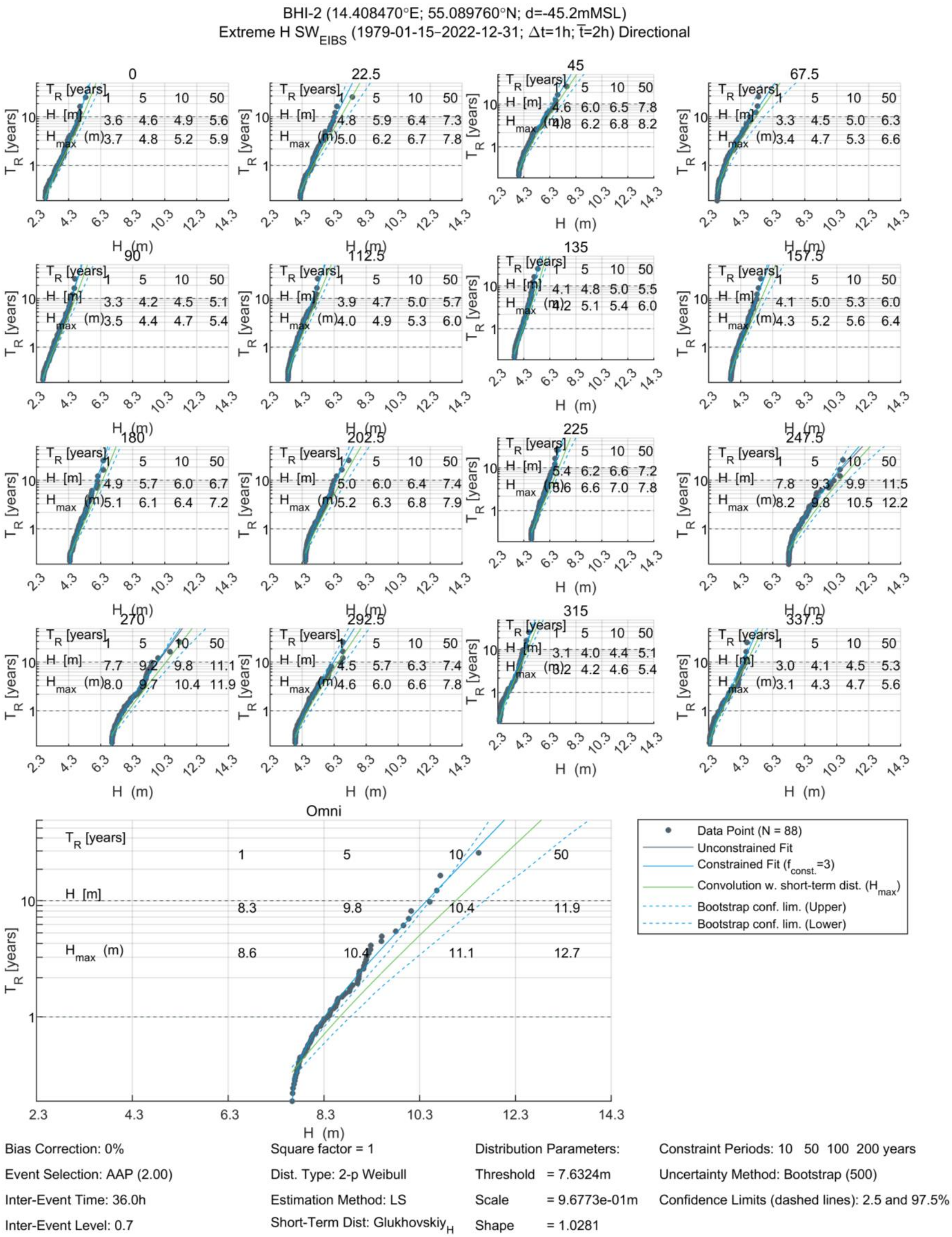

Figure 6.40 Extreme maximum wave height, H_{max}, at BHI-2

6.2.3 Extreme C_{max}

Table 6.7 and Figure 6.41 present the directional extreme maximum wave crest height to MSL, $C_{max,MSL}$, at BHI-2. Table 6.8 and Figure 6.42 present the directional extreme maximum wave crest height to SWL, $C_{max,SWL}$, at BHI-2.

Table 6.7 Extreme wave crest to MSL, $C_{max,MSL}$, at BHI-2

Direction	$C_{max,\,MSL}$ [m]			
	T_R 1 year	T_R 5 years	T_R 10 years	T_R 50 years
0°	3.4	4.1	4.4	5.0
22.5°	4.4	5.2	5.5	6.2
45°	4.3	5.2	5.6	6.5
67.5°	3.3	4.1	4.5	5.4
90°	2.9	3.4	3.6	4.0
112.5°	3.1	3.7	3.9	4.4
135°	3.1	3.5	3.7	4.0
157.5°	3.1	3.5	3.7	4.1
180°	3.6	4.0	4.2	4.7
202.5°	3.7	4.3	4.6	5.3
225°	3.8	4.3	4.5	5.0
247.5°	4.8	5.9	6.3	7.3
270°	4.8	5.9	6.3	7.3
292.5°	3.6	4.3	4.6	5.2
315°	2.8	3.3	3.5	4.0
337.5°	3.0	3.6	3.8	4.4
Omni	4.8	5.9	6.3	7.3

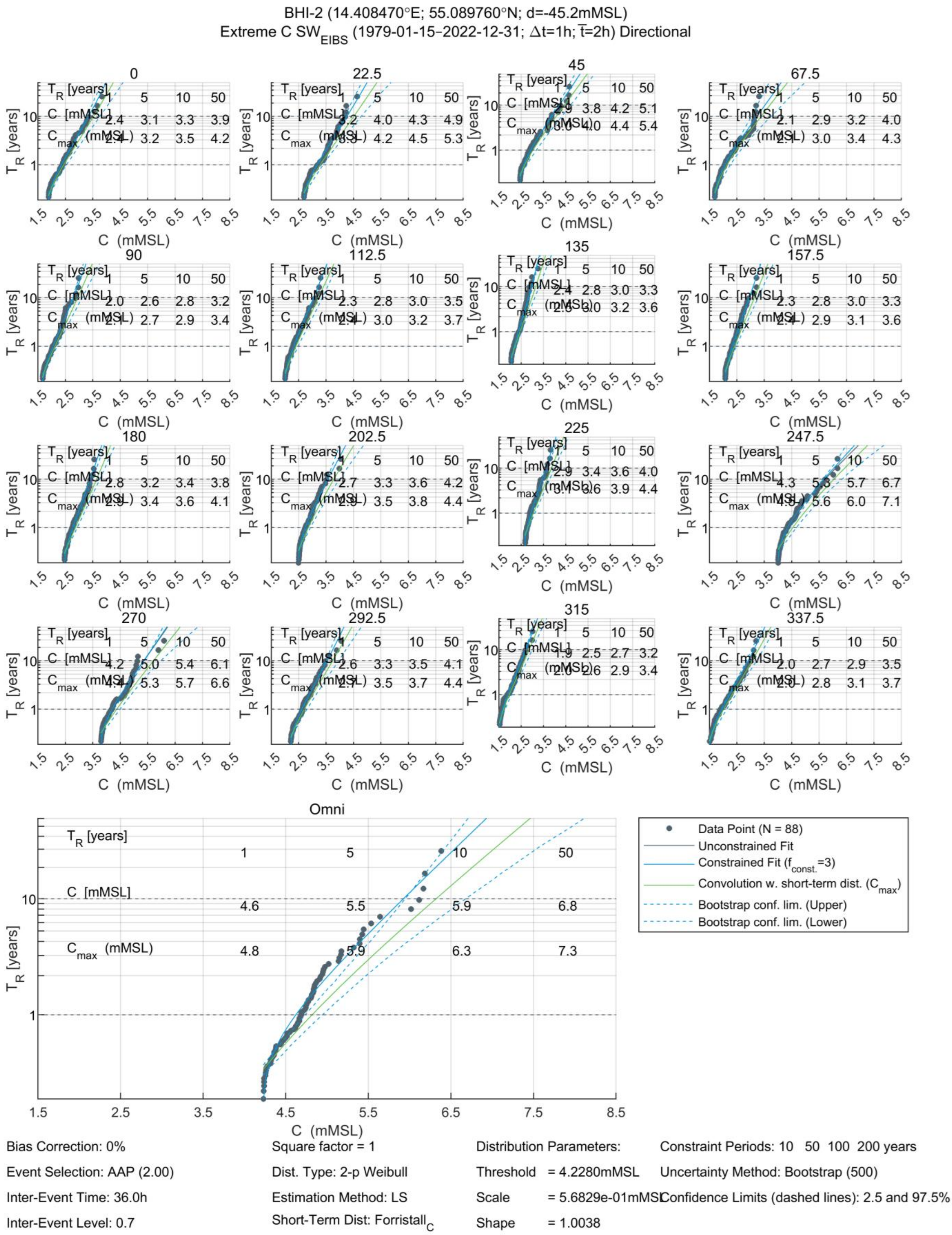

Figure 6.41 Extreme wave crest to MSL, $C_{max,MSL}$, at BHI-2

Table 6.8 Extreme wave crest to SWL, $C_{max,SWL}$, at BHI-2

Direction	$C_{max, SWL}$ [m]			
	T_R 1 year	T_R 5 years	T_R 10 years	T_R 50 years
0°	2.8	3.3	3.5	3.9
22.5°	3.7	4.4	4.7	5.3
45°	3.8	4.6	5.0	5.8
67.5°	2.9	3.7	4.0	4.9
90°	2.6	3.0	3.2	3.5
112.5°	2.9	3.4	3.6	4.0
135°	3.0	3.4	3.5	3.8
157.5°	3.1	3.6	3.8	4.3
180°	3.6	4.1	4.3	4.7
202.5°	3.8	4.5	4.8	5.4
225°	3.9	4.4	4.6	5.1
247.5°	5.0	6.1	6.6	7.6
270°	5.0	6.1	6.6	7.6
292.5°	3.6	4.4	4.7	5.5
315°	2.5	3.0	3.2	3.6
337.5°	2.5	3.1	3.3	3.8
Omni	5.0	6.1	6.6	7.6

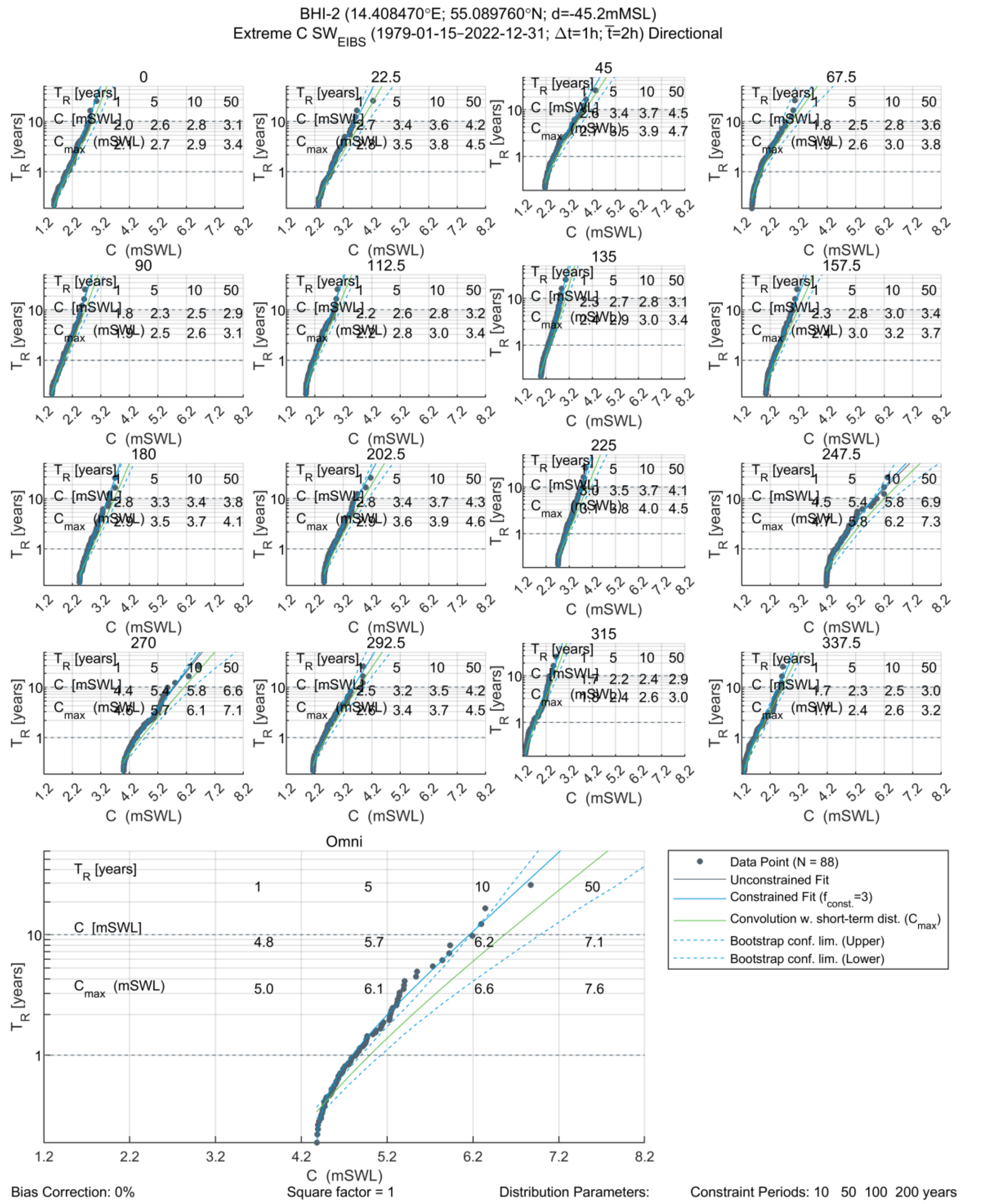

Bias Correction: 0%
Event Selection: AAP (2.00)
Inter-Event Time: 36.0h
Inter-Event Level: 0.7

Square factor = 1
Dist. Type: 2-p Weibull
Estimation Method: LS
Short-Term Dist: $Forristall_C$

Distribution Parameters:
Threshold = 4.3782mSWL
Scale = 5.9653e-01mSWL
Shape = 1.0034

Constraint Periods: 10 50 100 200 years
Uncertainty Method: Bootstrap (500)
Confidence Limits (dashed lines): 2.5 and 97.5%

Figure 6.42 Extreme wave crest to SWL, $C_{max,SWL}$, at BHI-2

6.2.4 Maps of extreme H_{m0}

Figure 6.43 to Figure 6.46 present the spatial variation of significant wave height across the EIBS OWF areas for return periods of 1, 5, 10, and 50-years based on traditional extreme value analysis at each mesh element. The highest extreme values can be found in the northern part of the study area, where it has a longer fetch for the strong westerly winds.

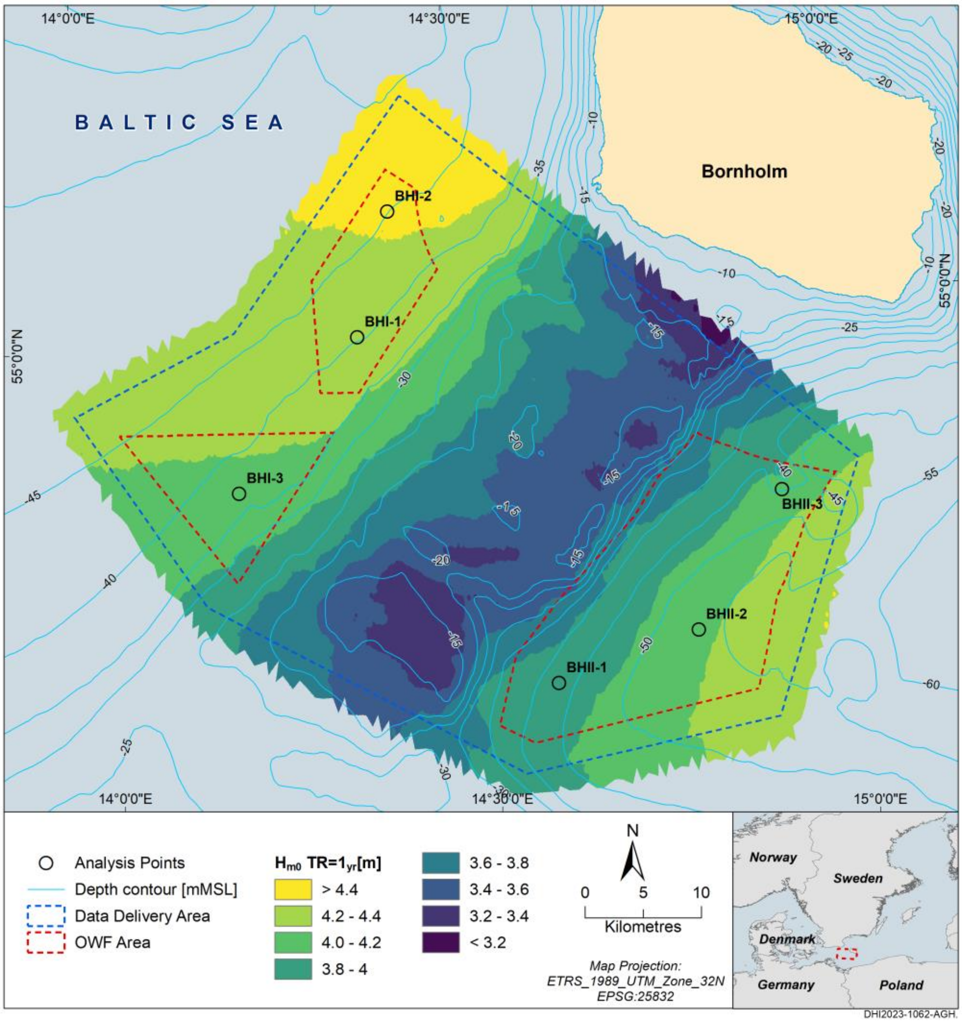

Figure 6.43 Spatial variation across EIBS OWF area of H_{m0} for return period of 1 year

The colour map shows the wave height, and the contours shows water depth.

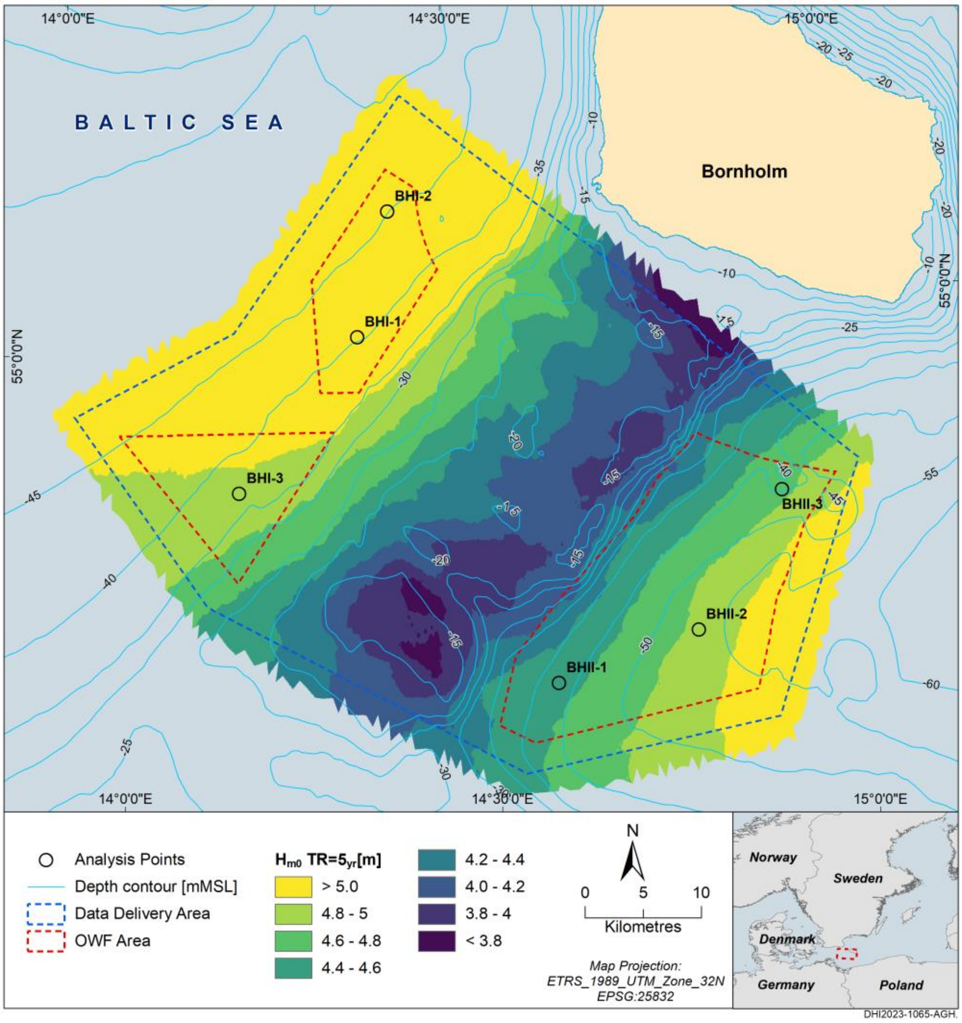

Figure 6.44 Spatial variation across EIBS OWF area of H_{m0} for return period of 5 years

The colour map shows the wave height, and the contours shows water depth.

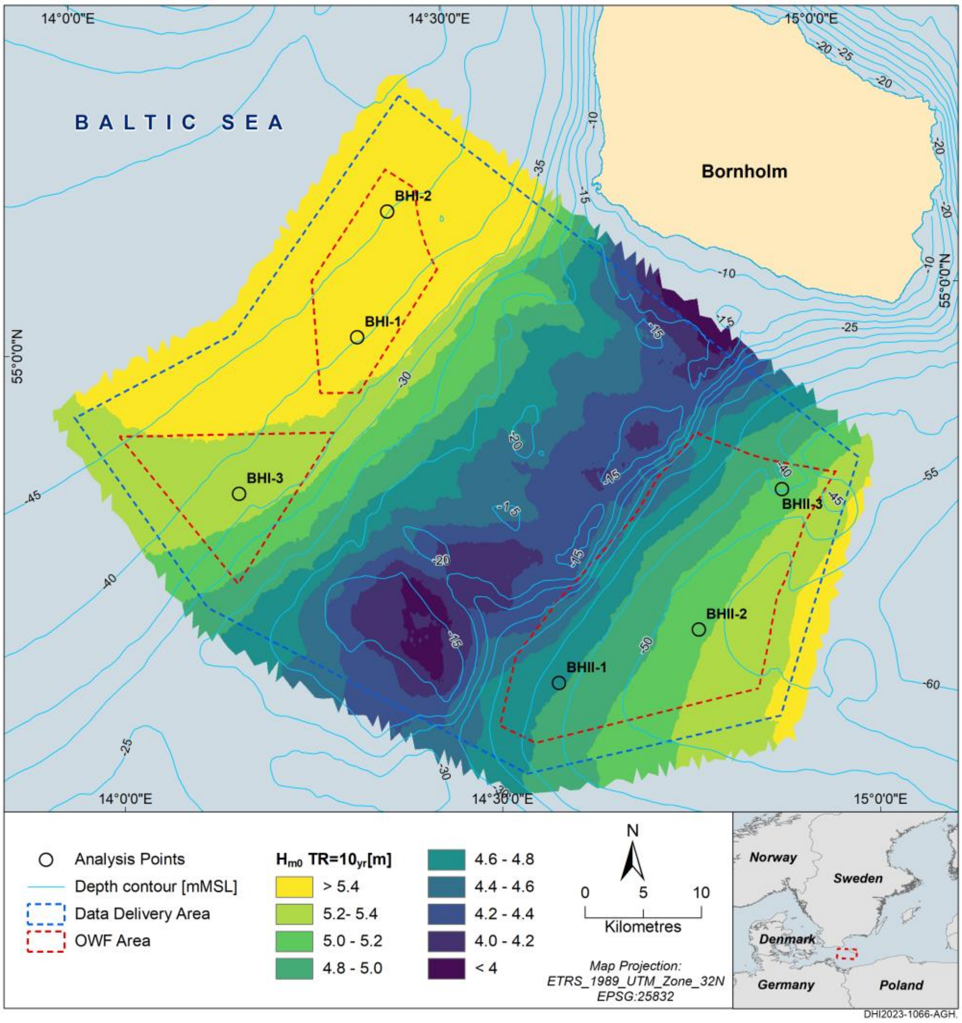

Figure 6.45 Spatial variation across EIBS OWF area of H_{m0} for return period of 10 years

The colour map shows the wave height, and the contours shows water depth.

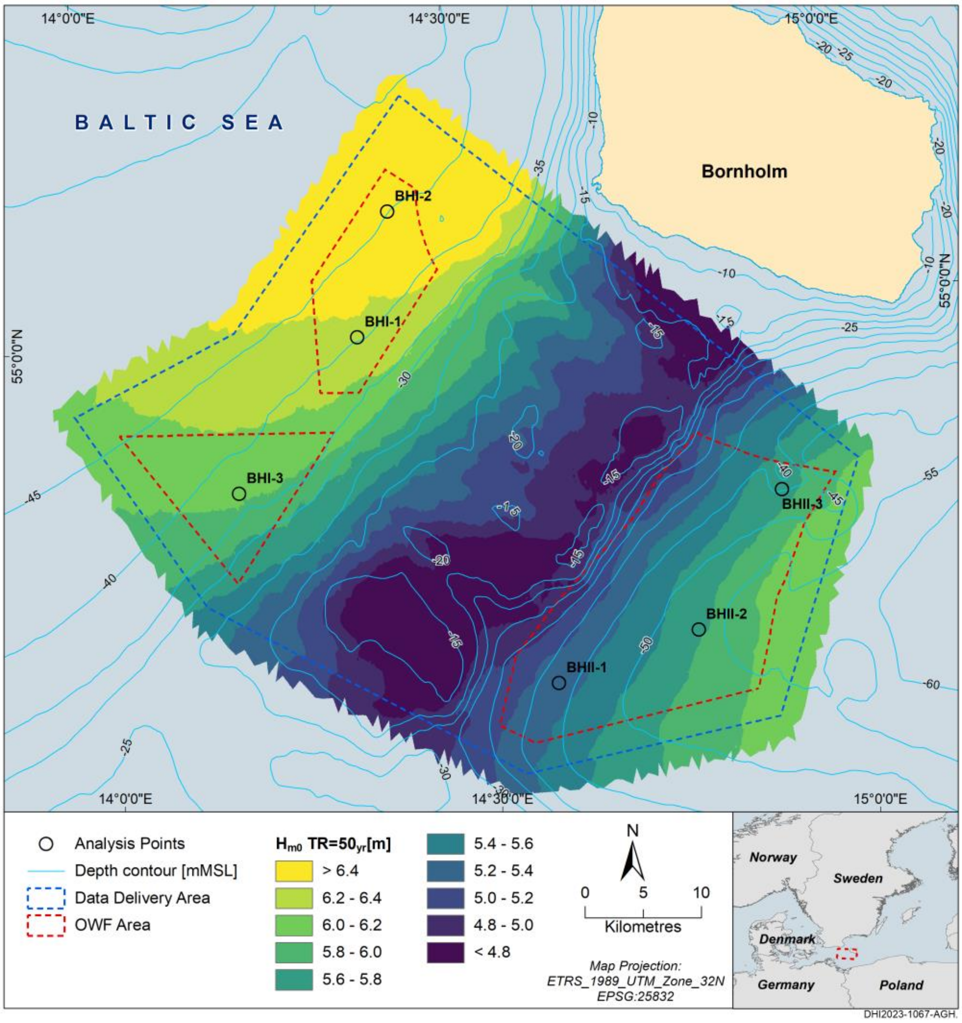

Figure 6.46 Spatial variation across EIBS OWF area of H_{m0} for return period of 50 years

The colour map shows the wave height, and the contours shows water depth.

6.3 Wave spectra

Recommendations of wave spectra wave spectra and parameters are given in Part A, [1], Section 6.4. For H_{m0} > 0.5 m, the spectrum is single-peaked and can be well represented by a JONSWAP spectrum. For information on JONSWAP gamma values, it is recommended to apply the guidelines in Section 3.5.5 of RP-C205 [3], i.e. defining γ based on T_p and H_{m0}.

6.4 Wave breaking and limitations

A commonly adopted criterion for steepness-induced wave breaking is given in Section 3.4.6.1 of DNV RP-C205, [3], see Eq. 6.1. This criterion is applicable to regular waves on a plane seabed. However, the extreme waves at EIBS are not regular, and it is well known that irregular and directionally spread (short-crested) sea states can support higher waves, hence, such a method should only be used with adequate mitigation measures.

$$\frac{H_b}{\lambda} = 0.142 \tanh\left(\frac{2\pi d}{\lambda}\right) \qquad \textbf{Eq. 6.1}$$

Where λ is the wavelength corresponding to water depth d. In deep water, the breaking wave limit corresponds to a maximum steepness of $S_{max} = H_b/\lambda = 1/7$.

Table 6.9 presents the recommended limits to H_{max} and C_{max} at all analysis points for 50 years return period.

Table 6.9 Recommended limits to H_{max} and C_{max}, 50 years return period, based on DNV steepness criteria

Name	d [mMSL]	1.13 x $T_{Hmax,50\%}$ [s]	$H_{max.Glukhovskiy}$ [m]	$H_{b.steepness}$ [m]	$C_{b.\,Steepness}$ [m] (=0.85 x H_b)
BHI-1	-40.5	9.8	12.2	19.1	16.2
BHI-2	-45.2	9.8	12.7	19.7	16.7
BHI-3	-37.0	9.5	11.5	17.7	15.1
BHII-1	-43.0	9.4	10.8	18.3	15.5
BHII-2	-53.6	10.6	11.6	23.1	19.7
BHII-3	-42.2	10.5	11.1	21.1	18.0

7 Other Atmospheric and Oceanographic Conditions

This section presents analyses of other atmospheric conditions wind and oceanographic conditions including air temperature, humidity, solar radiation, lightning. Other oceanographic conditions include seawater temperature and salinity. One point at BHI-2 is selected as representative for the area.

7.1 Air temperature, humidity, and solar radiation

Modelled air temperature at 2 m above sea level and relative humidity are based on NORA3 (1979-01-15 to 2022-12-31), whereas modelled downward solar radiation are based on CFSR (1979-01-15 to 2022-12-31), at analysis point BHI-2. The results are summarised in Table 7.1 to Table 7.3.

There is a clear seasonal variation for all three variables. Air temperature, relative humidity and solar radiation are larger during the summer months and lower during the winter months.

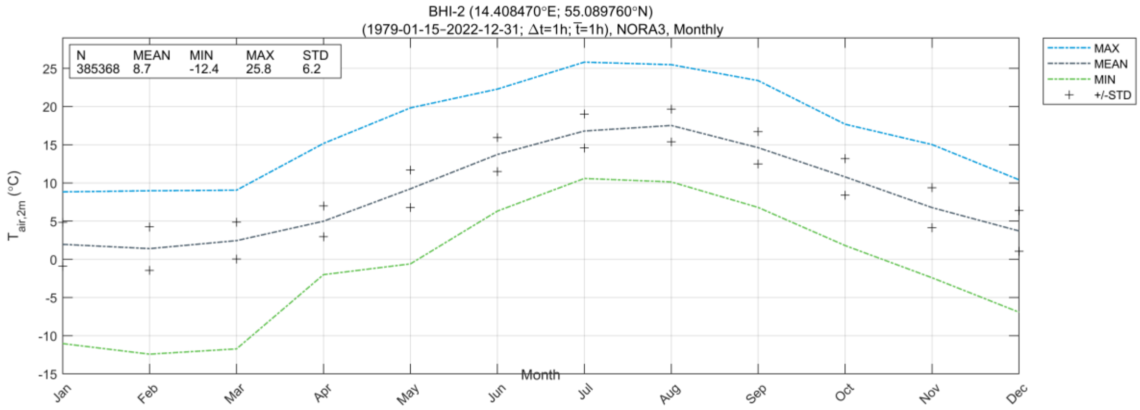

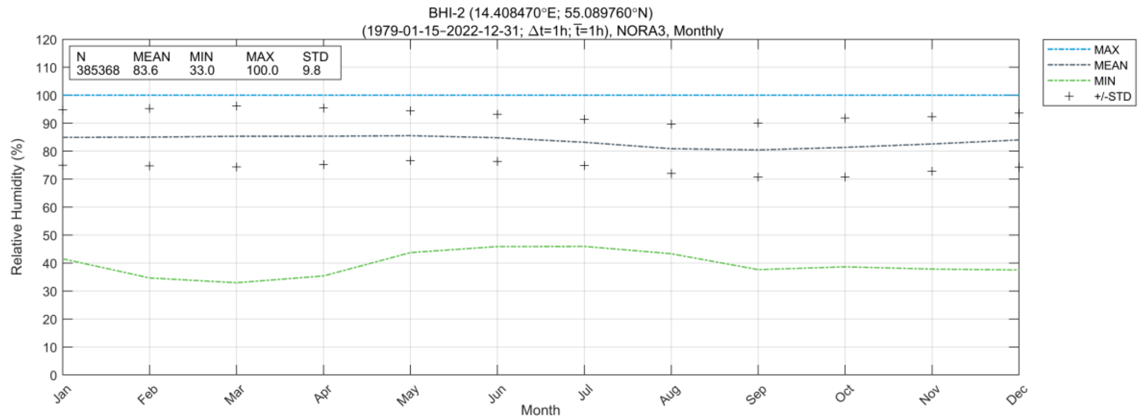

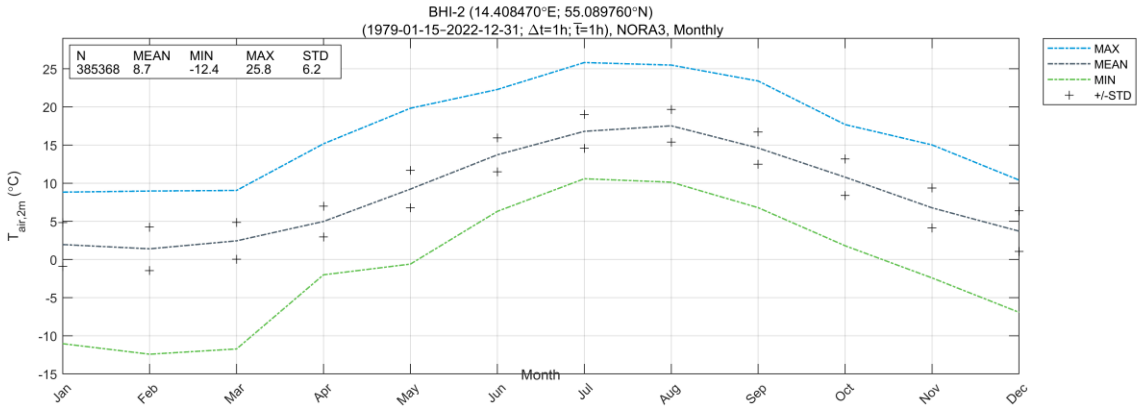

Figure 7.1 Monthly statistics of air temperature at 2 m above sea level (top), relative humidity (centre), and downward solar radiation (bottom) at BHI-2

Table 7.1 Annual and monthly statistics for air temperature at 2 m above sea level at BHI-2

Air temperature at 2 m above sea level at BHI-2 [°C]						
Statistical		№ of data points	Mean	Min.	Max.	STD.
Annual		385368	8.7	-12.4	25.8	6.2
Monthly	Jan.	32400	2	-11	8.8	2.9
	Feb.	29832	1.4	-12.4	9	2.8
	Mar.	32736	2.4	-11.7	9.1	2.4
	Apr.	31680	5	-2	15.2	2
	May	32736	9.2	-0.6	19.8	2.5
	Jun.	31680	13.7	6.3	22.3	2.2
	Jul.	32736	16.8	10.6	25.8	2.2
	Aug.	32736	17.5	10.1	25.5	2.1
	Sep.	31680	14.6	6.8	23.4	2.1
	Oct.	32736	10.8	1.8	17.7	2.4
	Nov.	31680	6.8	-2.4	15	2.6
	Dec.	32736	3.7	-6.9	10.4	2.6

Table 7.2 Annual and monthly statistics for relative humidity at BHI-2

Relative humidity at BHI-2 [%]						
Statistical		№ of data points	Mean	Min.	Max.	STD.
Annual		385368	83.6	33	100	9.8
Monthly	Jan.	32400	84.9	41.5	100	9.9
	Feb.	29832	85	34.7	100	10.2
	Mar.	32736	85.3	33	100	10.9
	Apr.	31680	85.3	35.4	100	10.1
	May	32736	85.5	43.7	100	8.9
	Jun.	31680	84.8	45.9	100	8.4
	Jul.	32736	83.2	45.9	100	8.3
	Aug.	32736	80.9	43.3	100	8.8
	Sep.	31680	80.4	37.6	100	9.7
	Oct.	32736	81.3	38.6	100	10.5
	Nov.	31680	82.6	37.8	100	9.7
	Dec.	32736	84	37.5	100	9.6

Table 7.3 Annual and monthly statistics for downward solar radiation at BHI-2

Downward solar radiation at BHI-2 [W/m²]						
Statistical		№ of data points	Mean	Min.	Max.	STD.
Annual		385368	139.7	0	861.7	212.4
Monthly	Jan.	32400	22	0	260.9	36.8
	Feb.	29832	52.2	0	443.6	78.5
	Mar.	32736	115.6	0	636.6	150.1
	Apr.	31680	198	0	762	228.6
	May	32736	263.4	0	839.7	279.6
	Jun.	31680	282.2	0	861.7	289.2
	Jul.	32736	264.3	0	836.7	278.1
	Aug.	32736	217.6	0	785.1	243
	Sep.	31680	142.6	0	651.8	175.3
	Oct.	32736	71.3	0	470.4	99.2
	Nov.	31680	26.9	0	269.7	42.9
	Dec.	32736	14.4	0	149.7	23.7

7.2 Seawater temperature and salinity

Information on the properties of seawater (temperature and salinity) was obtained from the EIBS-3DHD dataset. Time series of seawater temperature and seawater salinity were extracted for the near-surface, mid-depth, and near-seabed six (6) locations. The data cover a 25-year period (1998 to 2022) with a temporal resolution of 1-hour. Results of the analysis are presented only at the BHI-2 location, where model outputs were validated. Figure 7.2 and Figure 7.3 present the monthly variation of seawater temperature and salinity at three different layers.

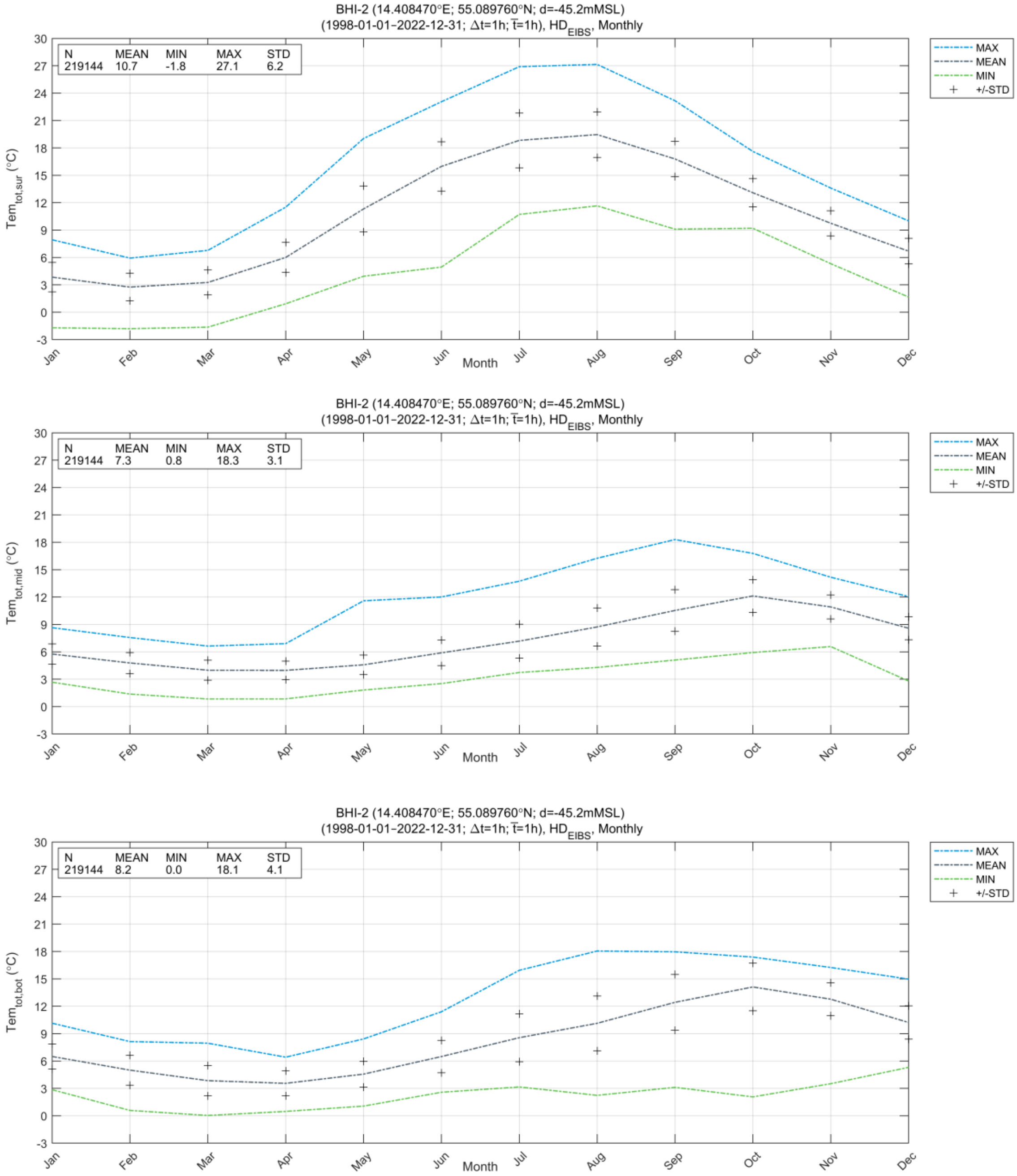

Figure 7.2 Monthly statistics of sea temperature at near-surface (top), mid-depth (centre), and near-seabed (bottom) at BHI-2

Table 7.4 Annual and monthly statistics for seawater temperature at near-surface at BHI-2

Seawater temperature at BHI-2 [°C] – Near-surface						
Statistical		№ of data points	Mean	Min.	Max.	STD.
Annual		219144	10.7	-1.8	27.1	6.2
Monthly	Jan.	18600	3.8	-1.7	7.9	1.6
	Feb.	16944	2.7	-1.8	5.9	1.5
	Mar.	18600	3.3	-1.6	6.8	1.4
	Apr.	18000	6	0.9	11.5	1.7
	May	18600	11.3	3.9	19	2.5
	Jun.	18000	16	4.9	23.1	2.7
	Jul.	18600	18.8	10.7	26.9	3
	Aug.	18600	19.5	11.7	27.1	2.5
	Sep.	18000	16.8	9.1	23.2	1.9
	Oct.	18600	13.1	9.2	17.6	1.5
	Nov.	18000	9.7	5.3	13.6	1.4
	Dec.	18600	6.7	1.7	10	1.4

Table 7.5 Annual and monthly statistics for seawater temperature at mid-depth at BHI-2

Seawater temperature at BHI-2 [°C] – Mid-depth						
Statistical		№ of data points	Mean	Min.	Max.	STD.
Annual		219144	7.3	0.8	18.3	3.1
Monthly	Jan.	18600	5.8	2.7	8.6	1.1
	Feb.	16944	4.8	1.4	7.6	1.2
	Mar.	18600	4	0.8	6.6	1.1
	Apr.	18000	4	0.8	6.9	1
	May	18600	4.6	1.8	11.6	1.1
	Jun.	18000	5.9	2.5	12	1.4
	Jul.	18600	7.2	3.7	13.7	1.9
	Aug.	18600	8.7	4.3	16.3	2.1
	Sep.	18000	10.5	5.1	18.3	2.3
	Oct.	18600	12.1	5.9	16.8	1.8
	Nov.	18000	10.9	6.6	14.2	1.3
	Dec.	18600	8.6	2.8	12.1	1.3

Table 7.6 Annual and monthly statistics for seawater temperature at near-seabed at BHI-2

Seawater temperature at BHI-2 [°C] – Near-seabed						
Statistical		№ of data points	Mean	Min.	Max.	STD.
Annual		219144	8.2	0	18.1	4.1
Monthly	Jan.	18600	6.5	2.9	10.1	1.4
	Feb.	16944	5	0.6	8.1	1.6
	Mar.	18600	3.8	0	8	1.7
	Apr.	18000	3.6	0.5	6.4	1.3
	May	18600	4.6	1.1	8.4	1.4
	Jun.	18000	6.5	2.6	11.4	1.8
	Jul.	18600	8.6	3.2	15.9	2.6
	Aug.	18600	10.1	2.2	18.1	3
	Sep.	18000	12.4	3.1	18	3.1
	Oct.	18600	14.1	2.1	17.4	2.6
	Nov.	18000	12.8	3.5	16.2	1.8
	Dec.	18600	10.2	5.3	15	1.8

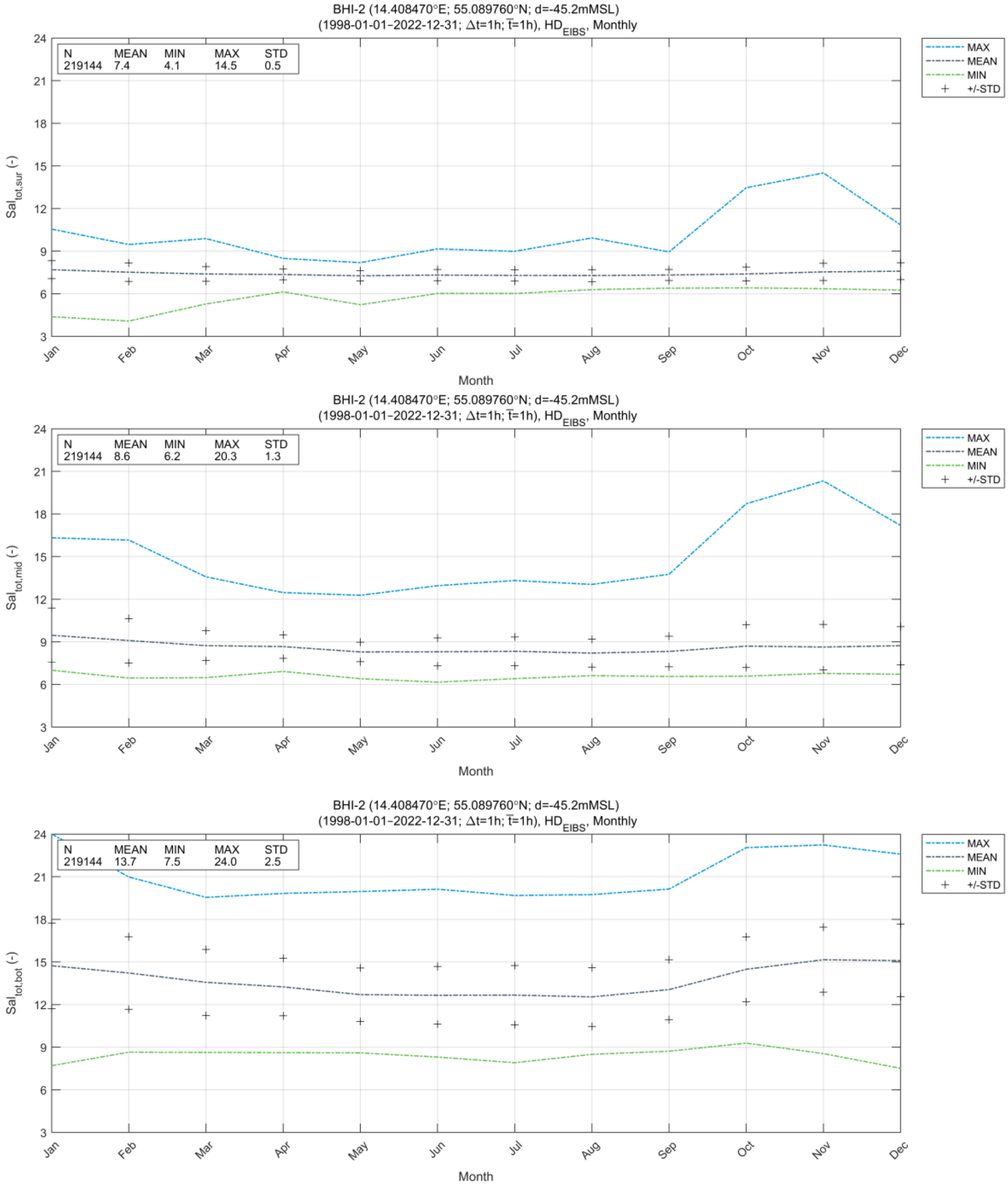

Figure 7.3 **Monthly statistics of salinity at near-surface (top), mid-depth (centre), and near-seabed (bottom) at BHI-2**

Table 7.7 Annual and monthly statistics for seawater salinity at near-surface at BHI-2

Seawater salinity at BHI-2 [] – Near-surface						
Statistical		№ of data points	Mean	Min.	Max.	STD.
Annual		219144	7.4	4.1	14.5	0.5
Monthly	Jan.	18600	7.7	4.4	10.6	0.6
	Feb.	16944	7.5	4.1	9.5	0.6
	Mar.	18600	7.4	5.3	9.9	0.5
	Apr.	18000	7.4	6.1	8.5	0.4
	May	18600	7.3	5.2	8.2	0.4
	Jun.	18000	7.3	6	9.2	0.4
	Jul.	18600	7.3	6	9	0.4
	Aug.	18600	7.3	6.3	9.9	0.4
	Sep.	18000	7.3	6.4	8.9	0.4
	Oct.	18600	7.4	6.4	13.5	0.5
	Nov.	18000	7.5	6.4	14.5	0.6
	Dec.	18600	7.6	6.3	10.9	0.6

Table 7.8 Annual and monthly statistics for seawater salinity at mid-depth at BHI-2

Seawater salinity at BHI-2 [] – Mid-depth						
Statistical		№ of data points	Mean	Min.	Max.	STD.
Annual		219144	8.6	6.2	20.3	1.3
Monthly	Jan.	18600	9.5	7	16.3	1.9
	Feb.	16944	9.1	6.5	16.2	1.6
	Mar.	18600	8.7	6.5	13.6	1.1
	Apr.	18000	8.7	6.9	12.5	0.8
	May	18600	8.3	6.4	12.3	0.7
	Jun.	18000	8.3	6.2	13	1
	Jul.	18600	8.3	6.4	13.3	1
	Aug.	18600	8.2	6.6	13	1
	Sep.	18000	8.3	6.6	13.8	1.1
	Oct.	18600	8.7	6.6	18.7	1.5
	Nov.	18000	8.6	6.8	20.3	1.6
	Dec.	18600	8.7	6.7	17.2	1.3

Table 7.9 Annual and monthly statistics for seawater salinity at near-seabed at BHI-2

Seawater salinity at BHI-2 [] – Near-seabed						
Statistical		№ of data points	Mean	Min.	Max.	STD.
Annual		219144	13.7	7.5	24	2.5
Monthly	Jan.	18600	14.7	7.7	24	3
	Feb.	16944	14.2	8.7	21	2.6
	Mar.	18600	13.6	8.6	19.5	2.3
	Apr.	18000	13.2	8.6	19.8	2
	May	18600	12.7	8.6	20	1.9
	Jun.	18000	12.7	8.3	20.1	2
	Jul.	18600	12.7	7.9	19.7	2.1
	Aug.	18600	12.5	8.5	19.7	2.1
	Sep.	18000	13.1	8.7	20.1	2.1
	Oct.	18600	14.5	9.3	23	2.3
	Nov.	18000	15.2	8.6	23.2	2.3
	Dec.	18600	15.1	7.5	22.6	2.5

7.3 Marine growth

Based on the detailed assessment presented in [1] of the predicted marine growth on submerged structures in the Baltic Sea, the recommended thickness and density at the EIBS OWFs and what the marine growth is expected to consist of is provided in Table 7.10.

Table 7.10 Summary of the marine growth on submerged structures at the planned EIBS OWFs

Water Depth	Description of marine growth on submerged structure	Thickness (mm) Recommendation for calculations (DNVGL-ST-0437) [10]	Density (kg/m³) Recommendation for calculations (DNVGL-ST-0437) [10]
0-1 m:	50-60% cover with barnacles (*Balanus improvisus*) extending to a maximum height of 15 mm above structure and with a dry weight in air of 250 g/m² – equivalent to ca. 80-100 g/m² in water		
1-7 m:	80-100% cover 2-3 stories high growth of mussels	100	1325
7-10 m:	50-75% cover 2 stories high growth of mussels		
10-15 m:	30-50% cover 1-2 stories high growth of mussels		
15-20 m:	10-25% cover in one layer of mussels		
>20 m:	Scattered individuals of mussels		

8 References

[1] DHI, “Energy Island Baltic Sea, Metocean Site Conditions Assessment, Part A: Description and verificatIon of data basis,” 2023.

[2] DHI, “Energy Island Baltic Sea, Metocean Site Conditions Assessment, Part D: Data Basis - Hindcast revalidation note, due Jan 2024,” 2023.

[3] DNV, “DNV-RP-C205 Environmental conditions and environmental loads,” DNV AS, 2021.

[4] IEC, “61400-3-1, Wind energy generation systems – Part 3-1: Design requirements for fixed offshore wind turbines,” 2019.

[5] H. B. Ø. F. B. R. R. M. B. P. &. A. O. J. Haakenstad, “NORA3: A nonhydrostatic high-resolution hindcast of the North Sea, the Norwegian Sea, and the Barents Sea,” *Journal of Applied Meteorology and Climatology,* vol. 60, no. 10, pp. 1443-1464, 2021.

[6] D. L. Codiga, Unified tidal analysis and prediction using the UTide Matlab functions, Narragansett: Graduate School of Oceanography, University of Rhode Island, 2011.

[7] R. Pawlowicz, B. Beardsley and S. Lentz, Classical tidal harmonic analysis including error estimates in MATLAB using T-TIDE, Computers & Geosciences, vol. 28, pp. 929-937, 2003.

[8] K. E. Leffer and D. A. Jay, Enhancing tidal harmonic analysis: Robust (hybrid L-1/L-2) solutions, Cont Shelf Res., vol 29, pp.78-88, 2009.

[9] M. G. G. Foreman, J. Y. Cherniawsky and V. A. Ballantyne, Versatile harmonic tidal analysis: improvements and applications, J. Atmos. Oceanic Tech., vol. 26, pp. 806-817, 2009.

[10] DNV, “DNVGL-ST-0437, Loads and site conditions for wind turbines,” (2016).

Appendix A List of Data Reports

This appendix presents a list of data reports attached to this report.

Table A.1 List of data reports (.xlsx) attached to this report
Normal and extreme conditions (based on T-EVA).

Filename
Normal and extreme conditions (based on T-EVA)
BHI-1_Metocean-Data-Report.xlsx
BHI--2_Metocean-Data-Report.xlsx
BHI-3_Metocean-Data-Report.xlsx
BHII-1_Metocean-Data-Report.xlsx
BHII-2_Metocean-Data-Report.xlsx
BHII-3_Metocean-Data-Report.xlsx

Appendix B Sensitivity of T-EVA to Distribution, Threshold, and Fitting

This section presents an assessment of the sensitivity of T-EVA to distribution, threshold, and fitting, leading to the choice of EVA settings.

It is good practice for conducting EVA to assess the sensitivity of the results using multiple thresholds, distributions, and fitting methods. Furthermore, one should consider the goodness of fit (visually), and magnitude (inter-compared), and water depth (waves), before deciding on an adequate EVA setup.

Figure B. 1 - Figure B. 8 sensitivity of T-EVA to distribution, threshold, and fitting for waves (H_{m0}), water levels (high and low, total, and residual), and current speed (total and residual) at BHI-2 (H_{m0} and WL) and BHI-2 (CS).

The plots depict the 100-year value vs. number of events per year for various long-term extreme value distributions and for two common fitting methods (Maximum likelihood (ML) and Least-Squares (LS). Based on the approach above, the applied EVA settings are chosen as follows:

- **Waves**: 2-p Weibull distribution fitted by least-square (LS) to the 88 (2x44) peak events separated by at least 36 hours.
- **Water level (high)**: 2-p Weibull distribution fitted by least-square (LS) to the 176 (4x44) peak events separated by at least 36 hours.
- **Water level (low)**: 2-p Weibull distribution fitted by least-square (LS) to the 88 (2x44) peak events separated by at least 36 hours.
- **Current speed**: 2-p Weibull distribution fitted by least-square (LS) to the 75 (3x25) peak events separated by at least 36 hours.

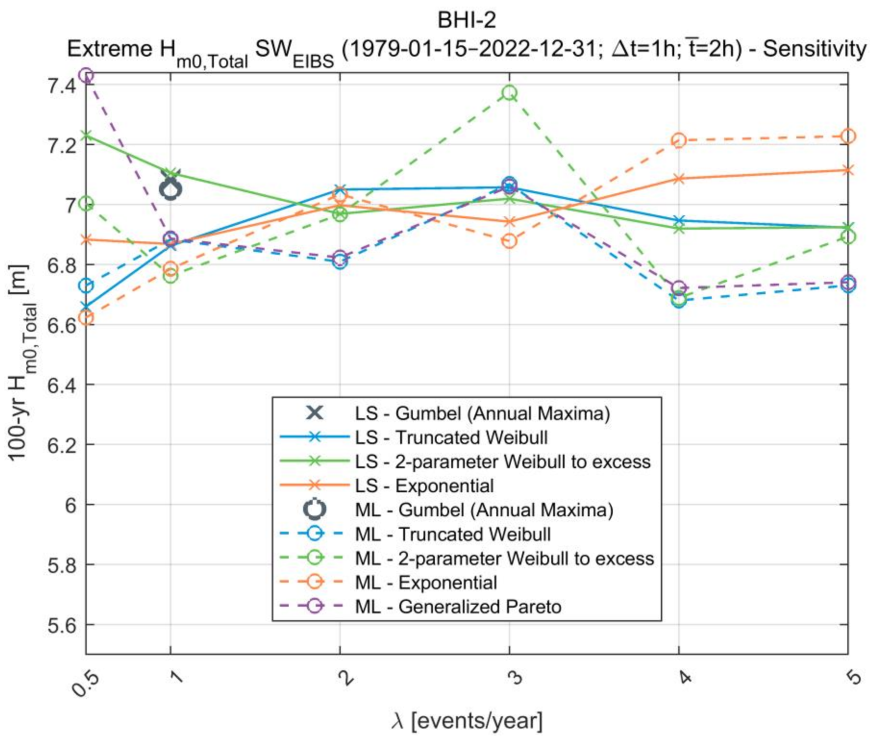

Figure B. 1 Sensitivity of T-EVA to distribution, threshold, and fitting at BHI-2
Variable: H_{m0}

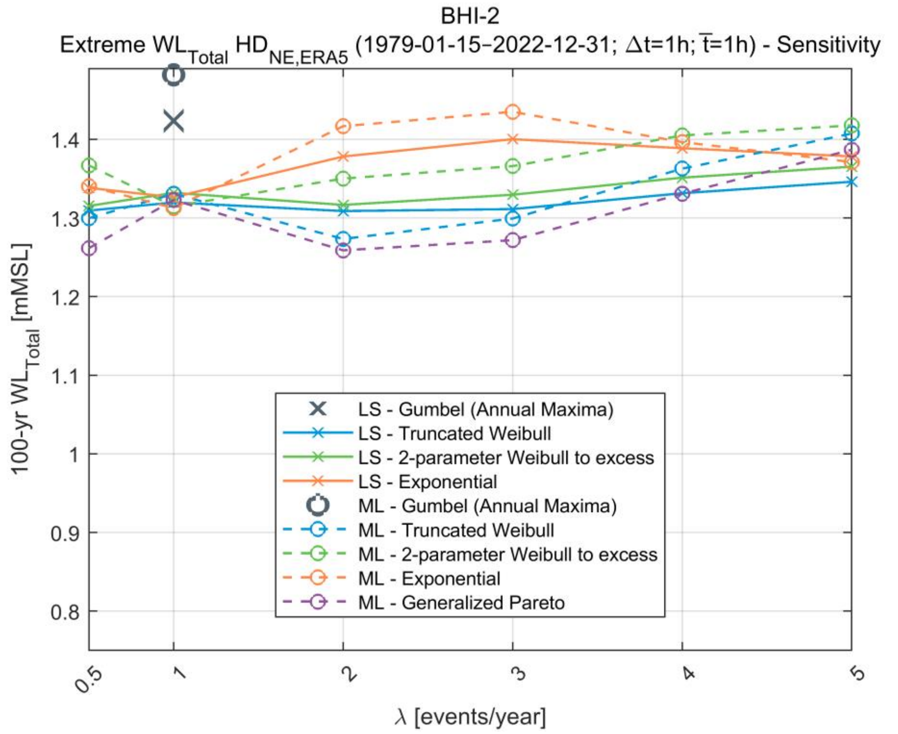

Figure B. 2 Sensitivity of T-EVA to distribution, threshold, and fitting at BHI-2
Variable: WL_{tot}

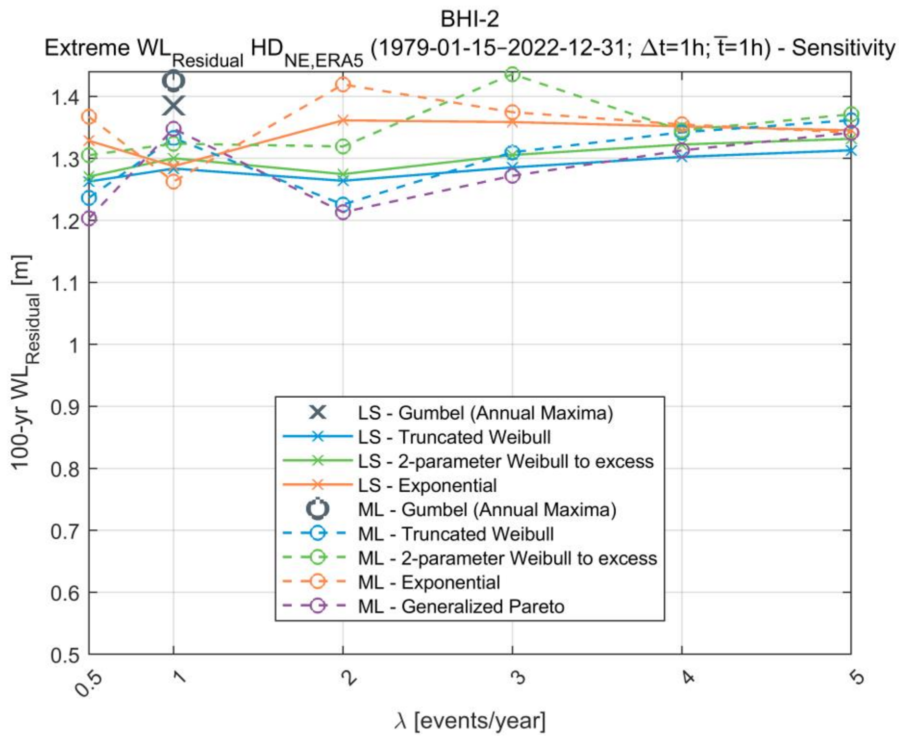

Figure B. 3 Sensitivity of T-EVA to distribution, threshold, and fitting at BHI-2
Variable: WL_{res}

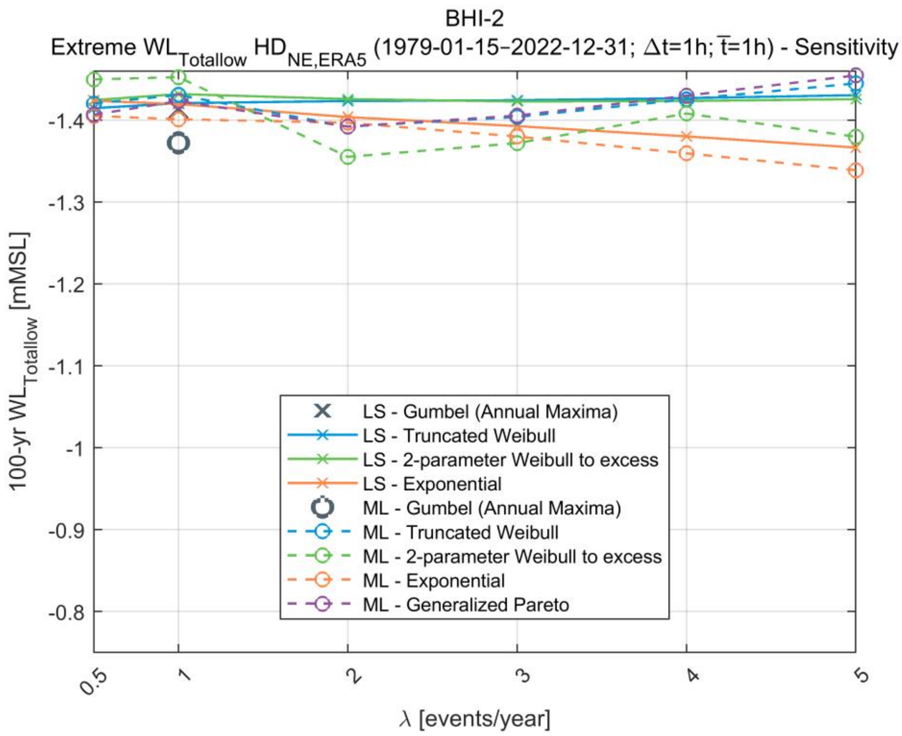

Figure B. 4 Sensitivity of T-EVA to distribution, threshold, and fitting at BHI-2
Variable: $WL_{tot,low}$

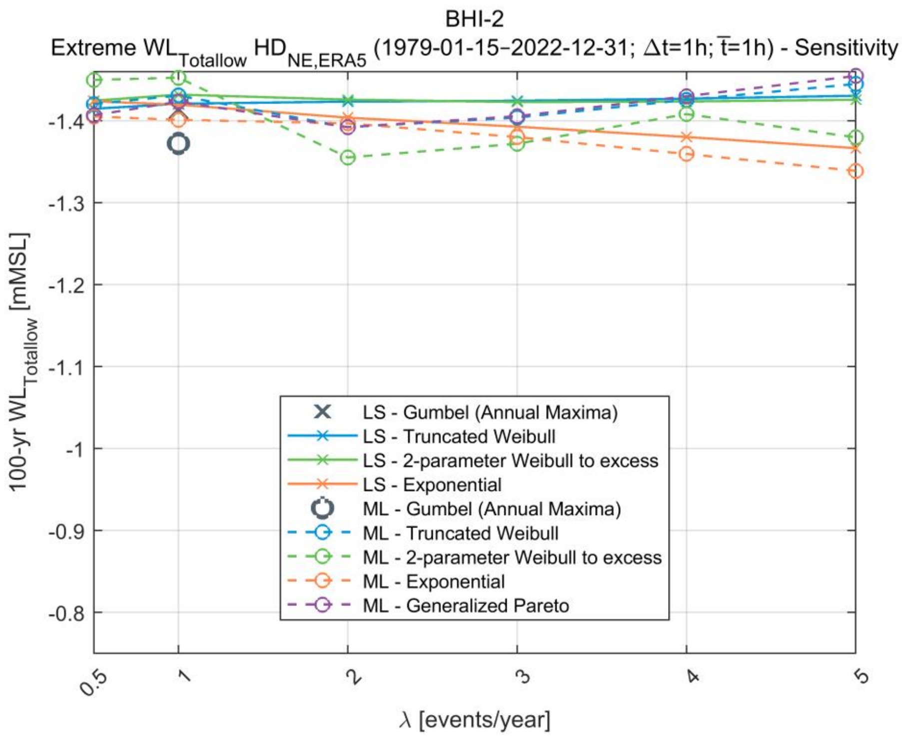

Figure B. 5 Sensitivity of T-EVA to distribution, threshold, and fitting at BHI-2
Variable: $WL_{res,low}$

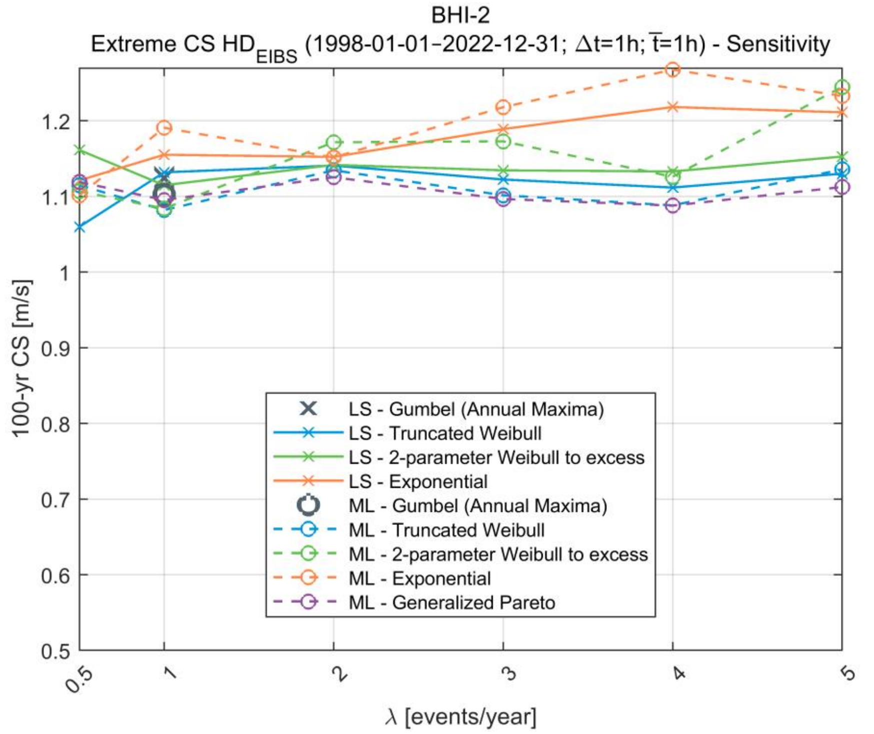

Figure B. 6 Sensitivity of T-EVA to distribution, threshold, and fitting at BHI-2
Variable: $CS_{tot,sur}$

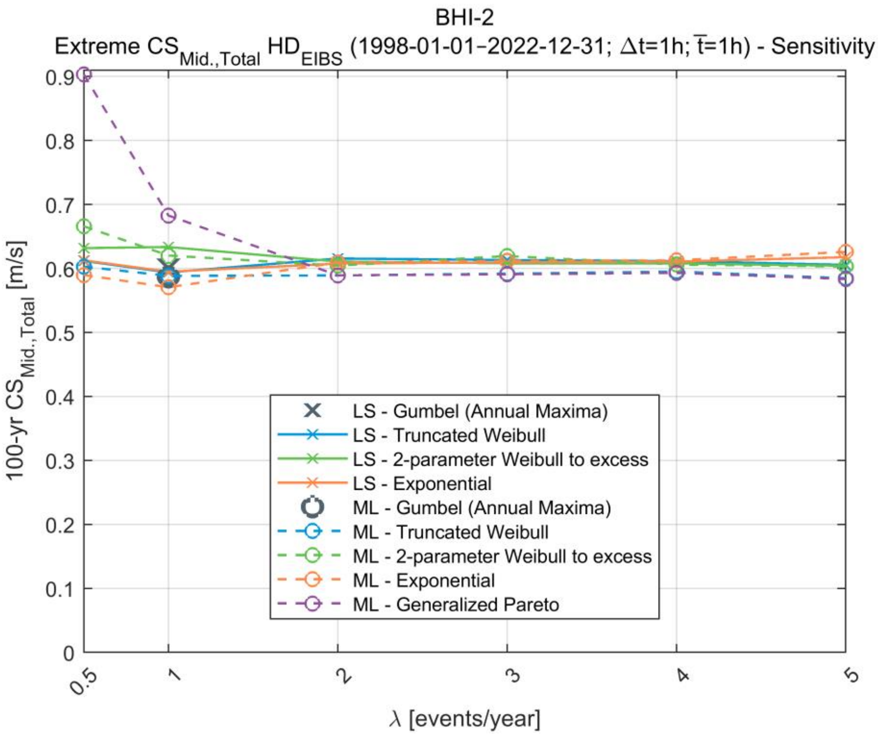

Figure B. 7 Sensitivity of T-EVA to distribution, threshold, and fitting at BHI-2
Variable: $CS_{tot,mid}$

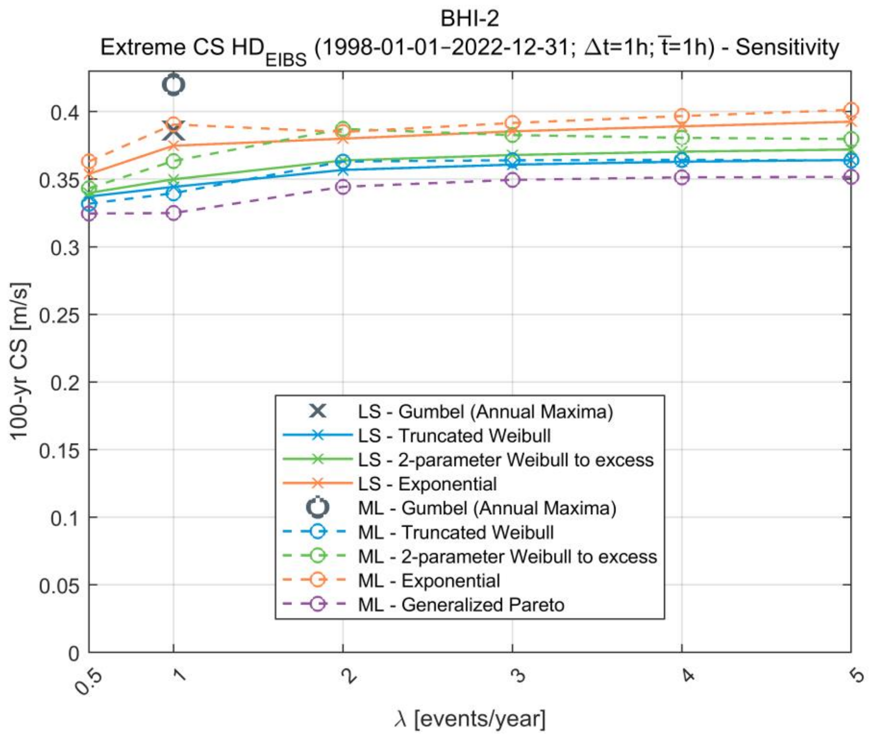

Figure B. 8 Sensitivity of T-EVA to distribution, threshold, and fitting at BHI-2
Variable: $CS_{tot,bot}$